THERMAL EFFECTS ON THE BEARING BEHAVIOR OF COMPOSITE JOINTS

A Dissertation presented to the Faculty of the

Graduate School of Engineering and Applied Science

at the

University of Virginia

In Partial Fulfillment of the Requirements for the Degree of

Doctor of Philosophy, Mechanical and Aerospace Engineering

By

Sandra Polesky Walker

May 2001

Abstract

Thermal effects on the pin-bearing behavior of an IM7/PETI5 composite laminate are studied comprehensively. A hypothesis presents factors influencing a change in pin-bearing strength with a change in temperature for a given joint design. The factors include the change in the state of residual cure stress, the material properties, and the fastener fit with a change in temperature.

Experiments are conducted to determine necessary lamina and laminate material property data for the IM7/PETI5 being utilized in this study. Lamina material properties are determined between the assumed stress free temperature of 460°F down to –200°F. Laminate strength properties are determined for several lay-ups at the operating temperatures of 350°F, 70°F, and –200°F.

A three-dimensional finite element analysis model of a composite laminate subject to compressive loading is developed. Both the resin rich layer located between lamina and the thermal residual stresses present in the laminate due to curing are determined to influence the state of stress significantly. For the laminate modeled, the effect of modeling temperature dependent material properties and nonlinear stress-strain behavior was found to be negligible. Simply using the material properties measured at the operating temperature of interest was sufficient for predicting stresses accurately in a linear analysis for the current problem.

Pin-bearing tests of several lay-ups were conducted to develop an understanding on the effect of temperature changes on the pin-bearing behavior of the material. As expected, for all lay-ups that failed in the bearing mode, pin-bearing strength decreased with an increase in temperature. Micrographs of failed specimens revealed severe damage in the outermost two plies with shear cracks emanating from that region.

A computational study investigating the factors influencing pin-bearing strength was performed. A finite element model was developed and used to determine the residual thermal cure stresses in the laminate containing a hole. Very high interlaminar stress concentrations were observed two elements away from the hole boundary at all three operating temperatures. The interlaminar stresses quickly reduced to zero within one laminate thickness from the hole boundary. Changes in fastener fit with a change in temperature were predicted to be insignificant on influencing changes in pin-bearing strength.

The pin-bearing problem was modeled assuming a rigid frictionless pin and restraining only radial displacements at the hole boundary. A uniform negative pressure load was then applied to the straight end of the model. A solution, where thermal residual stresses were combined with the state of stress due to pin-bearing loads was evaluated. The presence of thermal residual stresses intensified the interlaminar stresses predicted at the hole boundary in the pin-bearing problem. This dissertation shows that changes in material properties drives pin-bearing strength degradation with increasing temperature. The thermal residual cure stresses affect the extent that the pin-bearing strength

changes with temperature, where they can only lessen the strength degradation with increasing temperature.

Acknowledgements

The author would like to express her gratitude to the dissertation committee members for agreeing to serve on the committee and for their valuable suggestions. The author is especially grateful for her advisor, Professor Earl Thornton, whose patience, guidance, and wisdom gave me the opportunity to complete the dissertation work.

I also appreciate the support I have been given by employees of NASA Langley Research Center:

- Dr. Steve Scotti, whose support of the research made the dissertation possible
- Ronnie Long, Scott Wallace, Quinton Duncan, and Ron Penner for all there invaluable support in conducting experiments
- Members of the Metals and Thermal Structures Branch for all their compassion.

I must most of all thank my mother, Martha Polesky, for her love and devotion throughout my life gave me the strength to accomplish my goals. I am very thankful for my husband, Mitch, for all his support. I am dearly thankful for my children, Grayson and Kendra, who inspire me to be the best mother I possibly can.

Table of Contents

List of Figures

List of Tables

Nomenclature

Arabic	Description
[A]	laminate extensional stiffness matrix
B	fastener fit
[B]	laminate bending-extension coupling stiffness matrix
b	width
D	bolt hole diameter
d	pin diameter
E	modulus of elasticity
e	edge distance from center of bolt hole to laminate free end
F_{br}	pin-bearing strength
F_{bru}	pin-bearing yield strength
F_{bry}	pin-bearing ultimate strength
f	function
G	shear modulus
H	ply thickness
L	length
M	material properties
N	resultant force
N_x	axial load in x-coordinate direction
$\{N\}^T$	thermal force
P	load
Q	component of reduced stiffness matrix
r	radial coordinate in cylindrical coordinate system
S	state of residual stress
S_g	equivalent bearing stress
T	temperature
T_{ref}	reference temperature
T_g	glass transition temperature
T_{SFT}	stress free temperature
t	laminate thickness
[T]	transformation matrix
Ue	applied end load
W	laminate width
x	spatial coordinate
y	spatial coordinate
z	spatial coordinate

Greek	Description
α	coefficient of thermal expansion

Δ	change
ΔT	temperature change
ε	strain
ε_o	bearing strain at effective origin
γ	shear strain
λ	bolt hole clearance
θ	angular coordinate in cylindrical coordinate system
δ	bolt hole elongation
κ	curvature
σ	stress
τ	shear stress
ν	Poisson ratio

Subscripts	Description
1	spatial coordinate in lamina coordinate system
2	spatial coordinate in lamina coordinate system
3	spatial coordinate in lamina coordinate system
br	bearing
bry	bearing yield
bru	ultimate bearing
C	compression
i	i-th component of matrix
j	j-th component of matrix
max	maximum value
p	pin
r	resin layer
T	tension
x	spatial coordinate
Y	yield
y	spatial coordinate
z	spatial coordinate

Superscripts	Description
T	transpose
k	numbered identification
o	middle surface

Abbreviations	Description
ASTM	American Society of Testing and Materials
CLT	Classical Lamination Theory
ETW	Elevated Temperature Wet
IM7	graphite fibers
F.R.	Failure Ratio

LH2	Liquid Hydrogen
LO2	Liquid Oxygen
PCM	Polymer Matrix Composite
PETI-5	polyimide matrix material
RLV	Reusable Launch Vehicle
RTD	Room Temperature Dry
SFT	Stress Free Temperature

Chapter 1
Introduction

The desire for lighter weight aircraft and spacecraft has led to the utilization of polymer matrix composite materials for many structural components in advanced vehicle designs. Laminated composite panels have the ability to carry high mechanical loads while remaining lightweight in comparison to metallic panels. In advanced vehicle structural applications, the composite panels may be exposed to temperature extremes. This dissertation considers a critical area for application of composites at temperature extremes: the problem of mechanically fastened joints.

1.1 Background

To provide the rationale for the dissertation research, the necessity of mechanically fastened composite joints is briefly discussed. Next, the loading of composite joints at elevated and cryogenic temperatures is described followed by the topic of pin-bearing loads on a composite laminate and associated failure modes.

1.1.1 Mechanically Fastened Composite Joints

Size limitations in large-scale structures fabrication in addition to economic factors require that structural components be fabricated as components with subsequent assembly to produce a final vehicle. Due to the inability of adhesive bonds to transfer high mechanical loads between structural components, mechanically fastened joints are often used in vehicle design. A schematic drawing of a mechanically fastened composite joint concept as a component in an aircraft wing is illustrated in Figure 1.1. The joint concept shows two honeycomb sandwich panels with composite facesheets joined to a titanium splice plate through two rows of fasteners on each panel. By providing a load path through bolts and splice plates, the bolted splice joints transfer mechanical loads between structural components.

The need to join composite panels through bolted splice joints has raised many issues not encountered with metallic joints. Anisotropic, nonhomogeneous and viscoelastic properties of composite laminates in addition to their brittle nature require special attention in developing structurally reliable and efficient joints. The joining of composite laminates through bolted splice joints consequently became a major topic of research from the 1970s to the present. In 1986, the first U.S. government design guide was published that provides analysis tools (computer codes) and guidance for the design of composite bolted joints.[1.1]

1.1.2 Thermo-mechanical Loading

When a structure is exposed to a change in operating temperature, thermally induced stresses arise from constrained thermal expansion or contraction. In addition, both thermal and mechanical properties may change over the range of temperature. The combined effect of altered thermal

environment and additionally applied mechanical loading results in a complex thermo-mechanical loading of the structure.

Elevated Temperatures. During typical aircraft flight maneuvers, bending loads are induced along the span of the wing. Wing bending results in significant in-plane axial loads for the upper and lower wing surface panels. The loads may either be tension or compression; for example, when the upper surface is in compression, the lower surface is in tension. The axial load is depicted in Figure 1.2 for a surface wing panel joint experiencing a tensile load. A side view through the thickness of the wing joint is displayed in the figure with the applied mechanical load, N_x. For high speed aircraft structures, like that shown in Figure 1.1, the outer surface structural joints are also exposed to aerodynamic heating. For a Mach 2.5 civil transport, temperatures have been shown to reach 350°F on the outer surface of the aircraft.[1.2] Thermal effects in addition to the mechanically applied loads create a state of thermo-mechanical loading for the surface splice joint. The elevated temperatures may degrade the load carrying capabilities of the joint and consequently impose additional challenges in the joint design. Unfortunately, the design tools of Ramkumar et al. do not include temperature effects.[1.1]

Cryogenic Temperatures. On the other end of the spectrum, there is the possibility that laminated composite bolted splice joints will be necessary in cryogenic environments. Research studies have shown the necessity for composites as primary structure for a cost effective reusable launch vehicle(RLV) to replace the Space Shuttle.[1.3, 1.4] A schematic of a composite bolted splice joint in a RLV concept is illustrated in Figure 1.3. The figure shows an RLV concept with internal liquid oxygen (LO2) and liquid hydrogen (LH2) cryogenic tanks and an intertank structure located between the cryogenic tanks.[1.4] In such a design, a composite bolted splice joint is used as an assembly joint in mating the intertank structure with the cryogenic tank structures. As shown in the figure, the joint is subject to axial loading, N_x. Due to the joints proximity to the cryogenic tanks, the joint will be exposed to cryogenic temperatures. Consequently, the effect of cryogenic temperatures on the joint behavior requires consideration in the joint design.

1.1.3 Composite Laminate Subject to Pin-Bearing Loading

When the bolted splice joints shown in Figures 1.2 and 1.3 are subject to in-plane mechanical loads, the composite laminate facesheets experience complex loading, where bearing loads are a significant component. The bearing load is compressive due to the fastener bearing on a finite area of the composite laminate at the bolt hole boundary.

A simplistic case of pin-bearing where there is no out-of-plane compression of the composite laminate due to tightening of the bolt is shown in Figure 1.4. The composite laminate bearing specimen has width, w, edge distance, e, bolt hole diameter, D, and thickness, t. The figure also shows a tensile load, P, being transferred to the composite laminate through the pin with diameter, d. Due to the load transfer through the pin-laminate contact, the laminate is subject to

compressive bearing stresses in the vicinity of the bearing surface. The contact area varies as the load P increases.

A typical load-deformation curve obtained from a bearing test is shown in Figure 1.5.[1.5] For bearing testing, the deformation, δ, is measured across the bolt hole and is referred to as the bolt hole elongation. On the curve, the proportional limit represents the onset of nonlinear material behavior. The yield strength corresponds to 4% hole elongation in the composite laminate, and the ultimate load represents the maximum sustained load of the joint prior to failure. The bearing strength F_{br} of the laminate is calculated by:

$$F_{br} = P/tD \tag{1.1}$$

The subscripts bry and bru are also used to differentiate between yield and ultimate bearing strength, respectively.

The four basic laminate failure modes associated with composite bolted joints are illustrated in Figure 1.6.[1.5] The tension failure mode is characterized by a fracture of the laminate across its width from the hole to the edges, the shearout failure mode is characterized by a "pull-out" fracture between the hole and laminate end, and the cleavage-tension failure mode is characterized by a simultaneous fracture across the width to one edge and between the hole and the laminate end. The bearing failure mode is observed as a localized crushing of the laminate in front of the bearing surface. The type of failure mode observed during bearing testing is affected by the w/D and e/D ratios of the bearing specimens, which can easily be explained through strength of materials considerations. For a given laminate, the tension failure mode is associated with insufficient w/D ratios, where the specimen is not wide enough to prevent a tension failure. The shearout failure mode is dependent on the e/D ratio, where e can be made larger to prevent shearout failure. The cleavage-tension failure mode is a combined tension and shearout failure when the tension strength corresponds to the shear strength of a specimen. For sufficiently large e/D and w/D ratios, the bearing failure mode will result.

1.2 Previous Research

Previous research pertinent to this dissertation is reviewed in this section. Research on thermal effects on bearing behavior of composite joints is presented by first reviewing experimental investigations, followed by analytical studies. Residual stress concentrations at bolt holes is then reviewed. Finally, issues concerning previous studies are revealed.

1.2.1 Experimental Investigations on Bearing Behavior

Previous experimental investigations on pin-bearing strength, bolt bearing strength, and the effect of clamp-up forces for composite laminates with varying operating temperatures are reviewed.

Pin-bearing Strength. Three experimental investigations reported on the effect of temperature on the pin-bearing strength and failure mode for particular composite laminates. Pin bearing tests were conducted by Kim et al. (1976) at

room temperature and at 260°F on three different graphite/epoxy lay-ups.[1.6] About a 30 percent reduction in the pin bearing strength was observed for a temperature increase to 260°F for all three lay-ups. No change in the bearing failure mode was observed at the elevated temperature. Another study was conducted by Wilkins in 1977 which also investigated the effect of temperature on joint strength for the same graphite/epoxy material for five different lay-ups.[1.7] For all specimens, a moderate temperature increase from room temperature to 200°F showed no significant effect on the specimen strength. However, unlike Kim et al.'s study where the bearing specimens failed in a bearing mode, the bearing specimens here failed in a net tension mode. In contrast, a pin bearing strength reduction of approximately 40% with a temperature increase to 350°F from room temperature was reported by Wilson in 1979 for graphite/epoxy specimens with a range of geometric parameters.[1.8] Interestingly, for the 0 degree dominated lay-up tested, where the strength difference was pronounced for varying specimen width at room temperature, the strength became independent of specimen width at 350°F.

Bolt Bearing Strength. Several references encompassing both elevated temperature and cryogenic strength testing of graphite/polyimide composite bolted splice joint specimens were found in the literature. In 1979, Perry and Hyer established the testing procedures in their study.[1.9] Testing of 16-ply double lap quasi-isotropic specimens were conducted at temperatures of –250°F, 75°F, and 600°F. Wichorek observed a 30% reduction in bearing strength at the 600°F testing temperature in comparison to room temperature, and an 18% increase in bearing strength at the low temperature of –250°F in comparison to room temperature.[1.10,1.11] Other experimental investigations also revealed strength reductions at elevated temperatures for bolted composite material joints.[1.12,1.13, 1.14, 1.15, 1.16, 1.17] One study concluded that fracture load and mode can be predicted for joint geometry and temperature for a specific material system, where the authors proposed an empirical equation to estimate fracture load.[1.18] However, for carbon fiber composite joints tested at temperatures up to 285°F, negligible strength reductions were observed.[1.19] In general, past research suggests that the magnitude of strength reduction is at least somewhat dependent on the composite unnotched material properties variations with temperature.

The effect of lay-up on bearing strength at room temperature (RTD) and at a 250°F elevated temperature wet condition (ETW) was investigated by Garbo and Ogonowski for graphite-epoxy bolted joints.[1.20] Three lay-ups of varying percentage of 45° plies were tested in both tension and compression for a double shear two-fastener in-tandem specimen with a 50 in-lb torque. A 30-40 ksi loss in ultimate bearing strength was observed for all three lay-ups tested at the ETW condition. This result is in contrast to other reported pin-bearing strength results where the magnitude of the strength reduction was dependent on the lay-up of the material being tested.[1.6, 1.7, 1.8] Additionally, the effect of edge distance, e, and specimen width, w, (see Figure 1.4) on the bearing strength was also investigated by Garbo and Ogonowski. For a pin diameter d, they observed an

insensitivity to both e/d and w/d ratios, with a reduced bearing strength capacity for the ETW condition.

An extensive test program was conducted with the objective of providing information on the bearing behavior of graphite cloth epoxy in addition to quasi-isotropic tape laminate bolted joints at temperatures up to 450K.[1.21, 1.22] Strength degradations at elevated temperatures were observed for single and multifastener joint tests. The empirical approaches of Hart-Smith were utilized to explain elevated temperature test results. The techniques of Hart-Smith were developed from room temperature testing where stress concentration factors are computed based on composite bolted joint strength data from joints failing in tension.[1.23, 1.24] Baile et al.'s test results from tension failure specimens showed that raising the temperature produced significant increases in the stress concentration. This was explained to be due to higher temperatures reducing the resin strength and stiffness, thus lessening it's ability to support the fibers and transfer the load adjacent to the hole. Additionally, when tension failures occurred, there was little if any decrease in the joint stiffness as a function of temperature, but when bearing failures occurred, there was a clear decrease in joint stiffness over the linear load-deflection range.

The mechanical behavior of quasi-isotropic bolted joints was examined and discussed by Meakawa et al. in 1985, where test temperature, specimen width, and edge distance were all varied with zero bolt-torque clamping.[1.25] Examination of the results shows that at 120°C, all failure modes changed to bearing with a lower bearing strength than at room temperature. The change to a bearing failure mode was attributed to the actual decrease in the compressive strength for the laminate with increasing temperature. The width and edge distances required to raise the joint strength at room temperature did not provide any significant strength improvement at elevated temperatures where bearing failures occurred. In retrospect, these results are similar to those observed by Garbo and Ogonowski for graphite/epoxy bolted joints, where increasing specimen width and edge distance did not provide the increased strength capacity for the ETW case as it did for the RTD case.[1.20] Examination of the material properties of the lamina reported by Garbo and Ogonowski shows a 53% reduction in the fiber direction lamina compressive strength and a 33% reduction in the matrix direction lamina compression strength at the ETW condition and no change in the fiber direction tension ultimate strength with no reporting on the matrix direction tension strength at the ETW condition.

Bolt Clamp-up Effects. The beneficial effects of bolt clamp-up forces in increasing joint strength has been well documented for room temperature composite joints.[1.26, 1.27, 1.28] The increase in strength can be attributed to a combined effect of increasing the portion of load being transferred by friction at the joint, thus decreasing the bearing load at the bolt hole and also the lateral constraint increasing bearing strength by reducing out-of-plane displacement under contact and hence reducing the out-of-plane shear stress.[1.29] The effect of temperature on joint strength for varying clamp-up force was investigated by Horn and Schmitt in 1994.[1.30] They conducted tests of single-shear thermoplastic composite specimens with the objective of establishing a correlation between

bearing strength and clamp-up force. Their test results showed that increasing temperature decreased the bearing strength proportionally over the range of clamp-up force. Both the room temperature and elevated temperature results showed the same trend of increasing bearing strength with increasing clamp-up force. Wright et al.(1997) investigated the time- dependent bolt bearing behavior of thermoplastic joints at elevated temperature.[1.31] They observed time-dependent behavior of IM7/K3B joints only in a narrow band of loadings for an unclamped condition. For the clamp-up tests, no bearing creep behavior was observed up to 150% of the baseline load for the joint. Clamp-up force appeared to have the most significant effect on coupon bearing strength at temperature. They also conducted bearing bypass interaction static tests at temperature. The test results showed more significant reductions in strength under compressive loading at the elevated temperature than under tensile loading conditions.

Conclusions. The experimental investigations presented show that an increase in temperature leads to bearing strength reductions in many polymer matrix composite laminates. The extent of the bearing strength reduction has been shown to be affected by not only the temperature change, but also by the material system and lay-up being evaluated. The extent of bearing strength reduction with increasing temperature was also shown to be independent of clamp-up force for two material systems. Additionally researchers observed that the bearing failure mode is more likely to occur than the tension failure mode at elevated temperature due to a larger reduction in the laminate compressive strength at the elevated temperature in comparison to the laminate tensile strength. Consequently, based on the elevated temperature laminate tensile strength and bearing strength data for the bearing failure mode, one could easily design a joint with an optimum width, or distance between fasteners, for elevated temperature applications.

Additionally, a study was presented that showed increase bearing strength at the low test temperature of –250°F for graphite/polyimide specimens. Unfortunately, the material properties of the quasi-isotropic laminate tested were only reported at room temperature.

1.2.2 Analytical Studies on Bearing Behavior

Finite element analysis methods have been applied to investigate the bearing behavior of composite joints at elevated temperatures. A two-dimensional, in-plane, finite element analysis was employed by Maekawa et al. in 1985 to determine principal stresses in the vicinity of the bolt hole under bearing loading conditions.[1.25] By examining risk factors computed from the ratio of principal stresses to the compressive and tensile laminate strengths, the ability to predict the failure mode proved to be feasible. As the temperature increased, higher compressive risk factors were observed at the bolt hole, thus increasing the risk for a compressive failure mode. The risk assessment compared well with test results where bearing failures were more prominent at elevated temperatures.

An incremental finite element code was used by Chen and Lee to study the effect of temperature on the contact stresses at pin loaded holes in

composite laminates.[1.32, 1.33] A two-dimensional finite element plate model of the composite laminate with a constrained pin, as displayed in Figure 1.7, was developed for their investigations. They adopted a quadratic failure criterion to predict failure and study the failure process at different temperatures and for different lay-ups and materials. Their analysis results showed bearing strength degradations with increasing temperature, and that the extent of strength degradation with increasing temperature was dependent on the material system and lay-up being analyzed. Once again, analysis results showed a change in the failure mode with temperature, from that of a tension failure mode at room temperature to a bearing failure mode at elevated temperatures. In Chen and Lee, their analysis model was first subject to a temperature increase while a simply-supported boundary condition was imposed on the boundary where the mechanical load, U_e, was subsequently applied.[1.33] Initial thermally induced contact loads were observed at the hole boundary with the temperature increase prior to the introduction of the mechanical load. Increasing the pin clearance resulted in a decrease in the initial thermal load as would be expected for their joint model. The bearing capacity at temperature due to mechanical loading, which they defined as the residual bearing strength, consequently was strongly degraded by the initial thermal load.

Conclusions. In the literature presented, two-dimensional finite element analyses have been used in evaluating bearing behavior. The analysis results provide insight on the effect of temperature on the bearing failure mode, which was in agreement with experimental observations on the increased likelihood of a compressive failure mode at elevated temperatures. Analysis results also confirmed the dependency of strength degradation with increasing temperature on the material and lay-up being considered.

1.2.3 Residual Stress Concentrations at Bolt Holes

During the fabrication of a composite laminate, when layers are oriented in varying fiber directions, thermal residual stresses arise due to curing the orthotropic layers at high elevated temperatures and then cooling in a bonded state. The existence of the residual thermal stresses in composite laminates leads to thermal residual stress concentrations when bolt holes (or circular cutouts) are introduced into the laminate.

Three papers were found in the literature that included thermal residual stresses at bolt holes in composite laminates in their investigations. In 1976, Rybicki and Schmueser performed a three-dimensional finite element analysis on a composite laminate containing a circular hole.[1.34] A temperature loading condition of –200°F was applied for several lay-ups of graphite/epoxy laminates. Constant material properties were assumed for their linear analysis. Both significant in-plane and tensile transverse stress results were presented at the bolt hole only. No comparison was made to the stresses that would be present in the absence of a bolt hole. A nonlinear finite element approach was used by Chang in 1990 to study the stress concentrations at cutouts in asymmetric laminates.[1.35] His two-dimensional plate analysis model included temperature-dependent material properties and accounted for nonlinear geometric effects.

Large tensile tangential stress concentrations were observed for the various lay-ups studied. Stress concentrations were also shown to increase with decreasing hole diameter. In 1986, Smith and Pascal included the contribution of thermal residual stresses in estimating the interlaminar normal stress at a bolt hole subject to a pin-bearing load.[1.36] An approximate expression for interlaminar normal stress due to bearing loads was derived based on equilibrium considerations. Their simple estimate of the total interlaminar normal stress at a bolt hole showed a significant contribution due to thermal residual stresses.

These papers identify, through analysis, the existence of thermal residual stress concentrations in the vicinity of bolt holes in composite laminates. Consequently, these residual stress concentrations may affect the bearing strength of a composite laminate. Unfortunately, to this author's knowledge, no attempt has been made to measure the residual stress concentrations at the bolt hole in a composite laminate. This lack of data is due to the inability to measure strain accurately in the vicinity of very localized large gradients.

1.2.4 Issues

Although the literature has presented reduced joint strengths at elevated temperature conditions for many polymer matrix composite material systems, the actual mechanisms attributing to the bearing strength degradation have not been well defined. Additionally, the improved bearing strength that was observed at a low temperature requires further investigation as to the nature of the strength change. A basic understanding of thermal effects in a composite joint is key to producing a structurally efficient and reliable composite joint for high and low temperature operating environments. Knowledge of the factors attributing to the variation in strength can be used to improve joint designs for extreme temperature applications.

The literature has identified the possibility of significant thermal residual stresses at bolt holes in composite laminates. Although the residual thermal stresses were shown to have a significant contribution to the interlaminar normal stress at a bolt hole subject to bearing loading in one very simplified investigation[1.36], to this author's knowledge, the contribution the thermal residual stresses have in affecting the bearing strength has not been investigated. Furthermore, the existence of thermal residual stress concentrations has not been considered in any investigation found in the literature concerning the effect of operating temperature changes on bearing strength. A detailed three-dimensional analysis on the state of residual stress due to curing and the effect of temperature change coupled with bearing loads is necessary to provide more insight on the effect of temperature on bearing strength of composites. Also, with the recent development of materials cured at higher temperatures, thermal residual stresses become more significant and consequently require consideration in evaluating both laminate and bearing strength changes with changing temperature.

1.3 Hypothesis

When a composite laminate containing a bolted joint is subject to a uniform change in temperature, ΔT, the author hypothesizes that the pin-bearing strength change, $\Delta F_{br}(\Delta T)$, is due to the combined effect of three basic changes in the joint. The three basic changes are:

1. a change, ΔS, in the state of residual thermal stress at the hole boundary in the composite laminate due to a change in temperature,
2. a change, ΔM, in the material properties of the constituent materials, and
3. a change, ΔB, in the fastener fit due to changes in the bolt hole geometry and radial expansion or contraction of the fastener.

Thus, an expression for the change in pin-bearing strength as a function of a change in temperature is proposed as

$$\Delta F_{br}(\Delta T) = f(\Delta S, \Delta M, \Delta B) \tag{1.2}$$

where ΔS, ΔM, and ΔB are all dependent on ΔT for a given joint design. The significance each change, ΔS, ΔM, and ΔB, has on influencing the bearing strength may depend on the material system and joint configuration being considered. Consequently, the expression may need to be revisited when any change in a joint design occurs to determine what the significant factors are for that particular joint.

1.4 Goal and Objectives

The goal of the research is to develop a basic understanding of thermal effects on the pin-bearing behavior of a composite laminate. By examining in detail the extent the hypothesized changes of residual stress, material properties and fastener fit have on influencing the bearing behavior, a fundamental knowledge on the nature of the bearing strength change will be achieved. This knowledge can consequently be used to design more efficient and reliable flight vehicle joints.

The objectives of this dissertation are to:

1) characterize a material system within the applicable temperature range with the detail required to model structural response accurately under thermo-mechanical loading,
2) conduct pin-bearing experiments to provide data for evaluating and developing a general pin-bearing analysis model for analysis under thermo-mechanical loads, and
3) develop computational models with adequate detail to study the significance the hypothesized changes have in influencing the state of stress and consequently bearing behavior for the pin-bearing configuration.

1.5 Scope

The composite material system characterization is described in Chapter 2. The analysis of the composite laminate to establish laminate attributes necessary

in the pin-bearing finite element analyses is presented in Chapter 3. The pin-bearing test program for validation of the computational models is described in Chapter 4. The computational models for investigating thermal effects on stress concentrations at bolt holes, fastener fit, and the state of stress under pin-bearing loading are described in Chapter 5. Finally, the completed research is discussed and conclusions are made in Chapter 6.

1.6 References

1.1 Ramkumar, R.L., Saether, E.S., and Cheng, D.: Design Guide for Bolted Joints in Composite Structures. AFWAL-TR-86-3035, March 1986.

1.2 Williams, Louis J.: HSCT Research Gathers Speed. *Aerospace America*, April 1995, pp. 32-37.

1.3 Sawyer, J.: Graphite-Composite Primary Structure for Reusable Launch Vehicles, 1996 AIAA Space Programs and Technologies Conference, September 24-26, Huntsville, AL, AIAA-96-4268, 1996.

1.4 Stanley, D. O. and Piland, W.M.: Technology Requirements for Affordable Single-Stage Rocket Launch Vehicles, 44th Congress of the International Astronautical Federation, October 16-22, 1993, Graz, Austria, IAF 93-V.4.627, 1993.

1.5 MIL-HDBK-17, Military Handbook, Polymer Matrix Composites, Vol. 1. Guidelines, U.S. Dept. of Defense, 1994.

1.6 Kim, R.Y. and Whitney, J.M.: Effect of Temperature and Moisture on Pin Bearing Strength of Composite Laminates. *J. Composite Materials*, Vol. 10, April 1976, pp. 149-155.

1.7 Wilkins, D.J.: Enviromental Sensitivity Tests of Graphite-Epoxy Bolt Bearing Properties. Composite Materials: Testing and Design (Fourth Conference), ASTM STP 617, American Society for Testing and Materials, 1977, pp. 497-513.

1.8 Wilson, D.W. and Pipes, R.B.: Behavior of Composite Bolted Joints at Elevated Temperature. NASA CR-159137, Septermber 1979.

1.9 Perry, J.C. and Hyer, M.W.: Investigations into the Mechanical Behavior of Composite Bolted Joints. NASA CR-163295, June 1979.

1.10 Wichorek, G.R.: Preliminary Bolted Joint Data. In Graphite/Polimide Composites, NASA Conference Publication 2079, 1979, pp. 249-258.

1.11 Wichorek, G.R.:Experimental Data on Single-Bolt Joints in Quasi-Isotropic Graphite/Polyimide Laminates, NASA TP-2015, May 1982.

1.12 Kong, S.J.: Bolt Bearing Strengths of Graphite /Epoxy Laminates. AIAA/ASME/ASCE/AHS 22nd Structures, Structural Dynamics and Materials Conference, April 6-8, 1981, Atlanta, Georgia, AIAA Paper 81-0544, pp. 158-165.

1.13 Ramkumar, R.L. and Tossavainen, E.W: Bolted Joints in Composite Structures: Design, Analysis and Verification, Task 1 Test Results-Single Fastener Joints, AFWAL-TR-84-3047, August 1984.

1.14 Ramkumar, R.L. and Tossavainen, E.W.: Strenght and Lifetime of Bolted Joints. Fatigue in Mechanically Fastened Composite and Metallic Joints, ASTM STP 927, John M. Potter, Ed., American Society for Testing and Materials, Philadelphia, 1986, pp. 251-273.

1.15 Morgan, M.E. and Beckwith, S.W.: Bolt Torque Loading and Radial Gap Effects on Thick-Wall Composite Joint Strenght. Proceedings of 30th National SAMPLE Symposium, Anaheim, Ca, March 19-21, 1985, Vol. 30, pp.1321-1334.

1.16 Gerharz, J.J. and Huth, H.: Effect of Enviroment and Improvement Mearsures on Static and Fatigue Strenght of Bolted CRFP-Joints. AGARD-CP-427, March 1988, pp. 19.

1.17 Liu, D., Yi-Bing, L., and Bing-Zhang, Y.: Damage Detection and Damage Mechanisms Analyses in CFRP Laminate Bolted Joints. Composite Structures 5; Proceedings of the Fifth International Conference, Paisley, Scotland, July 24-26, 1989. Elsevier Applied Science, London and New York, 1989, pp. 591-601.

1.18 Kaji, A. and Hamada, H.: Influence of Test Temerature on the Strenght and Fracture Mode of Bolted-joint of Mat-FRP. *Japan Society of Materials Science, Journal* (ISSN 0514-5163), vol.33, July 1984, pp. 876-881. In Japanese, with abstract in English.

1.19 Nekrasov, Y.A., Nikolaev, V.P., and Stepanychev, E.I.: Bolted joints of Heavily-Loaded Structural Elements Made of Composites with a Polymer Matrix. *Mechanics of Composite Materials*, Vol.24 No.6, May 1989, pp. 827-831.

1.20 Garbo, S.P. and Ogonowski, J.M.: Effect of Variances and Manufacturing Tolerances on the Design Strength and Life of Mechanically Fastenened Composite Joints. AFWAL-TR-81-3041, Vol.1, April 1981.

1.21 Bailie, J.A.,Duggan,M.F.,Bradshaw,N.C.,and McKenzie,T.G.: Design Data for Graphite Cloth Epoxy Bolted Joints at Temperatures up to 450K. *Joining of Composite Materials*, ASTM STP 749,1981, pp.165-180.

1.22 Bailie, J.A.; Fisher, L.M.; Howard, S.A.; and Perry, K.G.: Some enviromental and geometric effects on the static strenght of graphite cloth epoxy bolted joints. Composite Structures; Proceedings of the First International Conference, Pailsey, Scotland, September 16-18, 1981. London, Applied Science Publishers, 1981, pp. 63-78

1.23 Hart-Smith, L.J.: Bolted Joints in Graphite Epoxy Composites. NASA CR-144899, June 1976.

1.24 Hart-Smith, L.J.: Mechanically-Fastenened Joints for Advanced Composites - Phenomenological Considerations and Simple Analyses. Proceedings of the Fourth Conference on Fiberous Composites in Structural Design, November 14-17, 1978, pp. 543-574.

1.25 Maekawa, Z., Kaji, A., Hamada, H., and Nagamori, M.: Failure Mode and Strenght Predictions of Mechanically Fastened Composite Joints. Proceedings of the Fifth International Conference on Composite Materials, The Metallurgical Society, July 29- August 1, 1985, pp.99-109.

1.26 Stockdale, J.H. and Mathews, F.L.: The effect of clamp-up pressure on bolt bearing loads in glass fibre-reinforced plastics. *Composites*, Vol.7, January 1976, pp.34-38.

1.27 Collings, T.A., On the Bearing Strenghts of CFRP Laminates, *Composites*, July 1982, pp. 241-252.

1.28 Smith, P.A., Ashby, M.F., and Pascoe, K.J.: Modelling Clamp-up Effects in Composite Bolted Joints. *Journal of Composite Materials*, Vol. 21, October 1987, pp. 879-897.

1.29 Wu, P.S. and Sun, C.T.: Bearing Failure in Pin Contact of Composite Laminates. Proceedings of the 38th AIAA/ASME/ASCE/AHS/ASC Structures, Structural Dynamics, and Materials Conference and Exhibit, April 7-10, 1997/Kissimmee, FL. Pt. 4, pp.1974-1983.

1.30 Horn, W.J. and Schmitt, R.R.: Influence of Clamp-up Force on the Strenght of Bolted Composite Joints. AIAA Journal, Vol.32 No. 3, March 1994, pp. 665-667.

1.31 Wright, R.J., Johnson, W.S., and Ahmad, H.: Bolt Bearing Behavior of Highly Loaded Composite Joints at Elevated Temperatures with and

without Clampup. Department of Material Science and Engineering, Georgia Institute of Technology, Atlanta, Georgia,1997.

1.32 Chen, W.H. and Lee, Y.J.: Failure Process and pin-bearing strength of laminated composites at elevated temperautre. *Journal of Reinforced Plastics and Composites*, Vol. 11, No. 7, July 1992, pp.743-771.

1.33 Chen, W. H. and Lee, Y. J.: Effect of Temperature on the Contact Stresses and Residual Bearing Strenght of Pin-Loaded Composite Laminates. *Journal of Thermal Stresses*, Vol. 15, Issue 3, September 1, 1992, pp. 419-437.

1.34 Rybicki, E.F. and Schmueser, D.W.: Three-dimensional Finite Element Stress Analysis of Laminated Plates Containing a Circular Hole. Technical Report AFML-TR-76-92, August 1976.

1.35 Chang, H.T.: Curing Stress Concentration on Advanced Composite Materials, 22nd International Sample Technical Conference, Vol.22 , November 6-8, 1990, pp. 733-746.

1.36 Smith, P.A. and Pascoe, K.J.: The Effect of Stacking Sequence on the Bearing Strengths of Quasi-isotropic Composite Laminates. *Composite Structures*, Vol. 6, Issue 1-3, 1986, pp. 1-20.

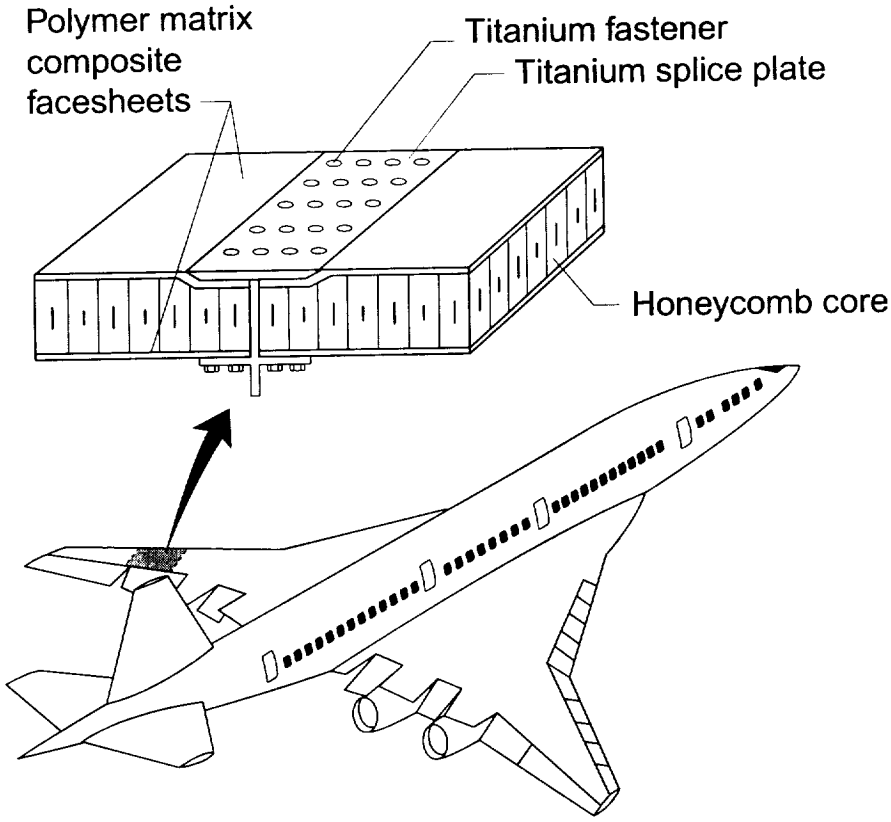

Figure 1.1. A mechanically fastened composite joint concept as a component in an aircraft wing.

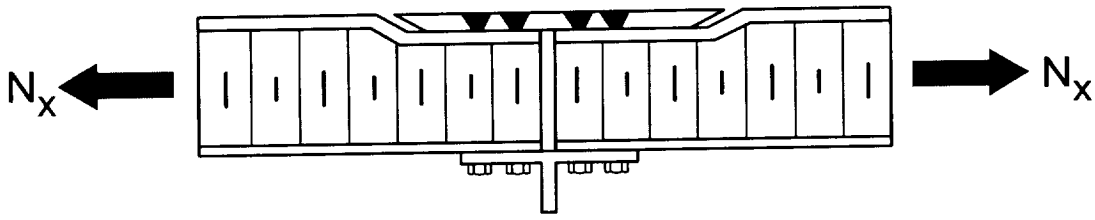

Figure 1.2. A composite wing panel splice joint concept subject to tensile axial loading.

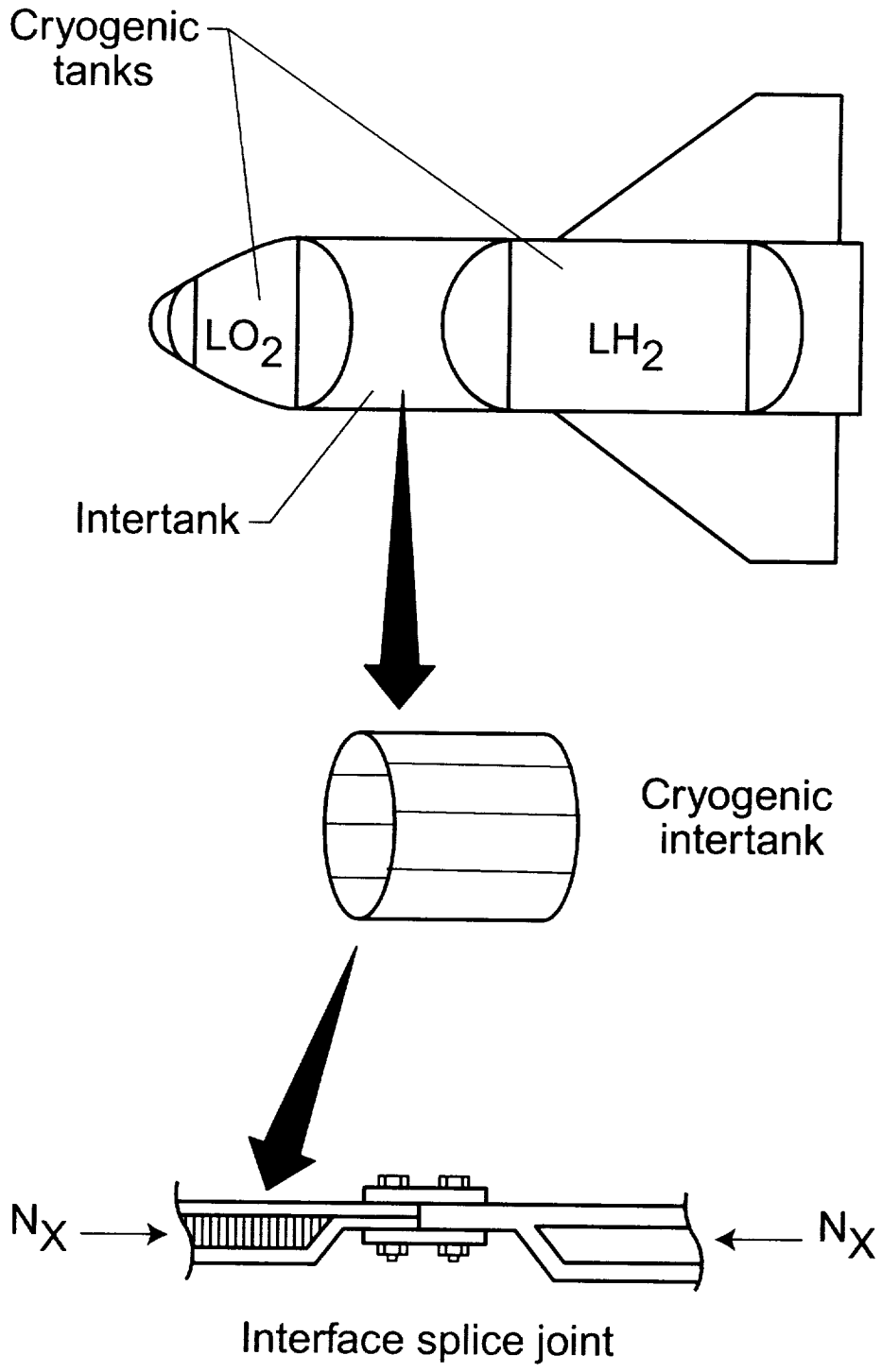

Figure 1.3. A mechanically fastened composite joint concept as a component in a reusable launch vehicles cryogenic intertank structure.

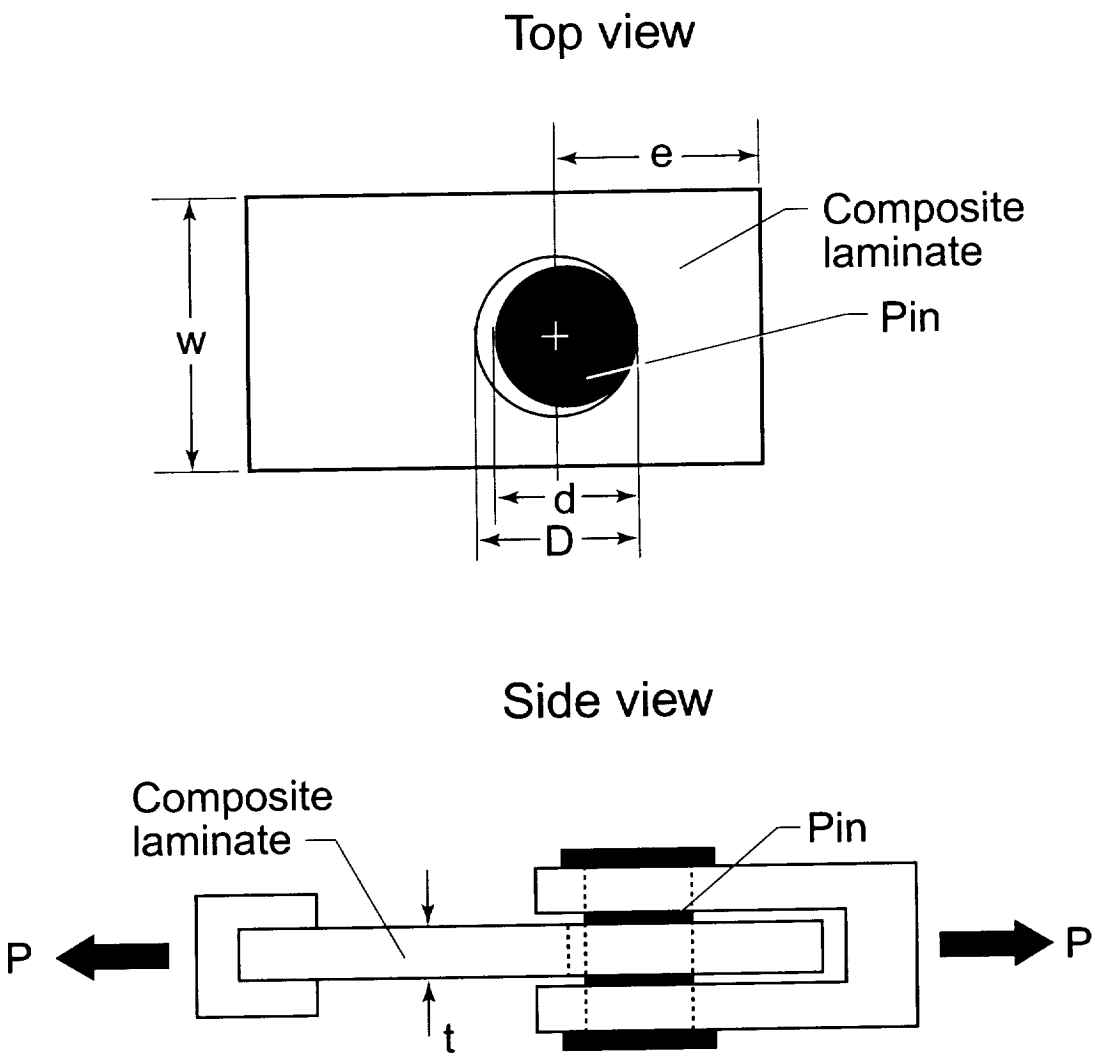

Figure 1.4. Pin-bearing tension test configuration.

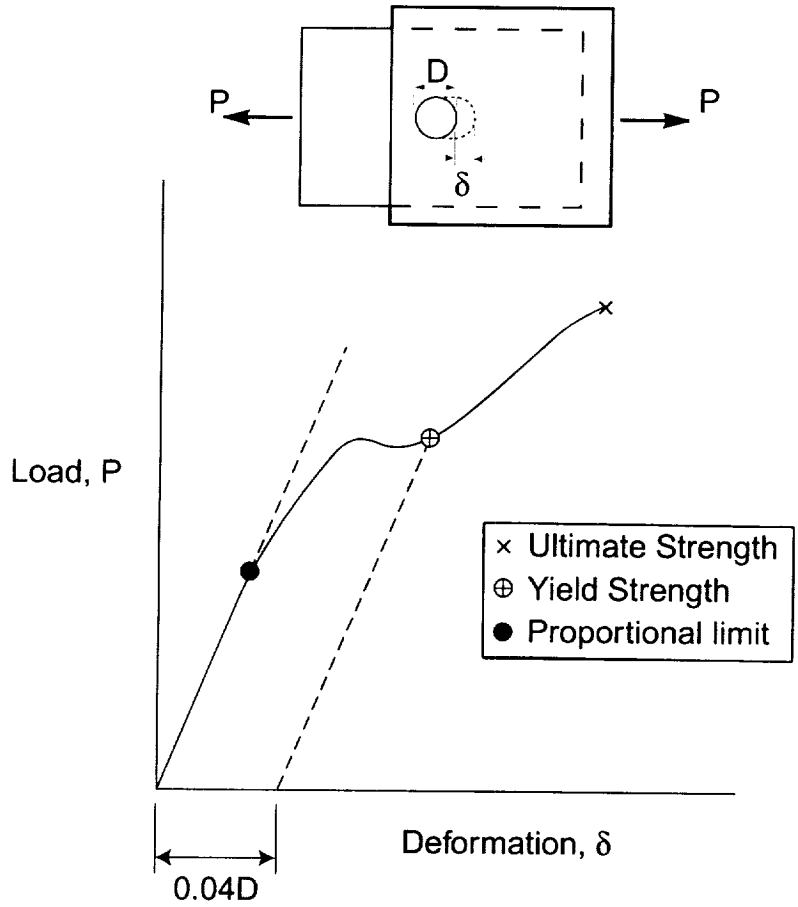

Figure 1.5. Typical load-displacement curve for a bearing test.

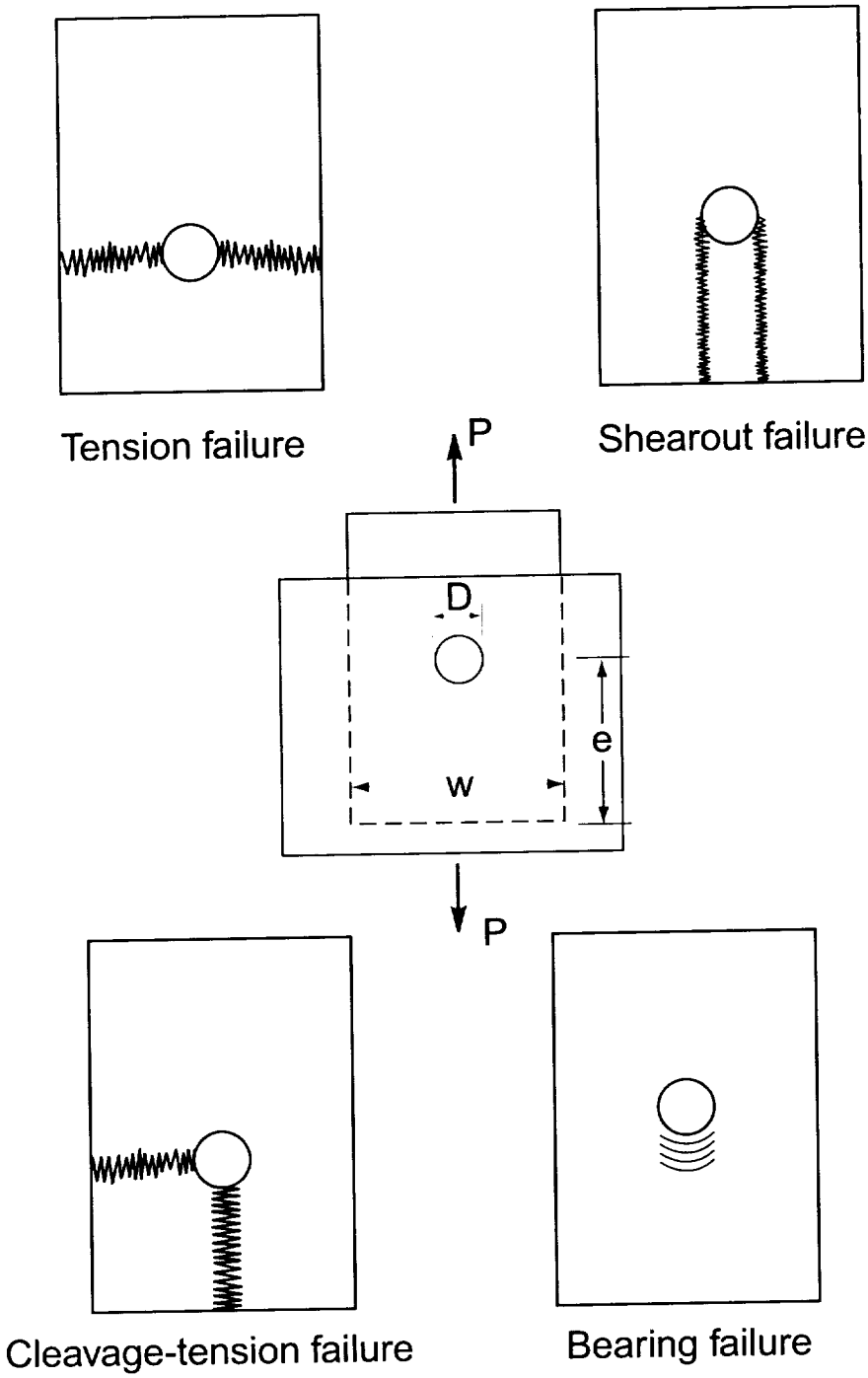

Figure 1.6. Four possible composite laminate failure modes associated with bolted joints.

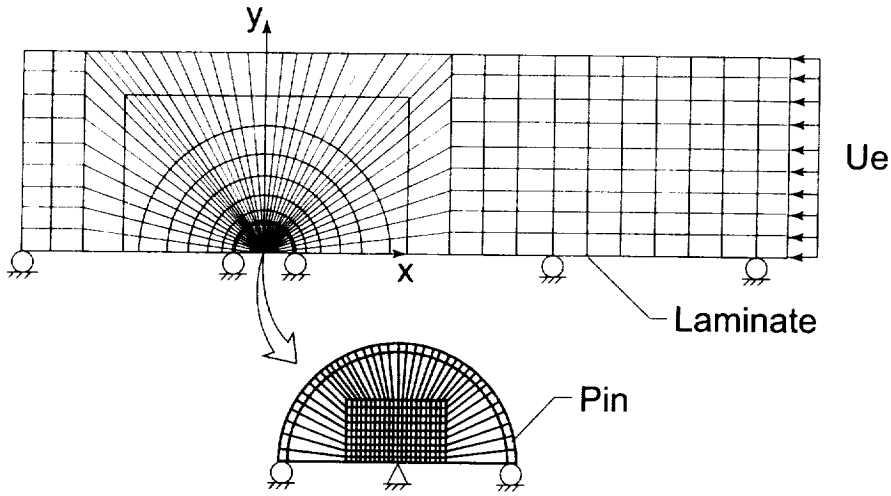

Figure 1.7. Two-dimensional finite element model of plate and pin, Ref. 1.33.

Chapter 2
Material System Characterization

In this chapter, a composite laminate is first described, followed by a description of the IM7/PETI5 material system being utilized for this study. The material properties for characterization of the material system are defined, which includes the temperature-dependent lamina properties, the nonlinear stress-strain behavior of the lamina, and finally the laminate strength properties.

2.1 Composite Laminate Description

A polymer matrix composite (PMC) laminate is composed of layers referred to as lamina. Each lamina consists of high strength fibers embedded in a lightweight polymer matrix resin material as illustrated in Figure 2.1. Also shown in the figure are the principal material directions. The 1-direction is parallel to the unidirectional fibers, and is also considered the fiber direction, since the properties in the 1-direction are dominated by the high strength fibers. The 2-direction is considered the matrix direction and is perpendicular to the fiber direction and in-plane to the lamina. The 3-direction is also perpendicular to the fiber and is out-of-plane to the lamina. The lamina material is subsequently used to construct laminates, where the layers of lamina are stacked in a lay-up with various orientations of the principal material directions. The direction of the layers and the stacking sequence are chosen to tailor the mechanical properties of the composite laminate. An example of an 8-ply laminate with a $(+45, -45,0,90)_s$ lay-up, where the subscript s denotes symmetric about the mid-plane z=0, is illustrated in Figure 2.2. Only the top half, or the top four plies, of the 8-ply laminate is shown in the figure. The laminate x, y, and z coordinate system is shown in the figure along with the orientations of the top four layers. Once stacked, the lay-up is cured in an autoclave at elevated temperatures and pressures to form a permanent bond between layers.

2.2 IM7/PETI5 Material System

The composite material being utilized for this study is a high strength PMC material designated IM7/PETI5 [2.1]. The material consists of IM7 graphite fibers with a PETI5 polyimide matrix material. A 100 lb batch of the lamina material in prepreg tape form was purchased from Cytec Fiberite for the study.

The IM7/PETI5 material system was chosen since the system offers potential for use in high-speed aircraft structural applications up to temperatures of 350°F. Additionally, IM7/PETI5 laminates are cured at 700°F, a temperature much greater then the approximately 300°F temperature used to cure most graphite/epoxy laminates. Due to the large temperature change in processing the laminates, there is potential for significant thermal residual stresses due to curing to be present in the laminates at their operating temperatures. The magnitude of the thermal cure stresses in IM7/PETI5 laminates has not been previously investigated and is consequently being investigated here to provide the necessary input to evaluating their effect on bearing behavior.

2.3 IM7/PETI5 Material Properties

Due to the lack of all necessary property data and the need for accurate material properties for the computational study, relevant material property data has been determined from the current batch of IM7/PETI5 prepreg. Both lamina properties and properties for the laminates of interest for the bearing study have been measured. The lamina properties are used in the analysis models for predicting the state of stress in the composite laminate. To aid in the development of the computational models, the laminate strength properties were measured for qualitative comparisons between lamina and laminate strength. Details on the property tests conducted herein are given in the Appendix.

2.3.1 Lamina Properties

The temperature-dependent orthotropic lamina properties obtained from testing in the IM7/PETI5 material are given in Table 2.1. The properties are given at the three operating temperatures of –200°F, 70°F, and 350°F and an upper bound temperature of 495°F. Since the variation in E_{11c} obtained from the tests at the different temperatures was negligible, the average E_{11c} from all test temperatures is presented in the table and it is concluded that E_{11c} is independent of temperature. For characterization of the material for non-linear analysis purposes including temperature dependent properties, the properties are assumed to vary with temperature piecewise linearly between the four given temperature values. The glass transition temperature, T_g, of the material was measured to be T_g = 460°F, after the properties were already determined up to 495°F.

For predicting residual cure stresses in the laminates under investigation in this dissertation, the T_g is assumed to be the stress free temperature(SFT) below which thermal curing stresses develop in the laminates. The choice of the T_g as the SFT is in accord with previous investigations on curing stresses in graphite/epoxy laminates, where a SFT of 350°F, the typical T_g of graphite/epoxy, was chosen.[2.2, 2.3] Therefore material stiffness and coefficient of thermal expansion properties are only utilized up to the T_g of 460°F, for predicting residual cure stresses in the laminates of interest.

The additional out-of-plane properties needed for a three-dimensional characterization of the composite material include E_{33}, G_{31}, G_{23}, ν_{31}, and α_3. These properties are assumed related to the in-plane properties as follows,

$$E_{33} = E_{22} \tag{2.1}$$

$$G_{31} = G_{12} \tag{2.2}$$

$$G_{23} = \frac{E_{22}}{2(1+\nu_{23})} \tag{2.3}$$

$$\nu_{31} = \frac{E_{22}}{E_{11}}\nu_{12} \quad \text{where} \quad \nu_{13} = \nu_{12} \tag{2.4}$$

$$\alpha_3 = \alpha_2 \tag{2.5}$$

and are determined from the values given in Table 2.1.

The properties of the resin rich layer between lamina, which will be discussed later in Chapter 3, are assumed to resemble the matrix direction properties of the IM7/PETI5 material, which are dominated by the PETI5 properties. The PETI5 resin layer is hence assumed to be an isotropic material with the following two independent properties,

$$E_r = E_{22} \tag{2.6}$$

$$\nu_r = 0.4 \tag{2.7}$$

where for isotropic materials,

$$G_r = \frac{E_r}{2(1+\nu_r)} \tag{2.8}$$

The simplifying assumption of constant material properties allows for a linear static analysis to be performed. When the assumption of constant properties is used to determine the stresses at a particular operating temperature within this dissertation, the properties at the operating temperatures given in Table 2.1 are all used along with the properties determined above at the operating temperature of interest.

2.3.2 Non-linear Stress-Strain Behavior

The moduli presented in Table 2.1 have been determined as a constant from a linear approximation of the slope of the stress-strain curve in accord with the procedures of the ASTM standard (see Appendix). However, the test data revealed that at all test temperature, G_{12}, and at the test temperature of 495°F and 350°F, E_{22c}, were not constant and alternatively were a function of strain. Using fourth order polynomial curve fitting of the actual stress-strain test data from the replicate specimens, an average curve was computed for evaluation. The average stress-strain curves derived from the tests conducted to determine G_{12} and E_{22c} are plotted in Figures 2.3 and 2.4, respectively. The tangent moduli computed from these curves at specific values of strain are presented in Table 2.2 and Table 2.3. Furthermore, the properties E_{33}, G_{23}, G_{31}, ν_{31}, E_r and G_r, being directly related to either G_{12} or E_{22} through Equations 2.1-2.7, are also strain dependent. Tables 2.2 and 2.3 along with Equations 2.1-2.7 characterize the material's nonlinear stress-strain behavior. The same characterization is assumed for both positive and negative values of shear strain.

As can be observed from Figures 2.3 and 2.4, the most significant nonlinear behavior is seen at the upper bound temperature of 495°F and at only relatively large stresses at the other temperatures. Since during curing, the magnitude of stress is assumed to increases from zero at the stress-free temperature of 460°F, and since the nonlinear stress-strain behavior dominates at only large stresses and high temperatures, no analyses with nonlinear stress-strain properties will be pursued in the context of this dissertation. Additional justification on the neglect of nonlinear material behavior will be discussed later in Chapter 3, in light of the analysis results. All finite element analyses within the context of the dissertation will assume linear elastic material properties.

2.3.3 Laminate Strength Properties

The measured laminate compressive strength, F_{xxc}, of the particular laminates of interest is presented in Table 2.4. The lay-ups of the laminates correspond to the lay-ups that will be evaluated in the bearing study. The compressive strength data will be used for qualitative comparisons with analysis result.

2.4 References

2.1 Hou, T.H., Jensen, B.J., and Hergenrother, P.M.: Processing and Properties of IM7/PETI Composites, *Journal of Composite Materials*, vol. 30, no. 1, pp.109-122, January 1996.

2.2 Chang, H.T.: Nonlinear Curing Analysis For Advanced Composite Materials. 35th International SAMPE Symposium, April 2-5, 1990, pp. 604-615.

2.3 Griffin, O.H.: Three-Dimensional Curing Stresses in Symmetric Cross-Ply Laminates with Temperature-Dependent Properties. Journal of Composite Materials, Vol. 17-September 1983, pp. 449-463.

Table 2.1 Experimental Data-Lamina Properties.

Material Property	Test Temperature (F)			
	-200	70	350	495
E_{11C}(Msi)	20.4	20.4	20.4	20.4
F_{11C} (ksi)	238.	225.	185.	
E_{11T}(Msi)	21.9*	21.9	22.9	25.8
F_{11T} *(ksi)*	336.	307.	307.	
E_{22C} *(Msi)*	2.	2.2	1.5	1.2
F_{22C}*(ksi)*	47.	37.	26.8	
E_{22T} *(Msi)*	1.6	1.4	.97	.6
F_{22T} *(ksi)*	6.6	9.	7.3	
G_{12}*(Msi)*	1.04	.92	.69	.62
F_{12}*(ksi)*	17.8	14.6	6.6	
ν_{12}	.34*	.34	.33	.34
ν_{23}	.4	.64	.52	.42
F_{1Z}(ksi) - ILSS	21.3	17.3	12.	
F_{ZZ}(ksi) - ILNS	5.2	4.5	2.7	
α_1(μin/in/F)	-.24	-.09	.9	.83+
α_2(μin/in/F)	10.1	15.5	16.7	17.3+

* data unavailable, extrapolated from closest value

\+ value given is at 460°F (α changed from value given to 0. at T=460°F)

Table 2.2 Nonlinear Stress-Strain Characterization for $G_{12}(\varepsilon,T)$.

Strain (in/in)	Temperature (°F)			
	-200	70	350	495
0.	.94	.96	.74	.82
.001	.97	.92	.67	.64
.002	1.22	.88	.60	.48
.003	1.15	.84	.54	.37
.004	1.1	.80	.49	.27
.005	1.07	.75	.44	.23
.007	1.01	.66	.35	.18
.01	.95	.53	.26	.12
.015	.85	.37	.16	.12

Table 2.3 Nonlinear Stress-Strain Characterization for E_{22} (ε,T).

Strain (in/in)	Temperature (°F)			
	-200	70	350	495
0.	2.	2.2	1.47	1.25
-.001	2.	2.2	1.48	1.25
-.002	2.	2.2	1.48	1.24
-.003	2.	2.2	1.48	1.22
-.004	2.	2.2	1.47	1.19
-.005	2.	2.2	1.45	1.16
-.007	2.	2.2	1.40	1.12
-.01	2.	2.2	1.30	0.95
-.015	2.	2.2	1.13	0.80

Table 2.4 Experimental Data – Laminate Compressive Strength Properties.

LAY-UP	Test Temperature (^{O}F)	Laminate Strength F_{xxc} (ksi)
1 $(90,0)_{8s}$	-200	144.
	70	126.
	350	95.
3 $(+45,-45,0,90)_{4s}$	-200	118.
	70	105.
	350	76.
4 $(+45,0,-45,90)_{4s}$	-200	115.
	70	93.
	350	69.
5 $(+45,0_2,-45,0_2,+45,0_2,-45,0_2,+45,90_2,-45)_s$	-200	144.
	70	126.
	350	79.

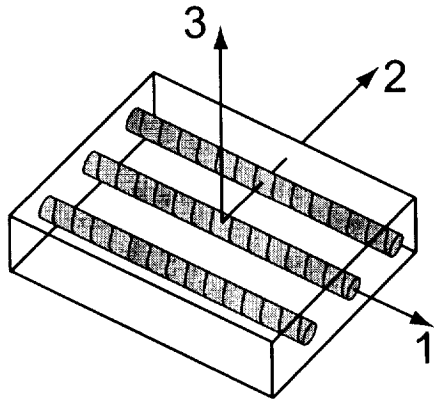

Figure 2.1. Unidirectional fiber reinforced lamina.

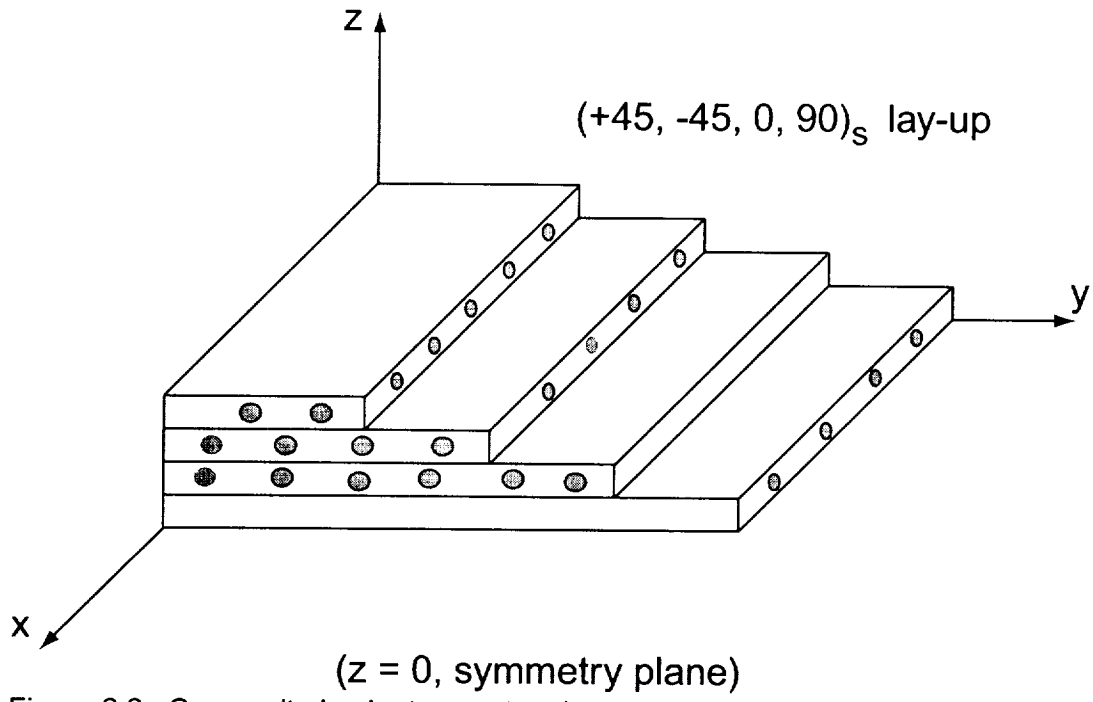

Figure 2.2. Composite laminate construction.

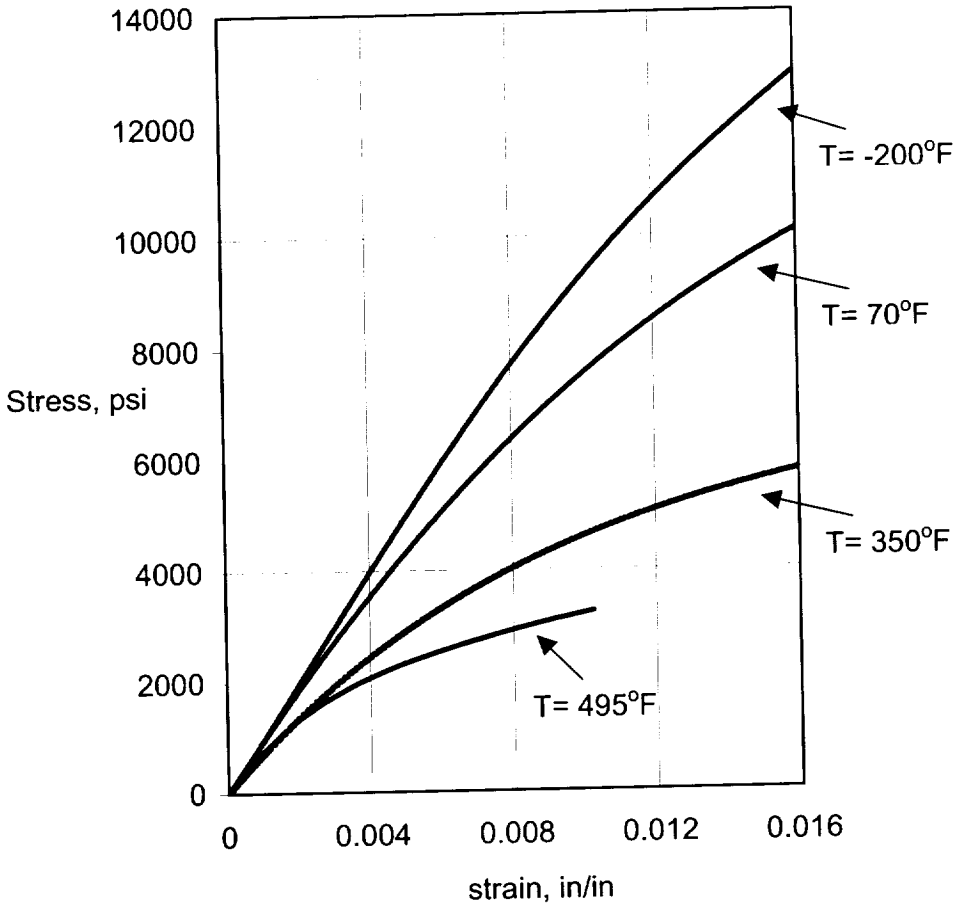

Figure 2.3. Nonlinear Stress-Strain curves for in-plane shear modulus, G_{12}.

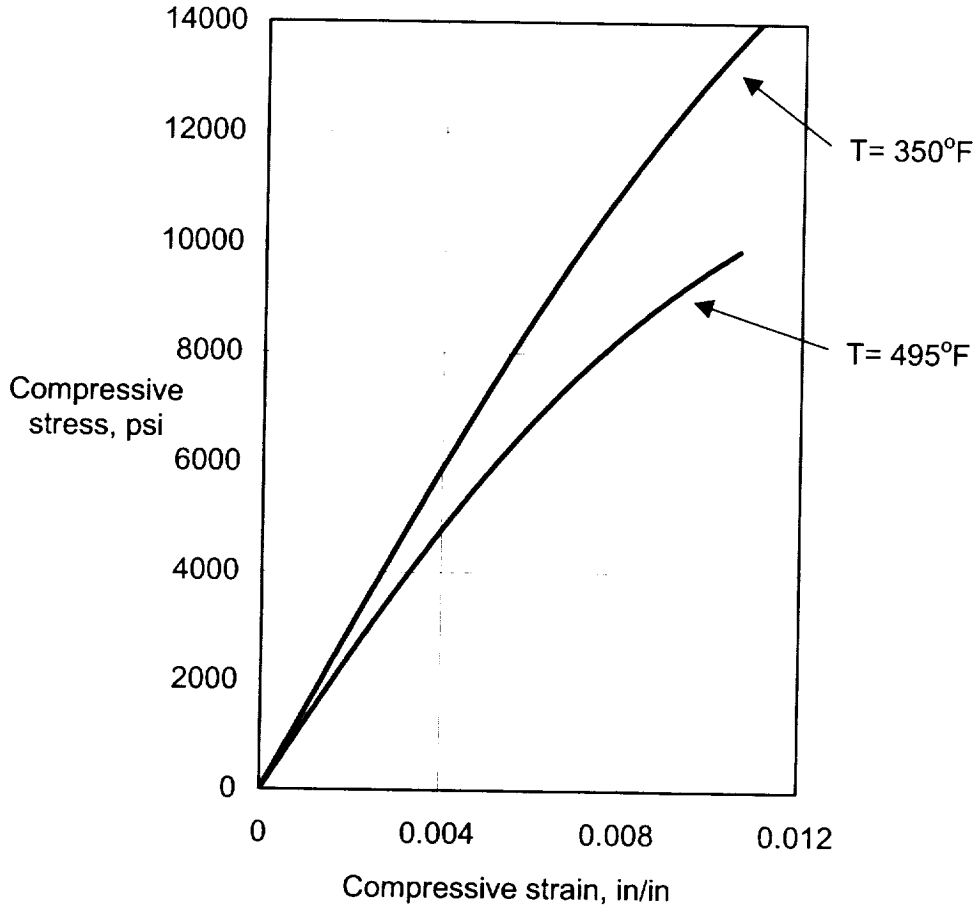

Figure 2.4. Nonlinear Stress-Strain curves for compressive matrix direction modulus, E_{22c}.

Chapter 3
Analysis of Composite Laminates

An understanding of the structural behavior of the unnotched composite laminate is essential to investigate pin-bearing behavior. The details required in the model of a composite laminate to predict behavior accurately need to be incorporated in the pin-bearing model to understand the bearing response.

In the following sections, the stresses in composite laminates, as pertains to this dissertation, are derived using classical lamination theory. The concepts of interlaminar stresses and residual thermal curing stresses follow. A verification model is then presented followed by the details of the three-dimensional analysis model development of an IM7/PETI5 composite laminate.

3.1 Classical Lamination Theory

Using the lamina orthotropic material properties, laminate behavior can be predicted using Classical Lamination Theory (CLT) and existing failure theories.[3.1] CLT assumes the lamina to be in a state of plane stress where the out of plane stresses, σ_3, τ_{13} and τ_{23}, are assumed to be zero. For an orthotropic lamina, the thermoelastic stress-strain relations in principal material coordinates are

$$\begin{Bmatrix}\sigma_1\\ \sigma_2\\ \tau_{12}\end{Bmatrix}=\begin{bmatrix}Q_{11} & Q_{12} & 0\\ Q_{12} & Q_{22} & 0\\ 0 & 0 & Q_{66}\end{bmatrix}\begin{Bmatrix}\varepsilon_1-\alpha_1\Delta T\\ \varepsilon_2-\alpha_2\Delta T\\ \gamma_{12}\end{Bmatrix} \tag{3.1}$$

or, equivalently, $$\{\sigma\}_{12}=[Q]\left(\{\varepsilon\}_{12}-\{\alpha\}_{12}\Delta T\right)$$

where the Q_{ij}'s are the reduced stiffnesses for the plane stress state. In terms of the engineering constants,

$$Q_{11}=\frac{E_{11}}{1-\nu_{12}\nu_{21}} \qquad Q_{22}=\frac{E_{22}}{1-\nu_{12}\nu_{21}}$$

$$Q_{12}=\frac{\nu_{12}E_{22}}{1-\nu_{12}\nu_{21}} \qquad Q_{66}=G_{12} \tag{3. 2}$$

Figure 3.1 illustrates the transformation between the material and laminate coordinate systems. The transformation matrix, [T] is written as

$$[T]=\begin{bmatrix}\cos^2\theta & \sin^2\theta & 2\sin\theta\cos\theta\\ \sin^2\theta & \cos^2\theta & -2\sin\theta\cos\theta\\ -\sin\theta\cos\theta & \sin\theta\cos\theta & \cos^2\theta-\sin^2\theta\end{bmatrix} \tag{3.3}$$

When relation (3.1) is transformed into the laminate coordinate system, the lamima stresses in the *kth* ply of the laminate are

$$\begin{Bmatrix}\sigma_x\\ \sigma_y\\ \tau_{xy}\end{Bmatrix}^k = \begin{bmatrix}\overline{Q_{11}} & \overline{Q_{12}} & \overline{Q_{16}}\\ \overline{Q_{12}} & \overline{Q_{22}} & \overline{Q_{26}}\\ \overline{Q_{16}} & \overline{Q_{26}} & \overline{Q_{66}}\end{bmatrix}^k \begin{Bmatrix}\varepsilon_x - \alpha_x \Delta T\\ \varepsilon_y - \alpha_y \Delta T\\ \gamma_{xy} - \alpha_{xy} \Delta T\end{Bmatrix}^k \tag{3.4}$$

or, equivalently, $\{\sigma\}^k = [\overline{Q}]^k (\{\varepsilon\}^k - \{\alpha\}^k_{xy} \Delta T)$

where $[\overline{Q}]$ is the transformed reduced stiffness matrix and is related to $[Q]$ by

$$[\overline{Q}] = [T]^{-1}[Q][T]^{-T} \tag{3.5}$$

and

$$\{\alpha\}^k_{xy} = [T]^T \{\alpha\}^k_{12} \tag{3.6}$$

CLT assumes that the laminate is thin and adopts the Kirchoff-Love hypothesis for plates by assuming that: 1) a normal to the middle surface of the laminate remains straight and normal which is equivalent to ignoring transverse shearing strains, $\gamma_{xz} = \gamma_{yz} = 0$ and 2) that normals have constant length, $\varepsilon_z = 0$. The remaining strains, as derived by Jones[3.1], can be expressed

$$\begin{Bmatrix}\varepsilon_x\\ \varepsilon_y\\ \gamma_{xy}\end{Bmatrix} = \begin{Bmatrix}\varepsilon^o_x\\ \varepsilon^o_y\\ \gamma^o_{xy}\end{Bmatrix} + z\begin{Bmatrix}\kappa_x\\ \kappa_y\\ \kappa_{xy}\end{Bmatrix}$$

or, equivalently, $\{\varepsilon\} = \{\varepsilon^o\} + z\{\kappa\}$ (3.7)

where $\{\varepsilon^o\}$ are the middle-surface strains and $\{\kappa\}$ are the middle-surface curvatures. When equation (3.7) is substituted in equation (3. 4), the stresses in the kth layer can be expressed in terms of the laminate middle-surface strains and curvatures as

$$\begin{Bmatrix}\sigma_x\\ \sigma_y\\ \tau_{xy}\end{Bmatrix}^k = \begin{bmatrix}\overline{Q_{11}} & \overline{Q_{12}} & \overline{Q_{16}}\\ \overline{Q_{12}} & \overline{Q_{22}} & \overline{Q_{26}}\\ \overline{Q_{16}} & \overline{Q_{26}} & \overline{Q_{66}}\end{bmatrix}^k \left[\begin{Bmatrix}\varepsilon^o_x\\ \varepsilon^o_y\\ \gamma^o_{xy}\end{Bmatrix} + z\begin{Bmatrix}\kappa_x\\ \kappa_y\\ \kappa_{xy}\end{Bmatrix}\right] - \begin{bmatrix}\overline{Q_{11}} & \overline{Q_{12}} & \overline{Q_{16}}\\ \overline{Q_{12}} & \overline{Q_{22}} & \overline{Q_{26}}\\ \overline{Q_{16}} & \overline{Q_{26}} & \overline{Q_{66}}\end{bmatrix}^k \begin{Bmatrix}\alpha_x\\ \alpha_y\\ \alpha_{xy}\end{Bmatrix}^k \Delta T$$

or, equivalently, $\{\sigma\}^k = [\overline{Q}]^k \{\varepsilon^o\} + [\overline{Q}]^k \{\kappa\}\, z - [\overline{Q}]^k \{\alpha\}^k \Delta T$ (3.8)

where ΔT is the change in temperature from the stress free temperature, T_{SFT}, to the operature temperature, T, which can be expressed,

$$\Delta T = T - T_{SFT} \tag{3.9}$$

Within the scope of this dissertation, only flat, symmetric composite laminates with a uniform temperature are considered, and all applied forces are in-plane as illustrated in Figure 3.2. The geometry through the laminate thickness is displayed in Figure 3.3. The resultant forces, $\{N\}$, acting on a laminate are obtained by integrating the stresses through the laminate thickness, t, and are defined as

$$\{N\} = \begin{Bmatrix} N_x \\ N_y \\ N_{xy} \end{Bmatrix} = \int_{\frac{-t}{2}}^{\frac{t}{2}} \begin{Bmatrix} \sigma_x \\ \sigma_y \\ \tau_{xy} \end{Bmatrix} dz = \sum_{k=1}^{N} \int_{z_{k-1}}^{z_k} \begin{Bmatrix} \sigma_x \\ \sigma_y \\ \tau_{xy} \end{Bmatrix} dz \tag{3.10}$$

Equation (3.8) can be substituted in equation (3.10), and assuming the lamina stiffnesses to be constant within a lamina, in addition to a uniform temperature throughout the laminate, the relationship can be expressed as

$$\{N\} = [A]\{\varepsilon\} + [B]\{\kappa\} - \{N\}^T \tag{3.11}$$

where

$$[A] = \sum_{k=1}^{N} [\overline{Q}]^k (z_k - z_{k-1}) \tag{3.12}$$

$$[B] = \sum_{k=1}^{N} [\overline{Q}]^k (z_k^2 - z_{k-1}^2) \tag{3.13}$$

$$\{N\}^T = \sum_{k=1}^{N} [\overline{Q}]^k \{\alpha\}^k (z_k - z_{k-1}) \Delta T \tag{3.14}$$

and $[A]$ is referred to as the laminate extensional stiffness, $[B]$ is the laminate bending-extension coupling stiffness, and $\{N\}^T$ are the thermal forces. For symmetric laminates, $[B]$ = 0, and inserting equation (3.14), equation (3.11) becomes

$$\begin{Bmatrix} N_x \\ N_y \\ N_{xy} \end{Bmatrix} = \begin{bmatrix} A_{11} & A_{12} & A_{16} \\ A_{12} & A_{22} & A_{26} \\ A_{16} & A_{26} & A_{66} \end{bmatrix} \begin{Bmatrix} \varepsilon_x^o \\ \varepsilon_y^o \\ \tau_{xy}^o \end{Bmatrix} - \sum_{k=1}^{N} \begin{bmatrix} \overline{Q_{11}} & \overline{Q_{12}} & \overline{Q_{16}} \\ \overline{Q_{12}} & \overline{Q_{22}} & \overline{Q_{26}} \\ \overline{Q_{16}} & \overline{Q_{26}} & \overline{Q_{66}} \end{bmatrix}^k \begin{Bmatrix} \alpha_x \\ \alpha_y \\ \alpha_{xy} \end{Bmatrix}^k (z_k - z_{k-1}) \Delta T$$

or, equivalently,

$$\{N\} = [A]\{\varepsilon^o\} - \sum_{k=1}^{N} [\overline{Q}]^k \{\alpha\}^k (z_k - z_{k-1}) \Delta T \tag{3.15}$$

Equation (3.15) can be solved for the middle-surface strains, which can be expressed

$$\{\varepsilon^o\} = [A]^{-1}\{N\} + \{\overline{\alpha}\}\Delta T \tag{3.16}$$

where

$$\{\overline{\alpha}\} = [A]^{-1} \sum_{k=1}^{N} [\overline{Q}]^k \{\alpha\}^k (z_k - z_{k-1}) \tag{3.17}$$

and $\{\overline{\alpha}\}$ is referred to as the average laminate coefficient of thermal expansion. Then, for in-plane loading only and $[B]$ = 0, the middle-surface curvatures are $\{\kappa\}$=0, so substituting equation (3.16) into (3.8), the lamina stresses are solved, using CLT, to be

$$\{\sigma\}^k = [\overline{Q}]^k [A]^{-1}\{N\} + [\overline{Q}]^k [\{\overline{\alpha}\} - \{\alpha\}^k]\Delta T \tag{3.18}$$

As can be observed from equation (3.18), CLT predicts in-plane lamina stresses, $\{\sigma\}^k$, due to applied external in-plane loading, $\{N\}$, and/or due to a change in temperature from the stress-free temperature, ΔT.

3.2 Interlaminar Stresses

The existence of interlaminar stresses in composite laminates was first studied by Pipes and Pagano where they used a quasi-three-dimensional elasticity approach, along with finite difference numerical approximations to predict the interlaminar stresses, γ_{xz}, γ_{yz}, and σ_z.[3.2] The problem studied is illustrated in Figure 3.4. For a symmetric laminate loaded axially along the ends x=constant, significant interlaminar stresses, γ_{xz}, γ_{yz}, and σ_z, were predicted at the laminate free edges, $y=\pm b$, for angle-ply laminates. At a distance of one laminate thickness away from the free-edge, the interlaminar stresses were shown to go to zero, and the stresses were equivalent to those predicted with classical lamination theory. Their observations included: 1) that there are no interlaminar stresses in unidirectional laminates, 2) interlaminar stresses are very high, perhaps singular, at the free edge of angle-ply laminates and 3) the magnitude of σ_z can be changed significantly by stacking sequence. Simplifications included: a) $[\pm\theta]$ laminates exhibit only shear coupling so γ_{xz} is the only non-zero interlaminar stress and b) [0/90] laminates exhibit only a Poisson mismatch between layers so γ_{yz} and σ_z are only non-zero interlaminar stresses.

Most importantly, high positive interlaminar normal stresses may lead to delaminations and hence failure of the composite laminate, and high interlaminar shear stresses may also lead to failure and thus cannot be ignored. Consequently, a three-dimensional analysis is necessary to determine the stresses that may lead to failure in a composite laminate.

Inclusion of resin-rich layers between plies, through the thickness of the laminate, was reported by Wu to affect significantly the interlaminar stresses.[3.3] A micrograph showing a 500 times magnification through the thickness of one of the $[0,90]_s$ IM7/PETI5 laminate specimens is displayed in Figure 3.5. The micrograph shows an entire 90 degree layer located between two 0 degree plies. As can be observed in the micrograph, indeed there are resin-rich layers between lamina in the current IM7/PETI5 laminates, which should be incorporated into analysis models for predicting interlaminar stresses.

3.3 Residual Thermal Stresses in Composite Laminates

Residual thermal stresses in composite laminates arise due to curing orthotropic lamina in bonded layers at various orientations, from an elevated temperature down to the operating temperature. Residual stresses in laminates have been studied by a myriad of authors and is currently an active area of research. One of the earliest studies was conducted by Chamis in 1971, where he used classical lamination theory to predict significant in-plane residual thermal stresses for various laminates.[3.4] Temperature dependent material properties were included in the nonlinear analysis of Pagano and Hahn in 1977.[3.5] Furthermore, a three-dimensional finite element analysis was performed by Chapin and Joshi in 1991.[3.6] Their investigation revealed significant interlaminar residual thermal stresses.

Since the magnitudes of both in-plane and interlaminar stresses developed in a composite laminate due to curing have been shown to be significant, the extent to which they vary with a change in operating temperature is of key interest in this study. The change in residual stresses with a change in temperature has the potential of playing an important role in the change of strength with a change in temperature and will consequently be included in the analysis models developed herein.

3.4 Validation of 3-D Finite Element Analysis Method

A finite element analysis model is developed to replicate the analysis results of a previously studied problem in the literature. The purpose of this model is to validate the use of the current analysis tools and procedures. The problem of interest is a $[+45,-45]_s$ graphite epoxy laminate subject to uniform axial extension of 0.00005 inches, on the ends x=constant, as previously illustrated in Figure 3.4. Each ply is modeled as an elastic orthotropic material with properties:

$E_{11} = 20. \times 10^6$ psi
$E_{22} = E_{33} = 2.1 \times 10^6$ psi
$G_{12} = G_{23} = G_{31} = 0.85 \times 10^6$ psi
$\nu_{12} = \nu_{13} = \nu_{23} = 0.21$
$\alpha_{11} = -0.5 \times 10^{-6}$ in/in°F
$\alpha_{22} = \alpha_{33} = 23. \times 10^{-6}$ in/in°F

The problem was studied by Pipes and Pagano in their investigation of interlaminar stresses.[3.2] They used a finite difference method along with an elasticity approach to solve for stresses in the y-z plane, where all stresses are independent of x. Their results showed extremely large interlaminar stresses, σ_z and σ_{xz}, at the intersection of the free-edge, y=b, and at interfaces between layers, but these stresses approached zero within one laminate thickness from the free edge. The possibility of stress singularities at the intersection was postulated. The existence of stress singularities was further investigated by Raju and Crews in 1980[3.7] and by Raju, Whitcomb, and Goree in 1980.[3.8] They analyzed the same problem using the finite element method with 8-node, two-dimensional quadrilateral elements. A comparison was made between solutions obtained from finite difference, perturbation and finite element methods. The interlaminar normal stress, σ_z, was shown to disagree in both magnitude and sign. The magnitude difference was expected due to the singularity and approximation differences with the numerical methods; however, the sign of the finite element solution was concluded to be the correct sign because the other methods made inaccurate assumptions for the boundary conditions.

Convergence studies conducted by Raju et al. showed the finite element solution to converge everywhere except very near the interface corner.[3.8] By looking as similar exact solution problems with singularities, finite element solutions were found to behave similarly near the singularity. Thus, the finite element method was concluded to be accurate except in a region involving the

two elements closest to the singularity, and that this region can be made arbitrarily small by refining the finite element model. Another study conducted by Reedy in 1988 showed that the singularity dominated an extremely small region near the free edge, and that this singularity is weak in that stresses changed by only 2% when the element size at the free edge was decreased by 50%.[3.9] Reedy also showed that rapidly varying interlaminar stresses exist even when there is no singularity present, and hence that there is a real interlaminar stress concentration as predicted by the finite element method. The two studies by Raju and Reedy give validity to the use of the finite element method for predicting interlaminar stress concentrations very close to the free edge. As a result, in the present study, interlaminar stresses will be evaluated everywhere except in the two elements closest to the free edge interface or apparent singularity, and these elements will be made as small as possible, so as to improve the approximate values for the interlaminar stresses.

In the current study, all finite element models are created within PATRAN, a commercially available finite element model generation code and then NASTRAN, a commercially available finite element analysis code, is used to perform the structural analyses.[3.10] As opposed to the quasi-three-dimensional models used by Raju et al. to predict stresses in the y-z plane, an actual three-dimensional finite element model using 20-node hexahedral elements is created here to solve the problem illustrated in Figure 3.4. The three-dimensional model is necessary for further investigation of the effect of thermal cure loading and pin-bearing behavior described in Chapter 5.

Figure 3.6 shows the discretization used in the y-z plane of the first quadrant of Mesh 1. Mesh 2, a more refined mesh, differed in that the three elements closest to the free edge in Mesh 1 were divided in half in the y-z plane. A model containing all four in-plane quadrants of the laminate were necessary for a three-dimensional model with accurate boundary conditions and the lack of in-plane symmetry for the $[+45,-45]_s$ lay-up. Mesh 1 was chosen to closely replicate the refined mesh used by Raju (Figure 9(c) in Ref.3.8). Unfortunately, the exact nodal locations were not given by Raju. With five elements used here in the x-direction and 576 elements in the y-z plane of the first quadrant, there is a total of 11,520 hexahedral elements in the model of all four quadrants.

The analysis results for the interlaminar stresses, σ_z and σ_{xz}, are plotted in Figures 3.7 and 3.8, respectively. The stresses are plotted along the interface, z=h, for the plane x=0. These stresses replicate the interlaminar stress distributions reported by Raju et al.[3.8] As expected due to the singularity, Mesh 2 predicted higher stresses in the two elements closest to the free edge than did Mesh 1. Most importantly, two elements away from the free-edge of Mesh 1, the magnitude of the stresses for Mesh 1, Mesh 2, and Raju's model all converge at the same value. The convergence of the interlaminar stress solution validates the analysis model developed here for evaluation of interlaminar stresses two elements from the free edge.

Analysis results, using Mesh 1, for the in-plane stresses, σ_x, σ_y, and τ_{xy}, are plotted in Figure 3.9. Also shown on the figure is the classical lamination theory (CLT) solution for the in-plane stresses. As previously observed by other

authors, the analysis results for in-plane stresses can be seen to approach the CLT solution at a distance of one laminate thickness, 4h, from the free edge.

The current finite element model was further utilized to investigate the thermal residual stresses that would be present in the laminate due to curing. A stress free temperature of T_{ref}=310°F was assumed, and the stresses were evaluated at an operating temperature of 70°F. The previously presented constant material properties were assumed, for simplicity, allowing for a linear static analysis.

The in-plane stresses, σ_x, σ_y, and τ_{xy}, obtained using Mesh 1 and the thermal curing load of ΔT= -240°F are plotted in Figure 3.10. Also shown is the classical lamination theory (CLT) solution for the in-plane stresses. As with the case of axial extension loading, the analysis results for in-plane stresses also approach the CLT solution at a distance of approximately one laminate thickness from the free edge from the free edge. The figure also reveals large in-plane stresses near the free edges due to curing. The large σ_x and σ_y stresses appear to be confined to the two elements closest to the free edge and, due to the singularity, are consequently not valid stresses.

The interlaminar normal, σ_z, and shear, σ_{xz}, stresses are displayed in Figures 3.11 and 3.12, respectively. Similar to the case of axial extension previously analyzed, a stress concentration and apparent singularity are present at the intersection of the free-edge and interface. However, in contrast to the case of axial extension, the interlaminar stresses σ_z and σ_{xz} are positive(tensile) in magnitude and more severe for curing. Since the thermal residual stresses are also much greater in magnitude than the interlaminar stresses due to extensional loading alone, their significance on the changes in the state of stress due to a change in temperature will be further investigated within Chapters 3 and 5.

3.5 Three-Dimensional Laminate Analysis

A three-dimensional analysis model of an IM7/PETI5 composite laminate is generated here for the purpose of establishing the laminate attributes that significantly affect the state of stress in the laminate. More specifically, the focus is on the attributes that influence the changes in stress with a change in temperature, and hence should be incorporated in the pin-bearing analysis model. The specific laminate attributes under investigation include: 1) the resin rich layer located between lamina in the laminate, 2) the residual thermal stresses that develop in a laminate due to the cure cycle, 3) the temperature dependent stiffness and thermal expansion coefficients for the IM7/PETI5 lamina, and 4) nonlinear stress-strain behavior of the IM7/PETI5 lamina.

Due to in-plane symmetry in the $[90,0]_{8s}$ laminates, and the formidable computational size of the full three-dimensional problem, only this lay-up was chosen for investigation, where taking advantage of symmetry, only one-eight of the laminate is modeled. Two finite element geometry models of the $[90,0]_{8s}$ laminate were created, one without a resin layer and one including the resin layer. The finite element model solid geometry including the resin-rich layer is shown in Figure 3.13. The model without the resin layer differed in that there

were no resin layers and a ply thickness of h=0.0055 inch is used, resulting in the same laminate half thickness of 0.088 inch. As approximated from the micrograph previously shown in Figure 3.5, for the model including the resin layer, the ply layer thickness, h, is 0.005 inch, where the resin layer thickness is 0.1h. All ply layers have a thickness of h and resin layers have a thickness of 0.1h except the top ply has a thickness of h+0.05h and the one resin solid adjacent to the z=0 symmetry plane has a thickness of 0.05h. Using a value of h=0.005 inch, the total thickness modeled is 0.088 inch, which is half of the total laminate thickness of t=0.176 inch. The three symmetry planes are z=0, the through the thickness symmetry, and x=0 and y=0, the in-plane symmetry planes.

The finite element models for Mesh 1 and the more refined mesh, Mesh 2, consisted of hexahedral solid elements with rectangular faces. A view of Mesh 1 in the x-y plane is displayed in Figure 3.14, where there are 20 uniformly spaced elements located in the x-direction and 30 elements in the y-direction. In the y-direction, 19 uniformly spaced elements are between y=0 and y=0.95W, and the remaining eleven elements were graded with the maximum concentration located at the free edge, y=W. A partial view of Mesh 1 in the x-z plane, including the resin layer, similar to the blow-up region depicted in Figure 3.13, is displayed in Figure 3.15, where there are 100 element layers through the thickness of the model. Each ply layer had 4 elements and each resin layer had 2 elements except for the two resin layers between the 0° and 90° plies located second and third from the z=0 symmetry plane, which had four elements. A total of 38,400 elements without the resin layer, and 60,000 elements with the resin layer, are in the model for Mesh 1. Mesh 2, the more refined mesh, differed from Mesh 1 with 35 elements in the y-direction, where the elements were made smaller than Mesh 1 between y=0.998W and the free edge. Also, there are 112 elements in the z-direction for Mesh 2 including the resin layer, which differed from Mesh 1 with 8 elements in the first 0° ply located closest to the z=0 symmetry plane, 8 elements in the resin layer between the first 0° and 90° ply and 4 elements per resin layer in the first resin layer adjacent to the z=0 symmetry plane and the resin layer between the first 90° and second 0° ply. A total of 48,960 elements without the resin layer, and 78,400 elements including the resin layer, are in the model for Mesh 2.

3.5.1 Resin Layer

To investigate the resin layer effect, the room temperature lamina engineering constants, as presented in Table 2.1 and Equations 2.1-2.7, are used as the properties in a linear static analysis of the composite laminate. For the $[90,0]_{8s}$ laminates, the average room temperature compressive strength of 126 ksi, as presented in Table 2.4, is used, along with the lamina moduli, E_{11c} and E_{22c}, to compute an equivalent applied displacement loading of d=-0.0028 inch for the analysis. The uniform displacement was applied on the surfaces at the end x=L on the finite element model as depicted in Figure 3.14.

Analysis results for the in-plane stresses, for the finite element model without the resin layer, subject to the applied displacement of d = -0.0028 inch,

are presented in Figure 3.16, along with the Classical Lamination Theory solution. The most severe in-plane stress, σ_x, occurred in the 0 degree plies. The plots show the stresses in the 0 degree ply at the intersection of the z=0 and x=0 symmetry planes and along the y-direction from y = 0.2 inch to the free edge, y=0.25 inch. The in-plane stress results closely replicate the Classical Lamination Theory solution except in a small region near the free edge. Analysis results for the interlaminar stresses σ_z and σ_{yz} are displayed in Figure 3.17 and 3.18, respectively. A maximum interlaminar normal stress, σ_z, is predicted in the laminate with a magnitude of approximately 7100 psi two elements from the free edge of Mesh 2, in the 0 degree ply along the z=0 symmetry plane. Interestingly, the maximum interlaminar shear stress did not occur directly at the free edge, but actually a very small distance away from the free edge as shown in Figure 3.18. A maximum σ_{yz} of –3200 psi occurred in Mesh 2 at the interface between the 90 degree and 0 degree ply adjacent to the z=0 symmetry plane. By comparison with Mesh 2 results, Mesh 1 appears to be adequate for obtaining a converged solution.

Analysis results of in-plane stresses from the finite element model including the resin layers and subject to the applied displacement, were basically identical to the results obtained in the absence of the resin layers, however the interlaminar stresses are different. The interlaminar stresses predicted in the model including the resin layers are displayed in Figures 3.19 and 3.20. A maximum interlaminar normal stress of σ_z = 8600 psi occurred two elements from the free edge of Mesh 2 along the z=0 symmetry plane. The maximum normal stress location was the same as obtained with the model without resin layers, however the magnitude was over 20% greater when the resin layers were included in the model. The maximum interlaminar shear stress, σ_{yz} = -6400 psi, two elements from free edge in Mesh 2, occurred at the interface between the resin layer and 90 degree ply closest to the z=0 symmetry plane. *This value was twice as much as the maximum interlaminar stress predicted from the model without the resin layers.* Since there is a great difference in interlaminar stresses between the models with and without the resin layers, only the more detailed model including the resin layers will be utilized in the forthcoming analyses.

3.5.2 Thermal Residual Cure Stresses

The residual cure stresses in the composite laminate are investigated here using a linear analysis. The properties at the relevant operating temperature as given in Table 2.1 are used. The interlaminar stresses were the most severe stresses in the laminate due to curing at all three operating temperatures of interest, -200°F, 70°F, and 350°F. Analysis results of the interlaminar stresses predicted at 70°F are plotted in Figure 3.21 and Figure 3.22. A maximum positive interlaminar normal stress of 7000 psi was predicted two elements from the free edge in the 90° ply at the interface of the first resin layer and 90 degree ply closest to z=0. A maximum interlaminar shear stress of 11500 psi was predicted two elements from the free edge in the resin layer at the interface of the first resin layer and 90 degree ply closest to z=0. Although the location of the maximum interlaminar stresses did not change at the different operating

temperatures under consideration, the magnitudes predicted did and are presented in Table 3.1.

3.5.3 Temperature-Dependent Material Properties

A nonlinear analysis of the composite laminate subject to the cure temperature changes is performed including temperature dependent material properties. A piecewise linear approximation of the material properties presented in Table 2.1 between the four temperatures given is incorporated in the finite element analysis. The temperature change loading was divided into ten increments with a convergence check made with a twenty increment division. The use of temperature dependent properties did not result in any change in the location of the maximum occurring interlaminar stresses and the difference in the magnitude in comparison to the analysis assuming constant properties was extremely insignificant at all operating temperatures. The maximum interlaminar stress results from the nonlinear analysis are presented in Table 3.1, in comparison to the linear analysis results.

3.5.4 Nonlinear Material Stress-Strain Behavior

The nonlinear elastic material stress-strain behavior was not included in the finite element analysis due to the following reasons,

1) NASTRAN does not have the capability to model nonlinear elastic material properties for orthotropic materials,
2) The in-plane shear stresses, τ_{12}, and interlaminar shear stress, τ_{31}, in the $[90,0]_{8s}$ composite laminate being analyzed were virtually zero, and since only the in-plane shear modulus, G_{12}, and interlaminar shear modulus, $G_{31}=G_{12}$, had any significant nonlinear characteristics as described in Section 2.3.2, the nonlinear elastic properties should not significantly alter the predicted stresses in the laminate analysis.

3.5.5 Combined Loading

The analysis of residual cure stresses occurs from the stress free temperature of 460°F to the operating temperature. Then, at the operating temperature of interest, the applied displacement loading occurs. The case of cure and the case of applied displacement loading at the operating temperature are analyzed independently where the states of stress are subsequently combined. The interlaminar stresses through the thickness of the laminate, two elements away from the free edge are presented in Figures 3.23, 3.24, and 3.25 at the three operating temperatures of 350°F, 70°F, and –200°F, respectively. Shown in each figure in the upper two plots are the σ_z and σ_{yz} stresses obtained independently for the case of cure loading (dashed line) and applied displacement loading (solid line). The bottom two plots then show the combined solution of cure and applied displacement loading for σ_z and σ_{yz}. As can be observed from the figures at all temperatures, (except for σ_z at 350°F), the applied displacement load decreases the interlaminar residual stresses that are

present in the laminate due to cure alone. As for the σ_z at 350°F, the σ_z due to cure is smaller than σ_z due to the applied displacement, and consequently the net σ_z in the combined case is larger than σ_z from cure alone. However, the combined maximum magnitude is only 2700 psi, which is much less the σ_z magnitudes of approximately 7000 psi observed due to cure only at the 70°F and 350°F operating temperatures.

The only significant in-plane stress in the analysis model is σ_x in the 0 degree plies, where τ_{xy} was virtually zero and σ_y was much less than the y-direction strength, F_{22c}, in the 90 degree plies. Table 3.2 shows σ_x due to cure only, applied displacement only, and the combined case of cure and applied displacement loading.

3.6 Discussion and Conclusions

From the analysis results of the IM7/PETI5 $[90,0]_{8s}$ composite laminate presented in Section 3.5, the significant laminate attributes that need to be included in the analysis of the laminate include: 1) the residual stresses due to cure and 2) the resin layer located between the lamina in the laminate. Moreover, analyses for this particular laminate at the temperatures being considered, establish that the temperature dependent material properties do not require a nonlinear analysis to provide an accurate stress solution. Just modeling the laminate assuming the properties to be constant at the operating temperature of interest as presented in Table 2.1 is sufficient for predicting stresses accurately. Also, due to the in-plane shear and interlaminar shear, τ_{13}, being virtually zero in the laminate under consideration, the nonlinear elastic characterization of the material is assumed not to be necessary to analyze the laminate behavior.

From the observation on the effect of an applied displacement load decreasing the interlaminar stresses present in the laminate due to cure alone, it is concluded that failure cannot be attributed to the interlaminar stresses in the composite laminate being studied when a compressive load is applied. The strength changes of F_{11c} and F_{xxc} for the $[90,0]_{8s}$ laminate, from Tables 2.1 and 2.4, respectively, are presented in Table 3.3 along with the change in the σ_x residual cure stress in the 0 degree plies. Unfortunately, due to the small changes in residual cure stresses, less than 15 ksi, and a scatter of up to 15 ksi in the average values of F_{11c} and F_{xxc} data presented in Table 2.1, the effect of residual cure stresses and changes in lamina compared to laminate strength cannot be clearly perceived. One can conclude that the increase in compressive strength of the $[90,0]_{8s}$ laminate due to a decrease in temperature is most likely governed by the increase is lamina strength, F_{11c}, with a decrease in temperature in addition to possible effects with the changes in residual stress lessening the strength change for the laminate as compared to the lamina. Although interlaminar stresses do not appear to cause failure in a compression specimen, investigating the three-dimensional state of stress including thermal residual stresses was necessary to make the determination. Similarly, the three-dimensional state of stress in a pin-bearing specimen must be studied to determine the role of interlaminar stresses in the pin-bearing problem.

3.7 References

3.1 Jones, Robert M.: Mechanics of Composite Materials, 2nd Edition, Taylor & Francis, Inc., Philadelphia, PA, 1998.

3.2 Pipes, R. B. and Pagano, N.J.: Interlaminar Stresses in Composite Laminates Under Uniform Axial Extension. *J. Composite Materials*, Vol. 4, October 1970, pp. 538-548.

3.3 Wu, C.M.L.: Nonlinear Thermal and Mechanical Analysis of Edge Effects in Angle-Ply Laminates. *Computers and Structures*, Vol. 35, No.6, 1990, pp. 705-717.

3.4 Chamis, Christos C.: Lamination Residual Stresses in Multilayered Fiber Composites. *NASA TN D-6146*, February 1971.

3.5 Pagano, N.J. and Hahn, H.T.: Evaluation of Composite Curing Stresses. Composite Materials: Testing and Design (Fourth Conference), *ASTM STP 617*, American Society for Testing and Materials, 1977, pp. 317-329.

3.6 Chapin, C.M. and Joshi, S. P.: Variation of Residual Thermal Stresses in Graphite/Epoxy Laminates. *Composites: Proceedings of the 8th International Conference on Composite Materials*, Honolulu, HI, July 15-19, 1991, pp. 30-D-1 to 30-D-10.

3.7 Raju, I.S. and Crews, J.H.: Interlaminar Stress Singularities at a Straight Free Edge in Composite Laminates. NASA TM 81876, August 1980.

3.8 Raju, I.S., Whitcomb, J.D., and Goree, J.G.: A New Look at Numerical Analysis of Free-Edge Stresses in Composite Laminates. *NASA Technical Paper 1751*, December 1980.

3.9 Reedy, E.D., Jr.: On Free-edge Interlaminar Stress Distributions. *Composites Science and Technology*, Vol. 34, 1989, pp. 259-266.

3.10 MSC/PATRAN/NASTRAN, Structural Analysis, Version 7, Vol. 1, The MacNeal-Schwendler Corperation, Los Angeles, CA, July, 1997.

Table 3.1 Comparison of Predicted Maximum Residual Cure Stresses Two Elements Away from Free Edge.

Temperature (°F)	Linear Analysis Constant Properties		Nonlinear Analysis Temperature-Dependent Properties	
	σ_z(psi)	σ_{yz}(psi)	σ_z(psi)	σ_{yz}(psi)
350	1521.	2439.	1524.	2439.
70	7081.	11467.	7174.	11491.
-200	7691.	12375.	7782.	12408.

Table 3.2 Maximum In-Plane Stress, σ_x, Predicted in the Laminate.

Temperature (°F)	σ_x (ksi)		
	Cure Only	Applied Displacement	Combined
350	-3.	-230.	-233.
70	-15.	-231.	-246.
-200	-16.	-231.	-247.

Table 3.3 Comparison of Changes in Lamina Strength, F_{11c}, $[90,0]_{8s}$ Laminate Strength, F_{xxc}, and σ_x Cure Stress in 0 degree Ply with a Change in Temperature.

Temperature Change	ΔF_{11c} Lamina (ksi)	ΔF_{xxc} Laminate (ksi)	Cure Stress, $\Delta\sigma_x$ (ksi)
350°F to 70°F	40	31	-12
350°F to -200°F	53	49	-13

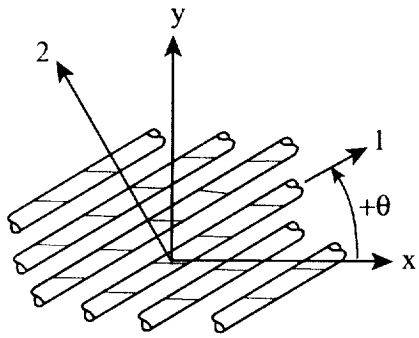

Figure 3.1. Illustration of transformation between the material and laminate coordinate systems.

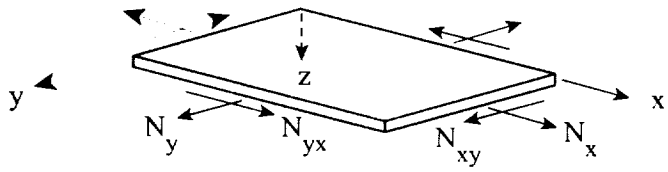

Figure 3.2. Composite laminate subject to in-plane applied forces.

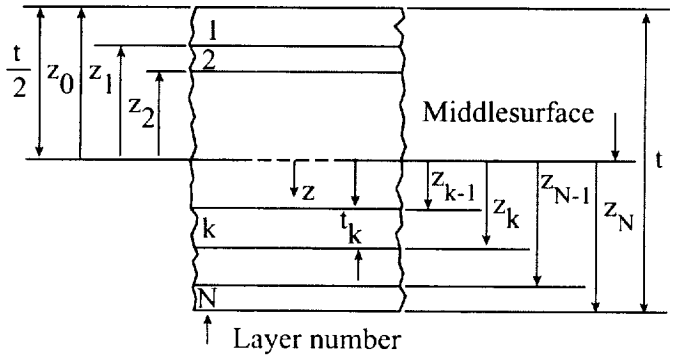

Figure 3.3. Geometry through the thickness of an N-layered laminate.

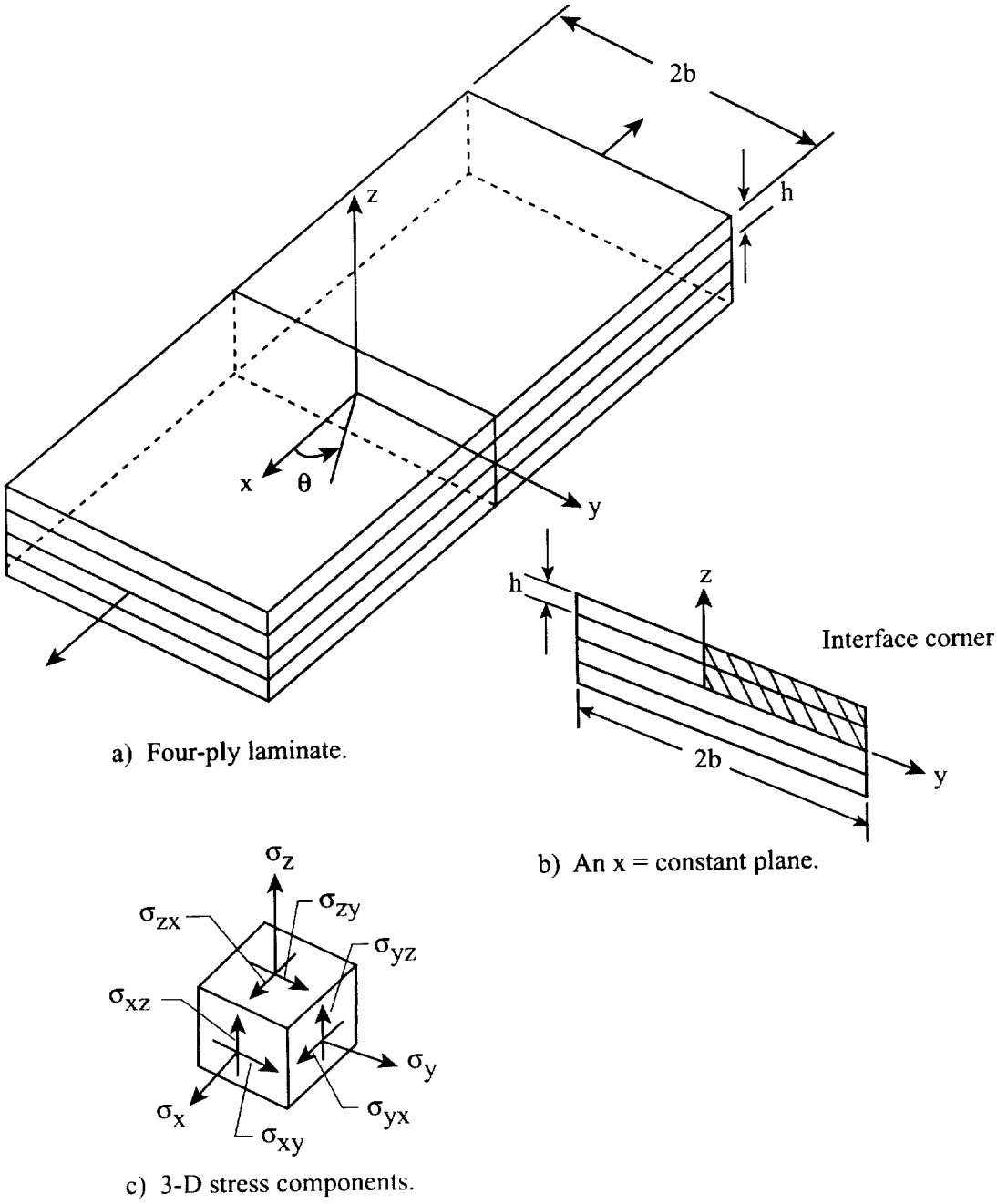

Figure 3.4. Illustration of the problem of a four-ply laminate under uniform axial extension and the resultant stress components, Ref.3.2.

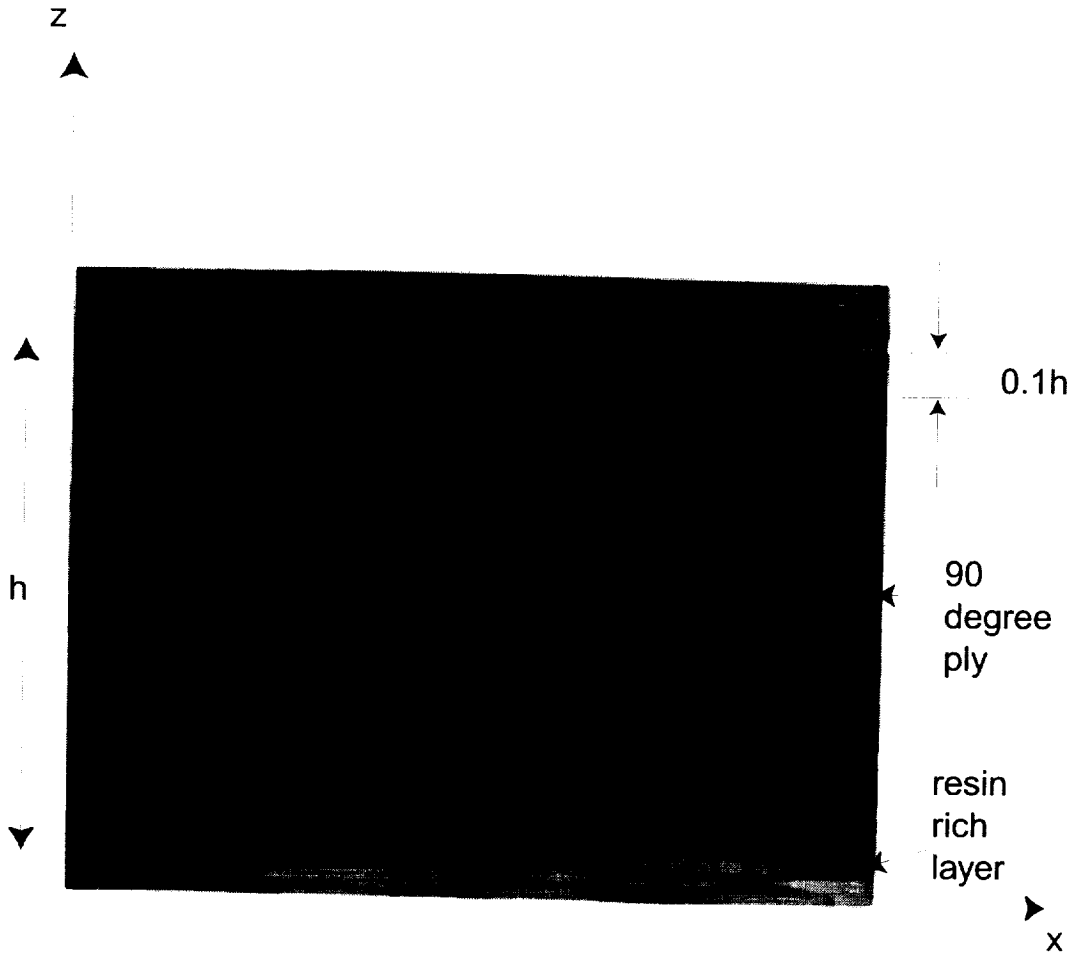

Figure 3.5. Micrograph showing a 500 times magnification of a portion through the thickness of a $(90,0)_s$ IM7/PETI5 laminate.

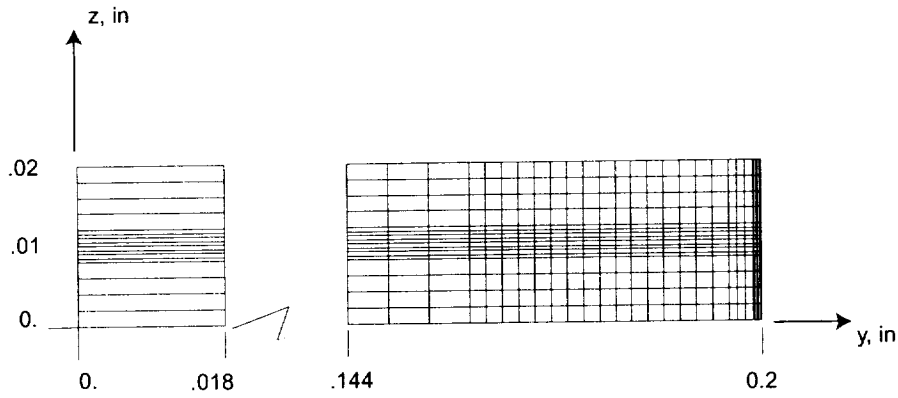

Figure 3.6. Finite element model discretization of Mesh 1 in first quadrant of the y-z plane.

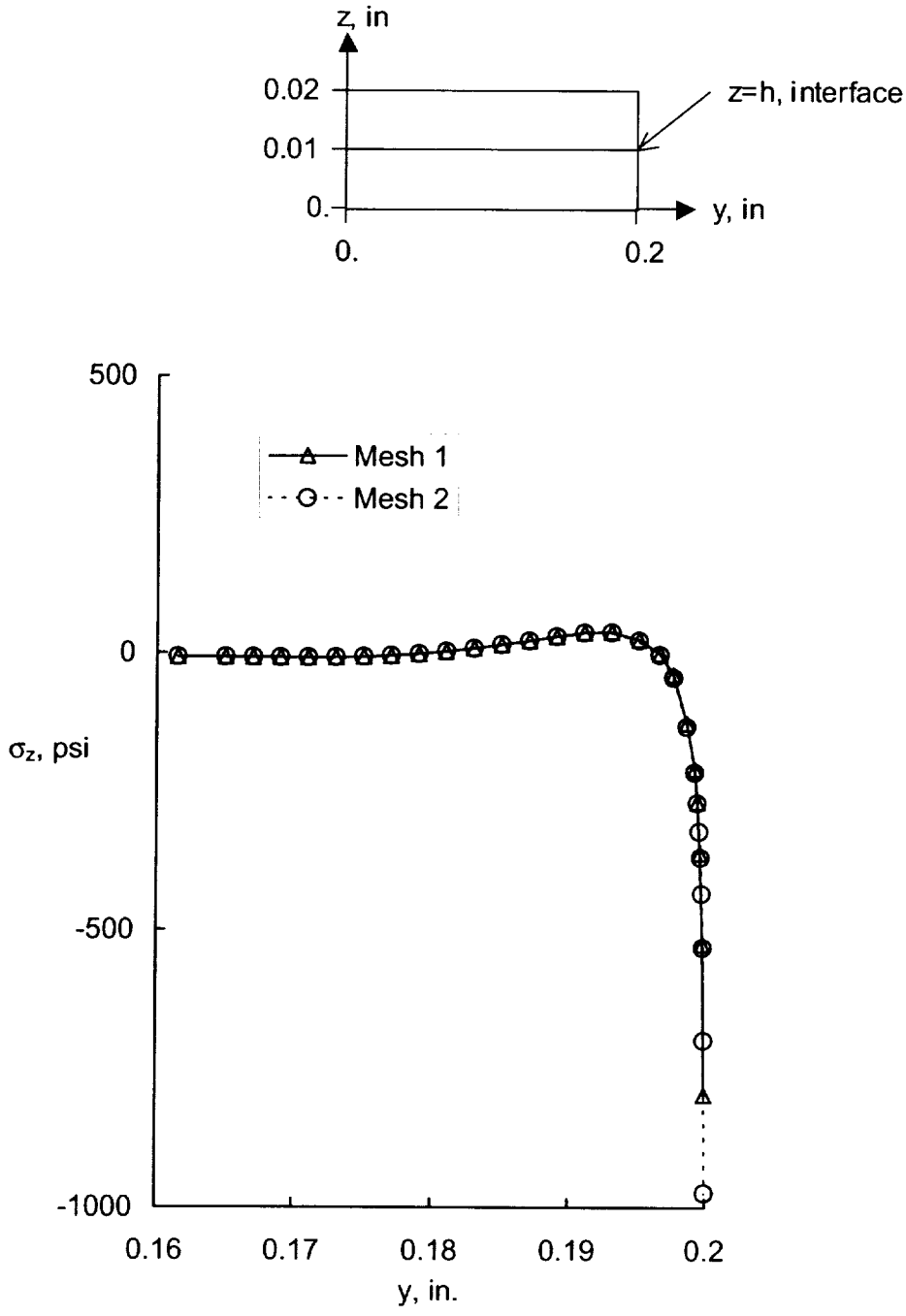

Figure 3.7. The interlaminar normal stress, σ_z, along the interface, z=h.

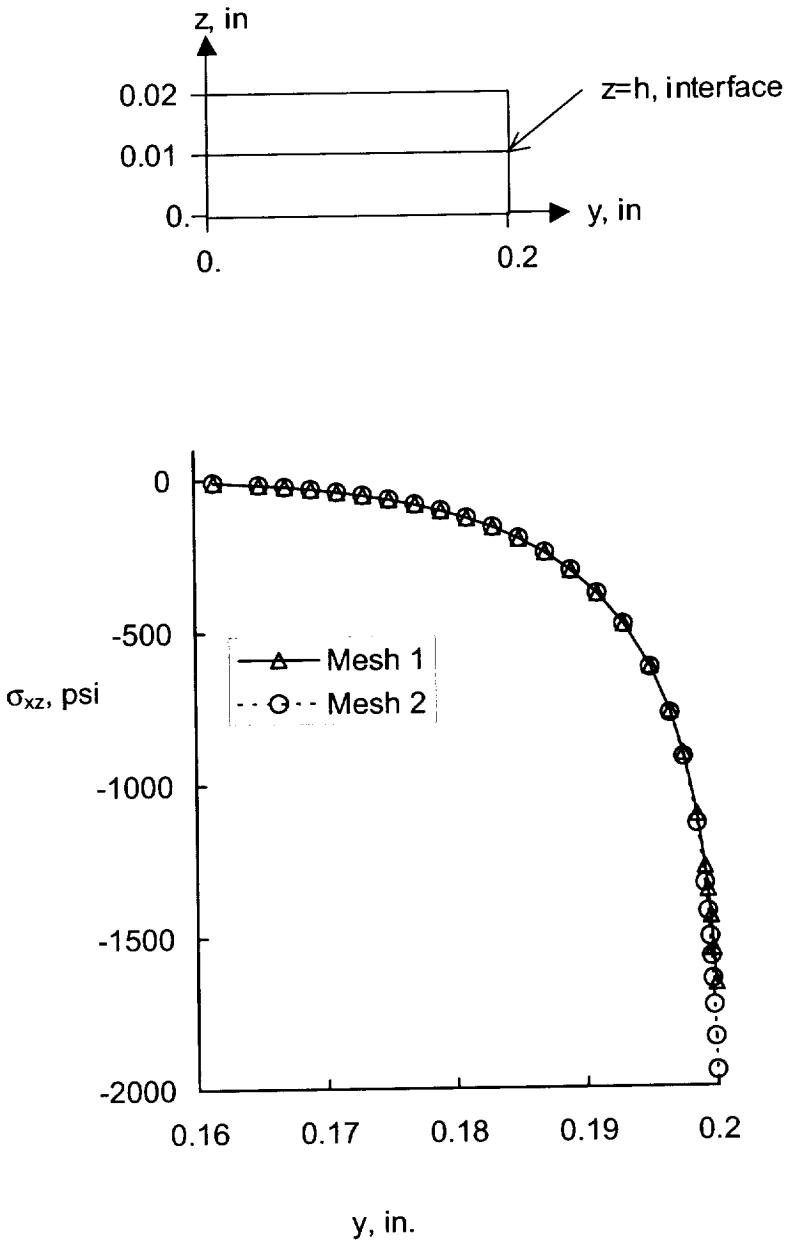

Figure 3.8. The interlaminar shear stress, σ_{xz}, along the interface, z=h.

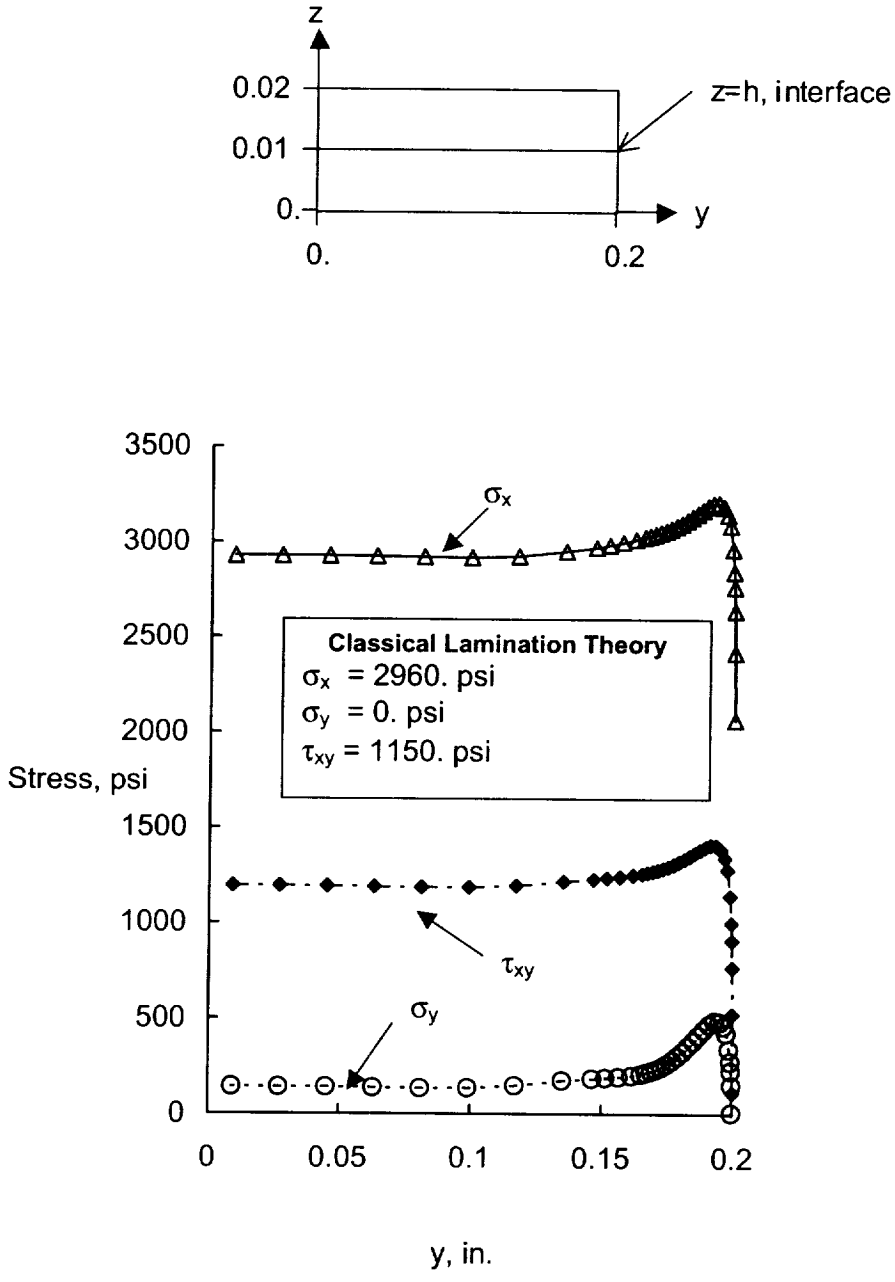

Figure 3.9. Analysis results of in-plane stresses along the interface, z=h.

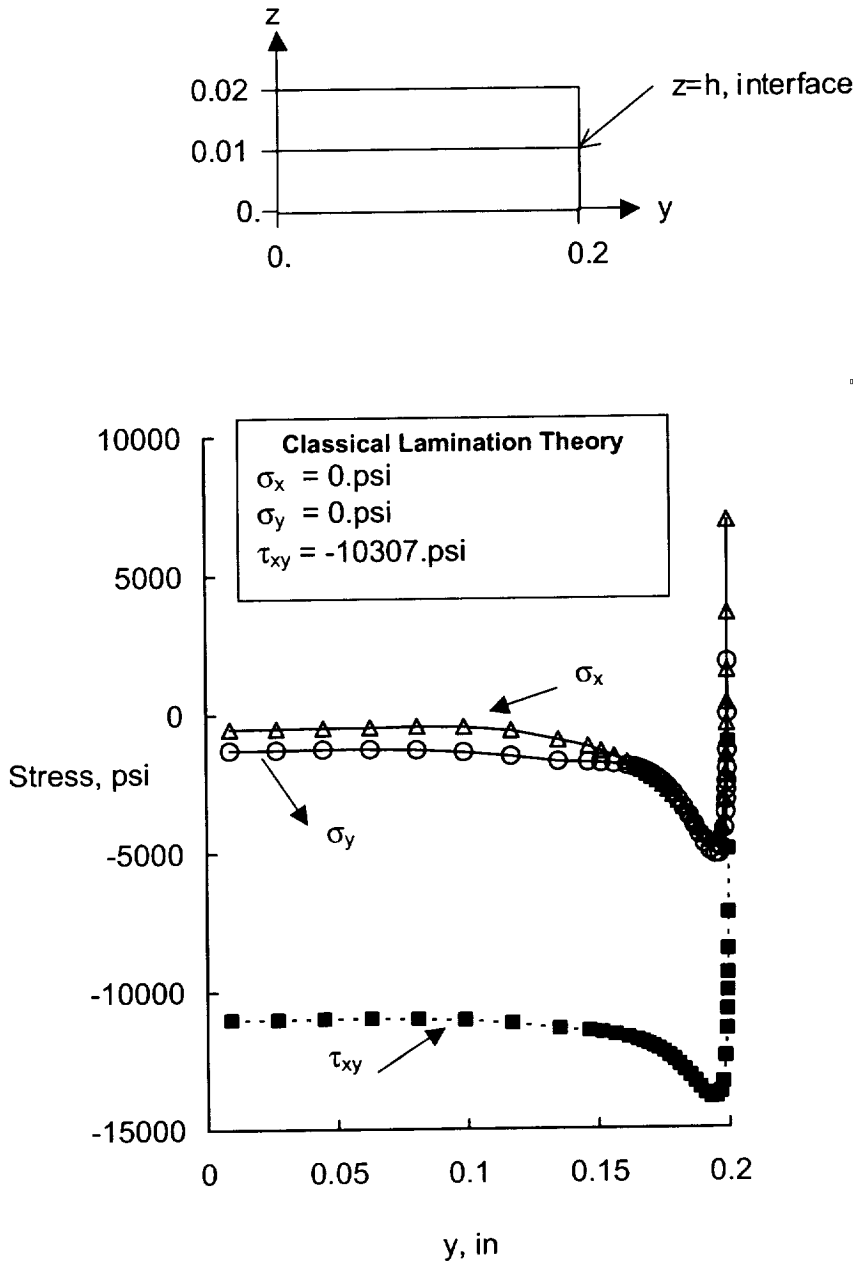

Figure 3.10. Analysis results of in-plane stresses along the interface, z=h, due to curing.

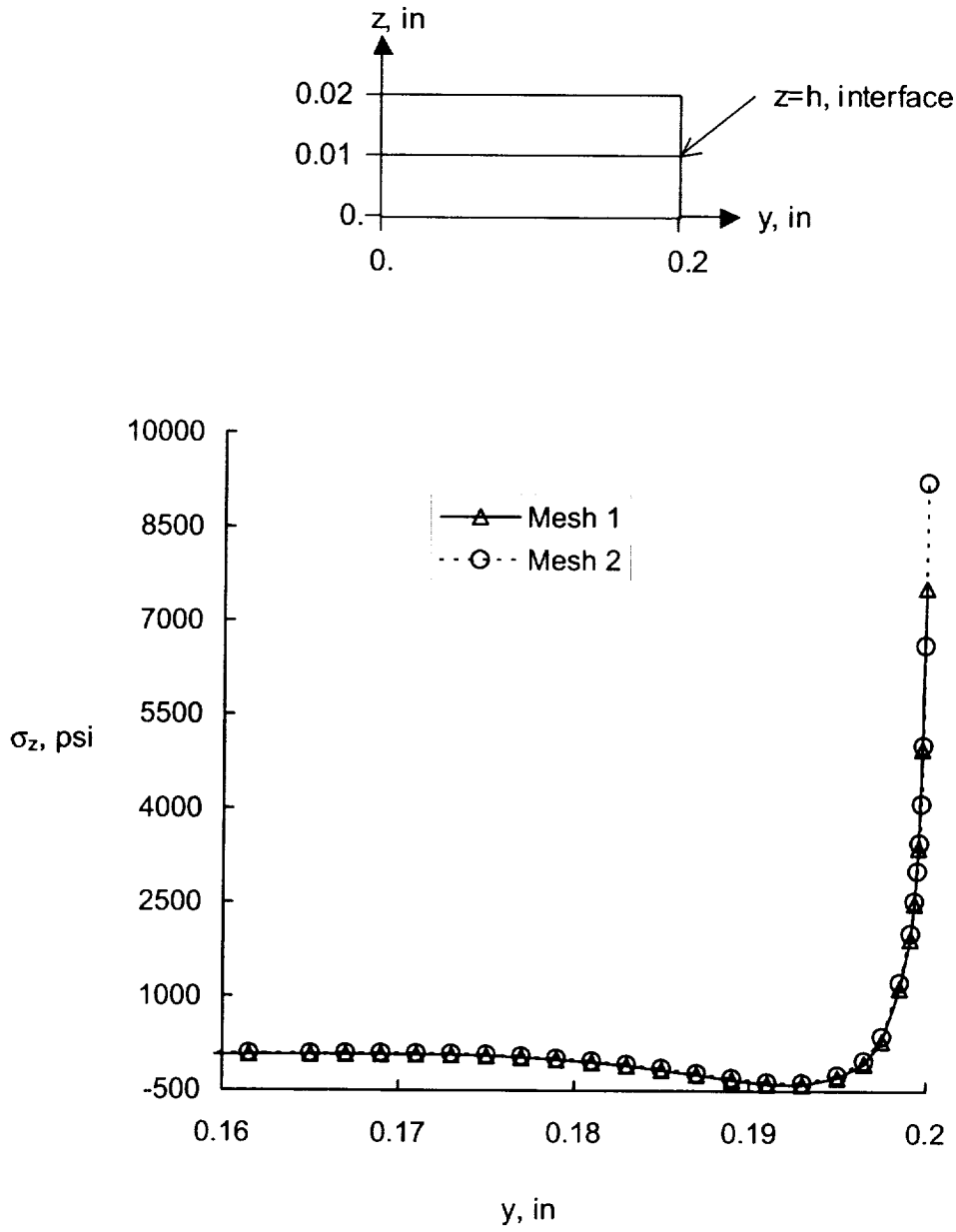

Figure 3.11. The interlaminar normal stress, σ_z, along the interface, z=h, due to curing.

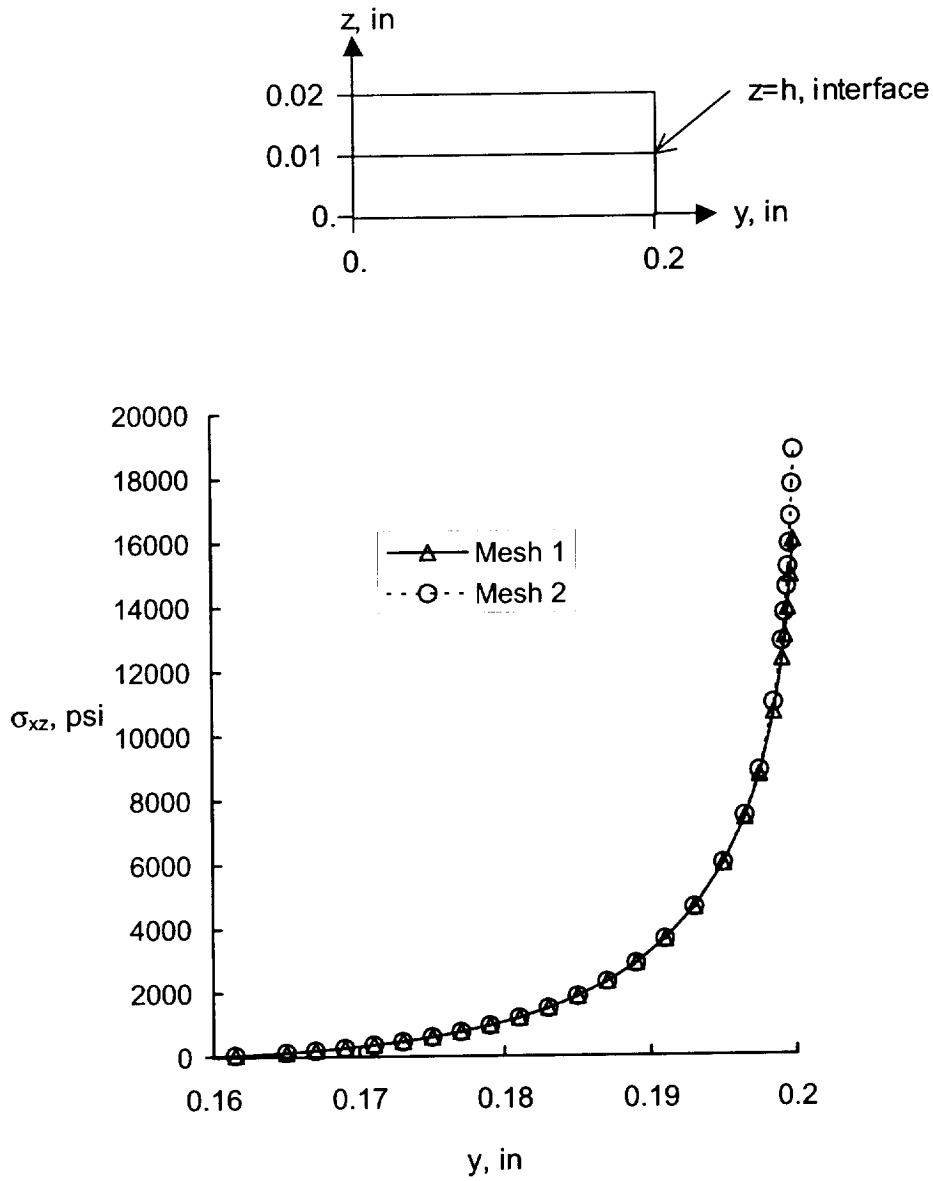

Figure 3.12. The interlaminar shear stress, σ_{xz}, along the interface, z=h, due to curing.

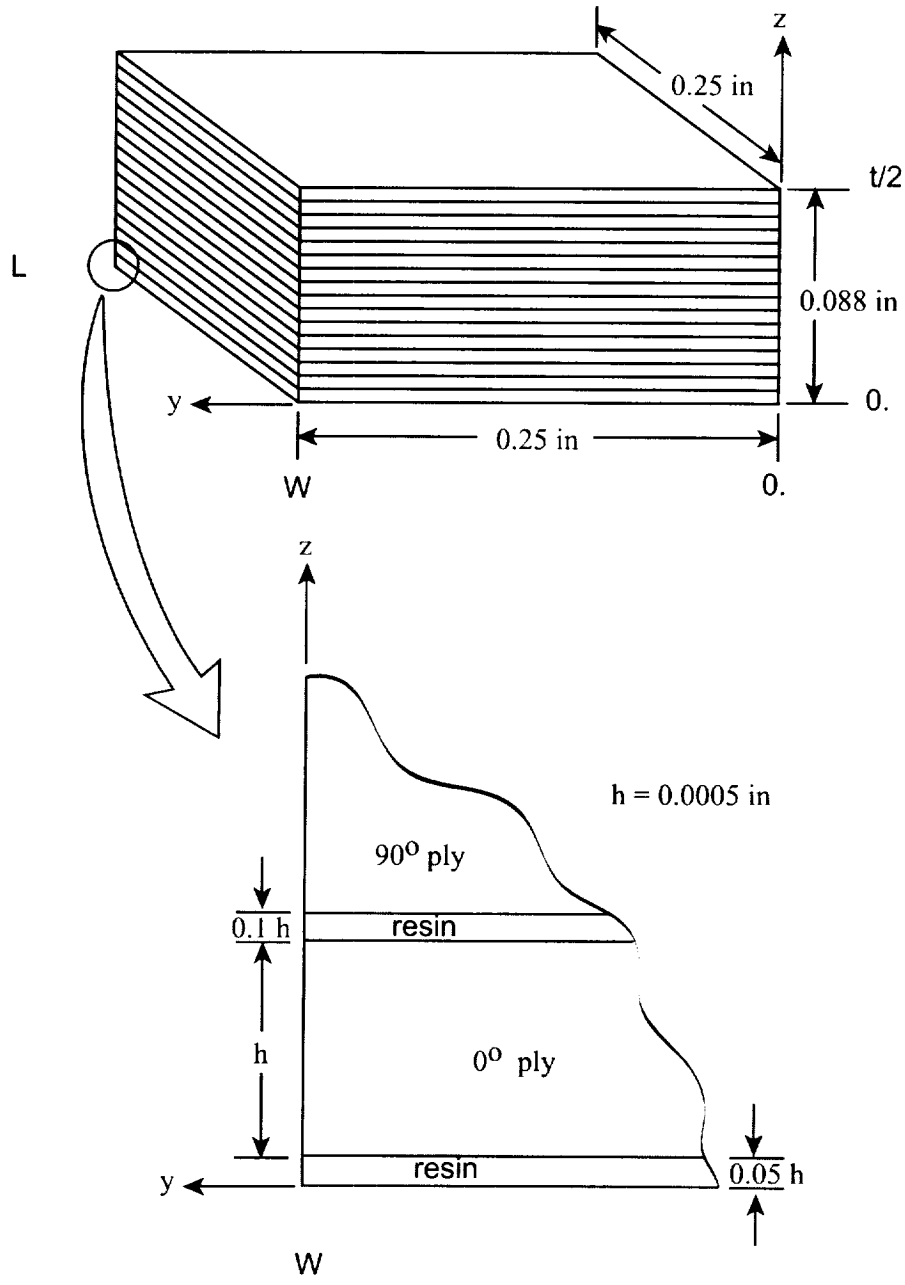

Figure 3.13. Finite element model solid geometry including resin-rich layer.

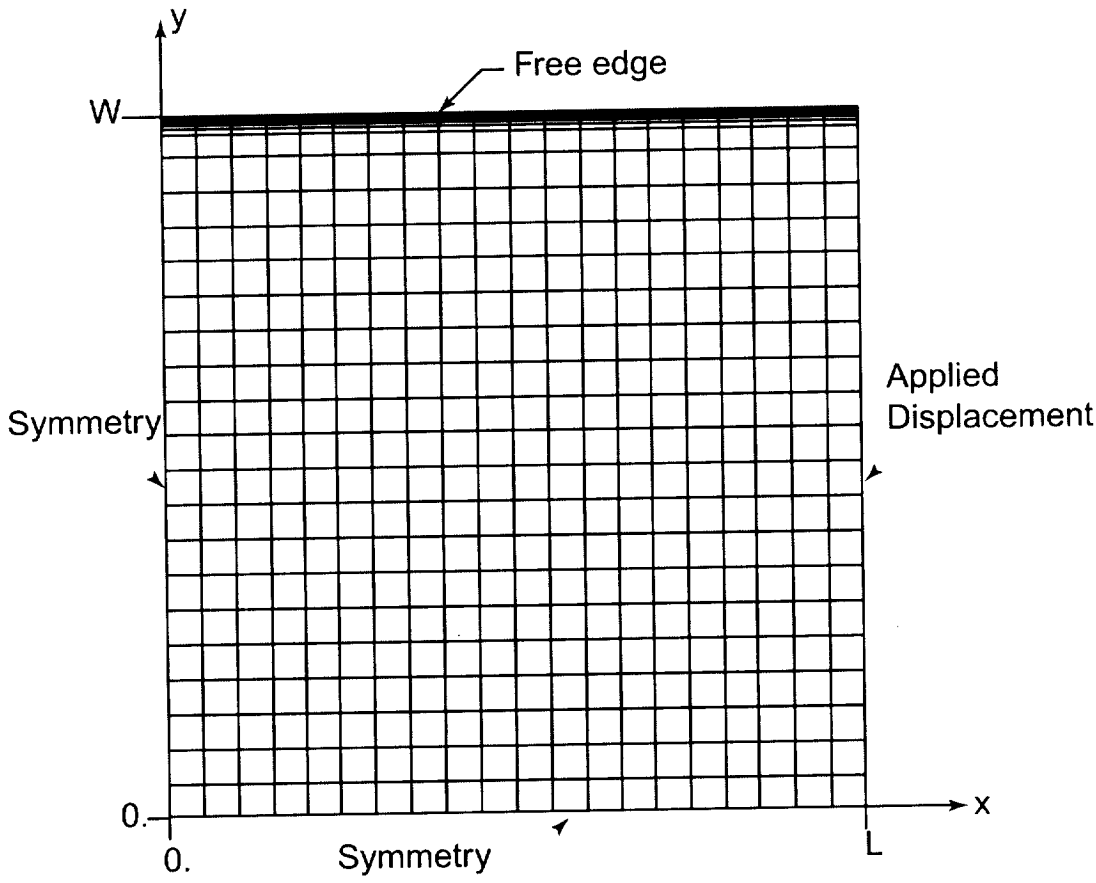

Figure 3.14. Finite element discretization in the x-y plane for Mesh 1.

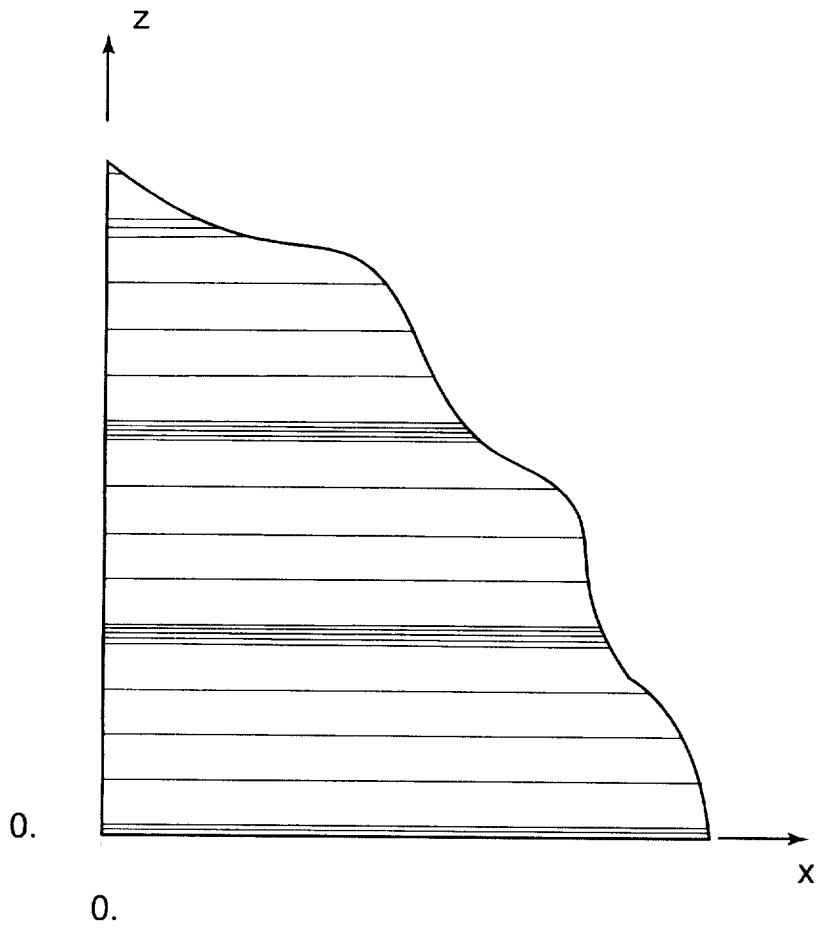

Figure 3.15. Partial view of the finite element discretization in the x-z plane for Mesh 1 with resin layers.

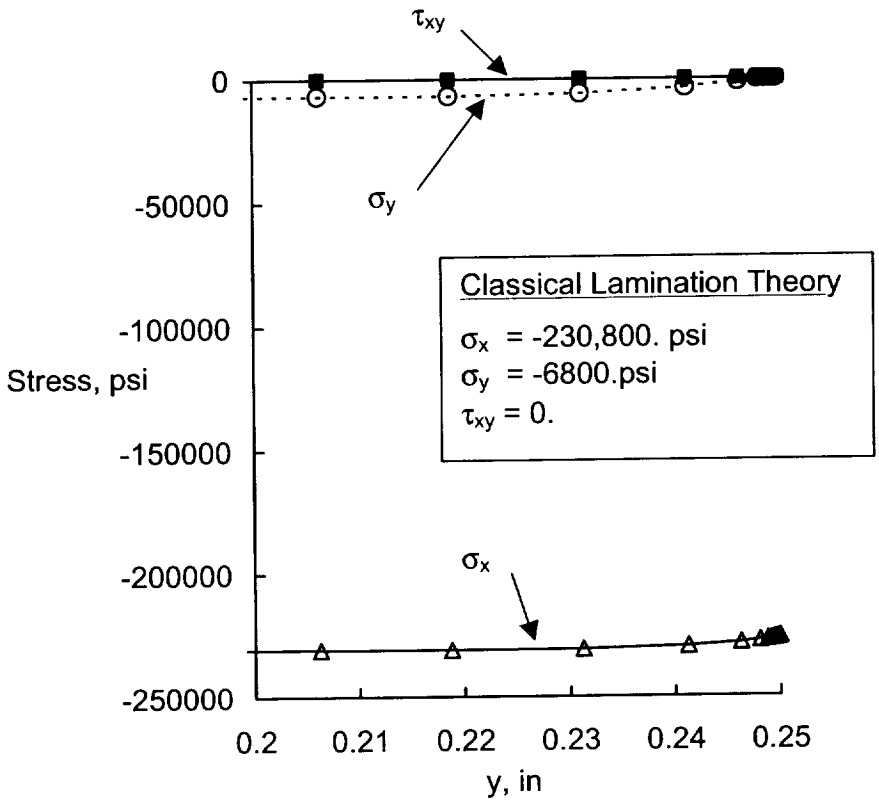

Figure 3.16. In-plane stresses in 0° ply of $[90,0]_{8s}$ laminate, subject to applied displacement, plotted along the z=0 and x=0 symmetry planes.

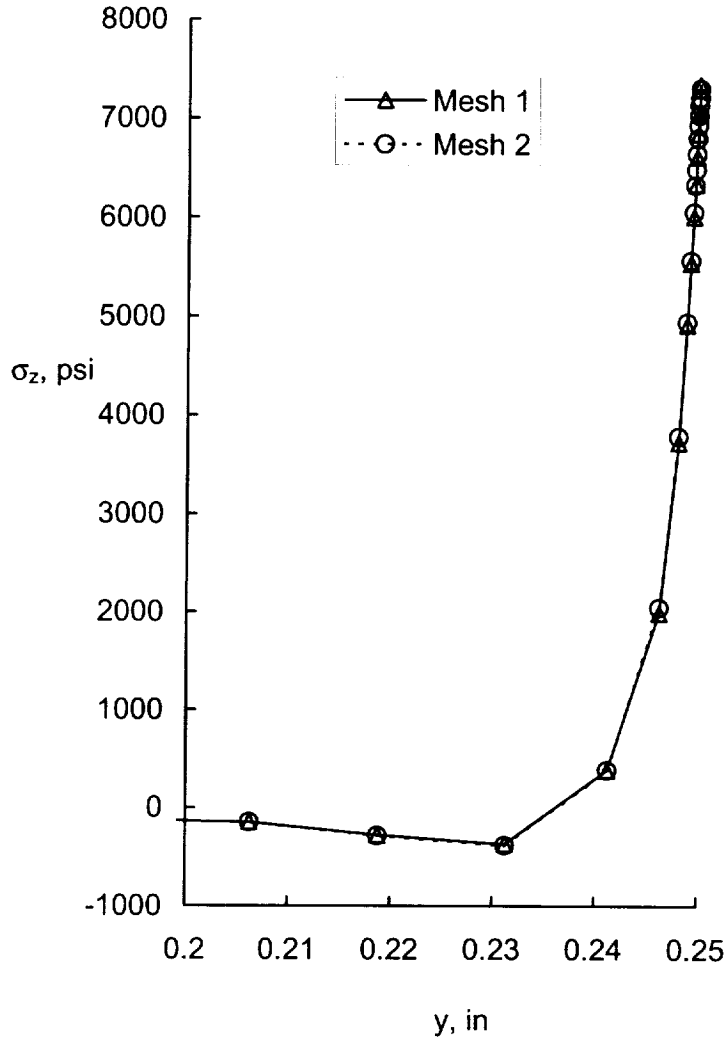

Figure 3.17. Interlaminar normal stress in $[90,0]_{8s}$ laminate without the resin layer, subject to applied displacement, plotted along the z=0 and x=0 symmetry planes.

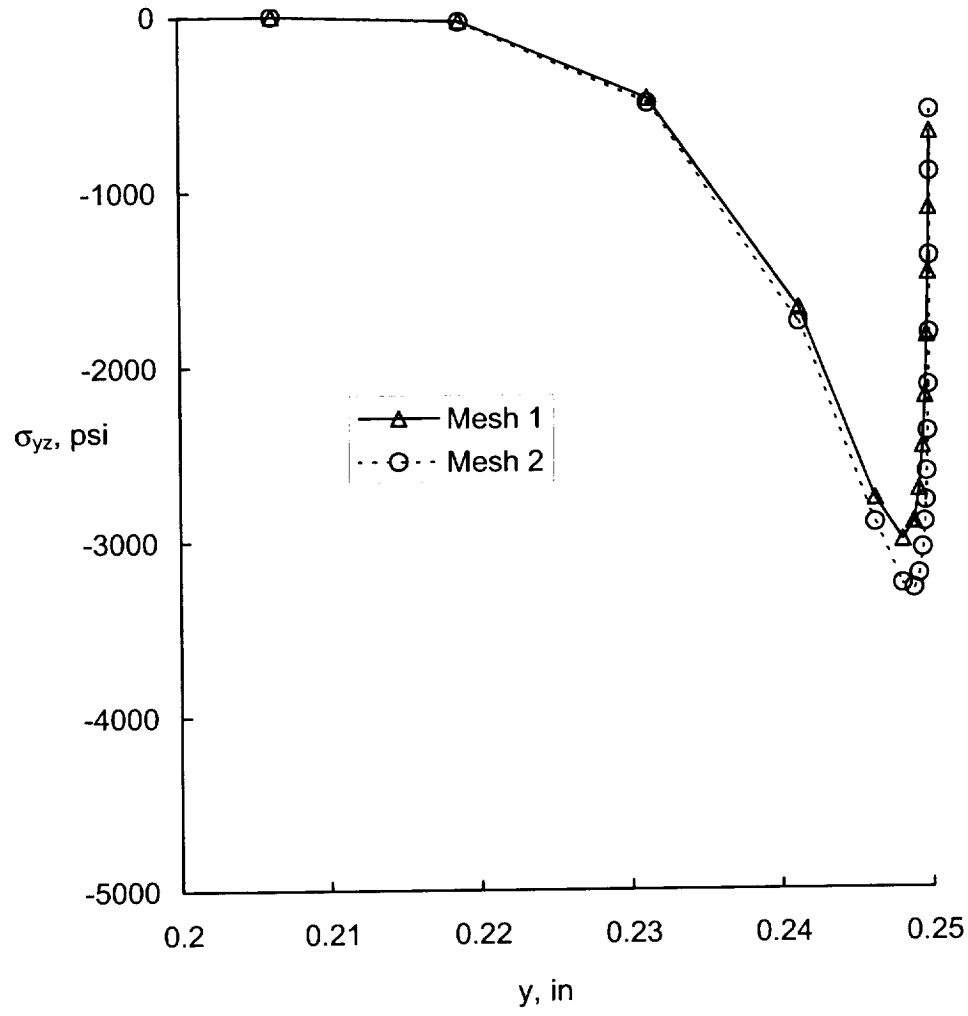

Figure 3.18. Interlaminar shear stress in $[90,0]_{8s}$ laminate without resin layers, plotted along x=0 and the interface between the first 90 degree and 0 degree ply adjacent to the z=0 symmetry plane.

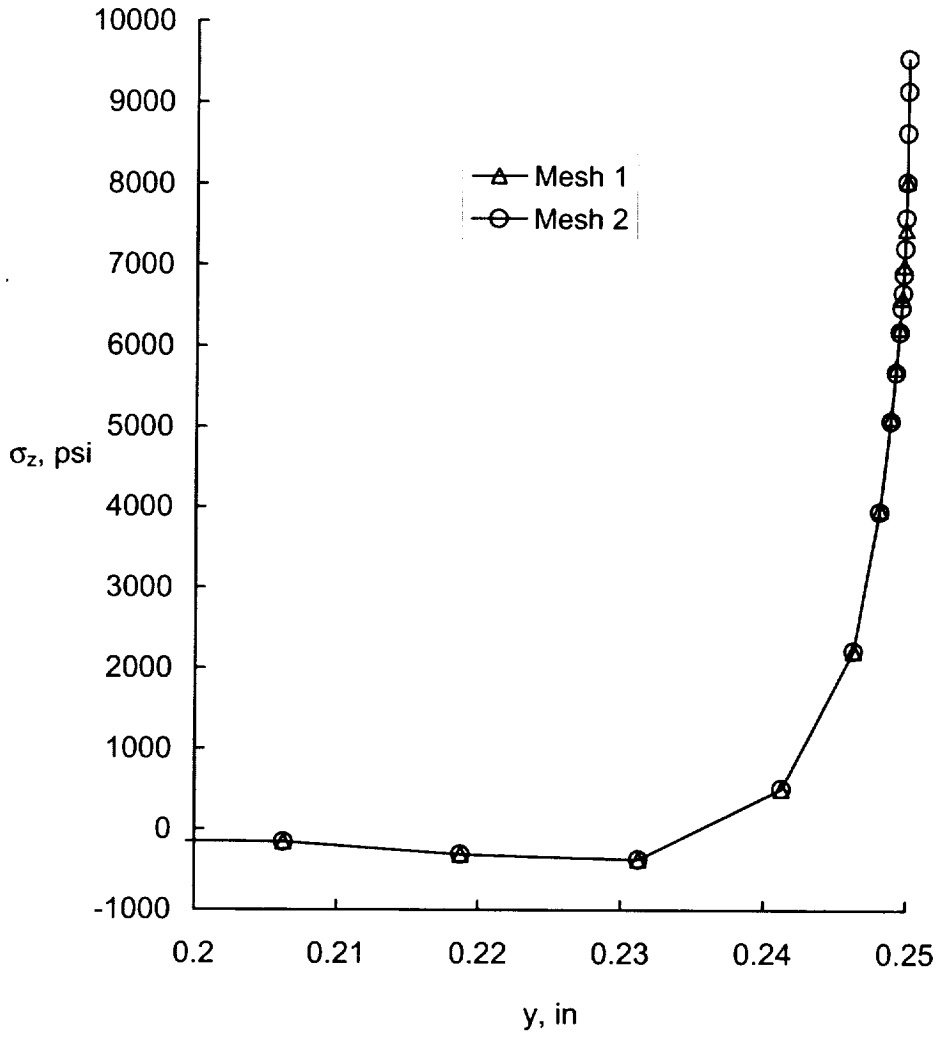

Figure 3.19. Interlaminar normal stress in $[90,0]_{8s}$ laminate including resin layers, subject to applied displacement, plotted along the z=0 and x=0 symmetry planes.

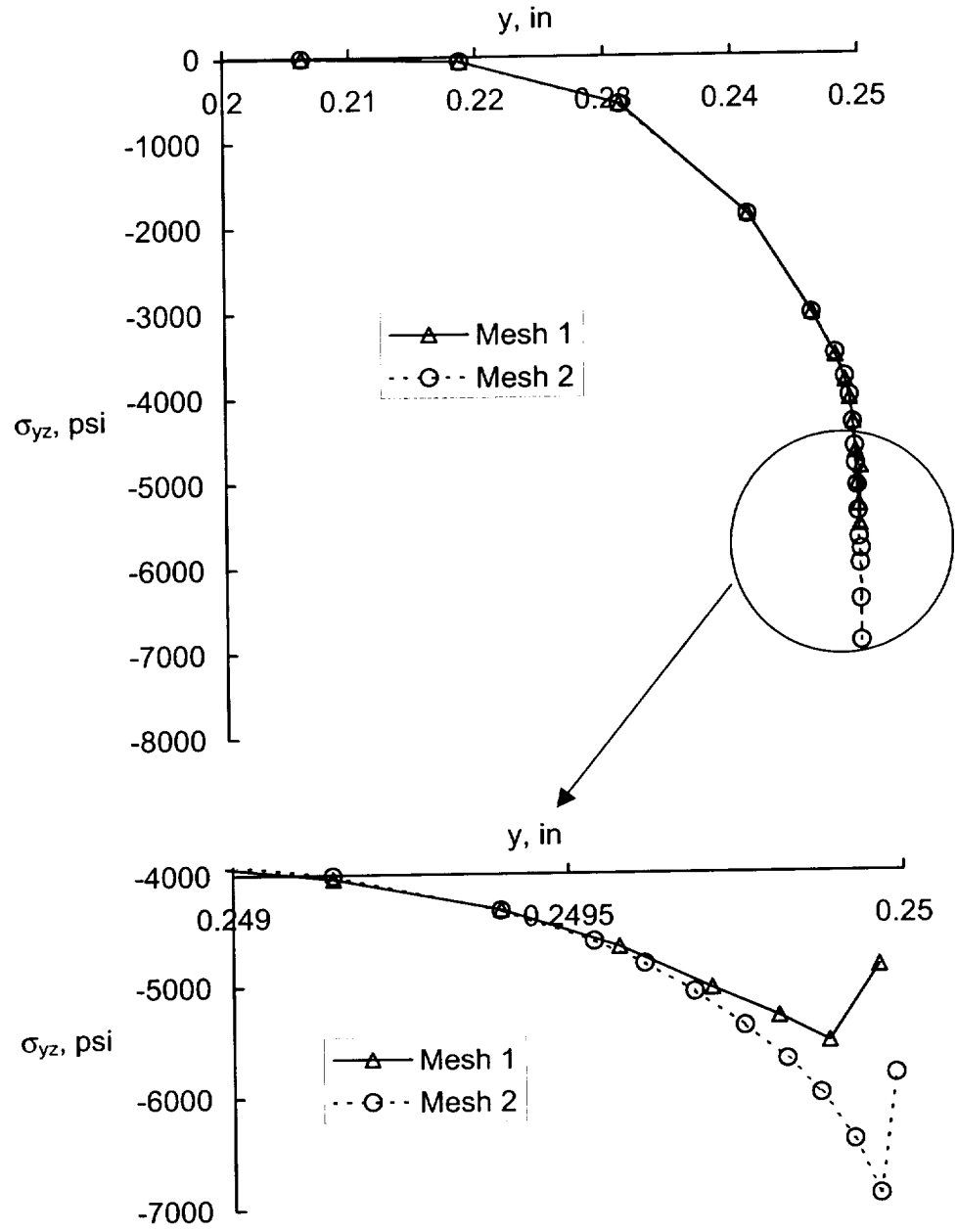

Figure 3.20. Interlaminar shear stress in $[90,0]_{8s}$ laminate including resin layers, subject to applied displacement, plotted along x=0 and the interface of the first resin layer and 90 degree ply closest to z=0.

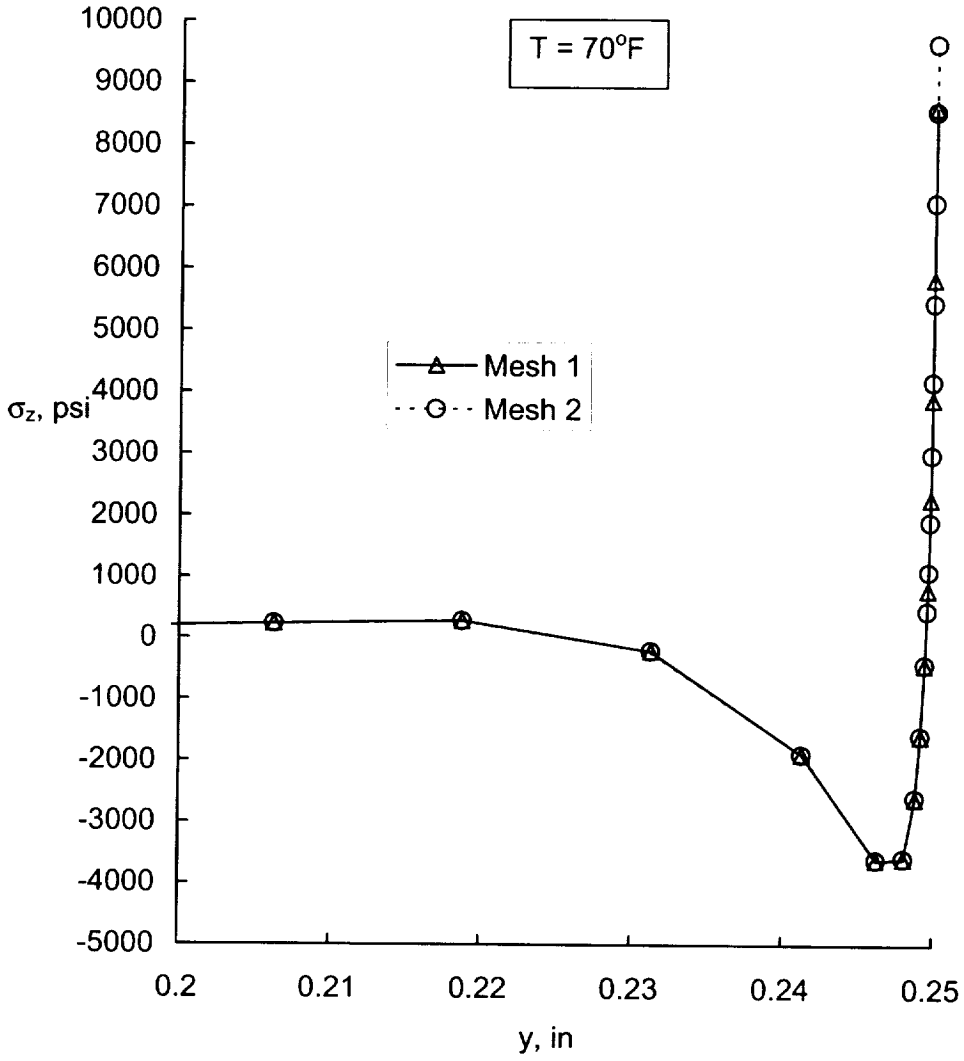

Figure 3.21. Interlaminar normal stress in $[90,0]_{8s}$ laminate at 70°F due to curing only, plotted along x=0 in the 90° ply at the interface of the first resin layer and 90 degree ply closest to z=0.

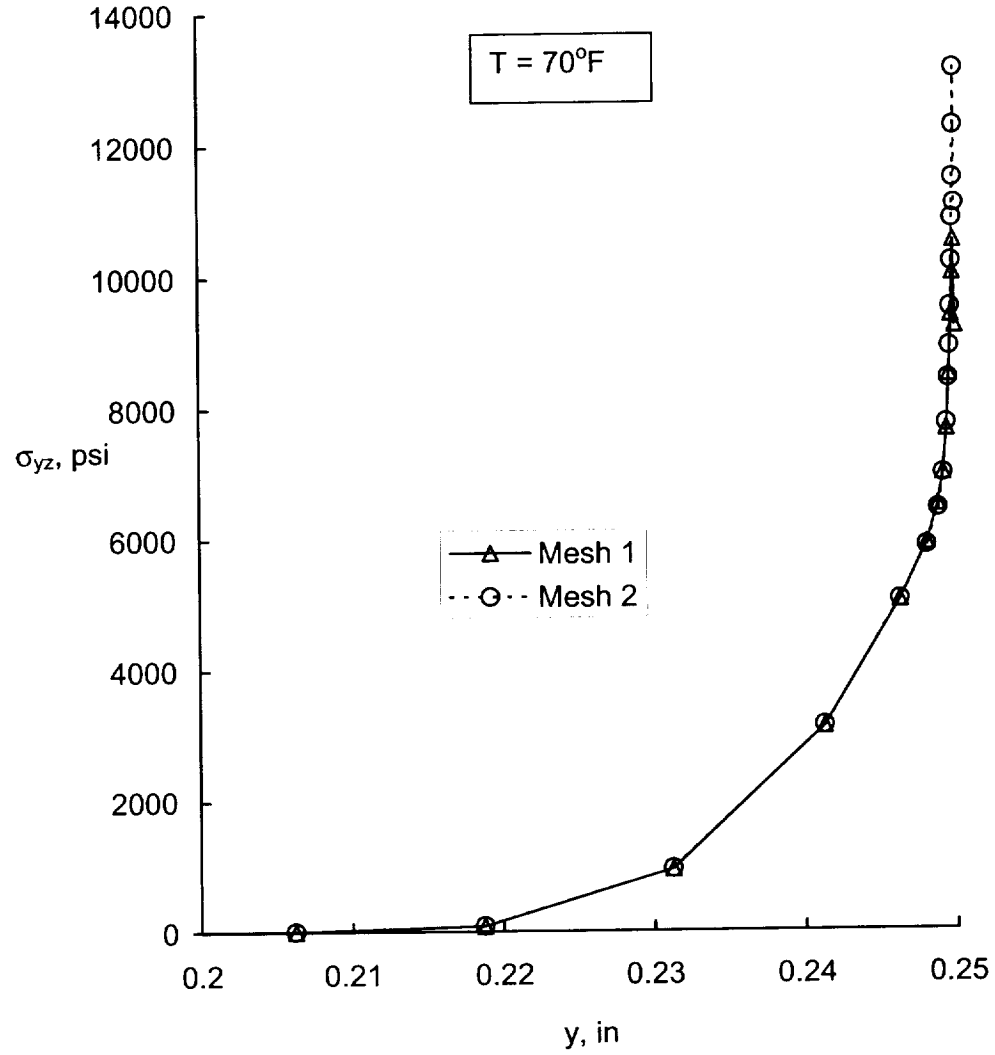

Figure 3.22. Interlaminar shear stress in $[90,0]_{8s}$ laminate at 70°F due to curing only, plotted along x=0 in the resin layer at the interface of the first resin layer and 90 degree ply closest to z=0.

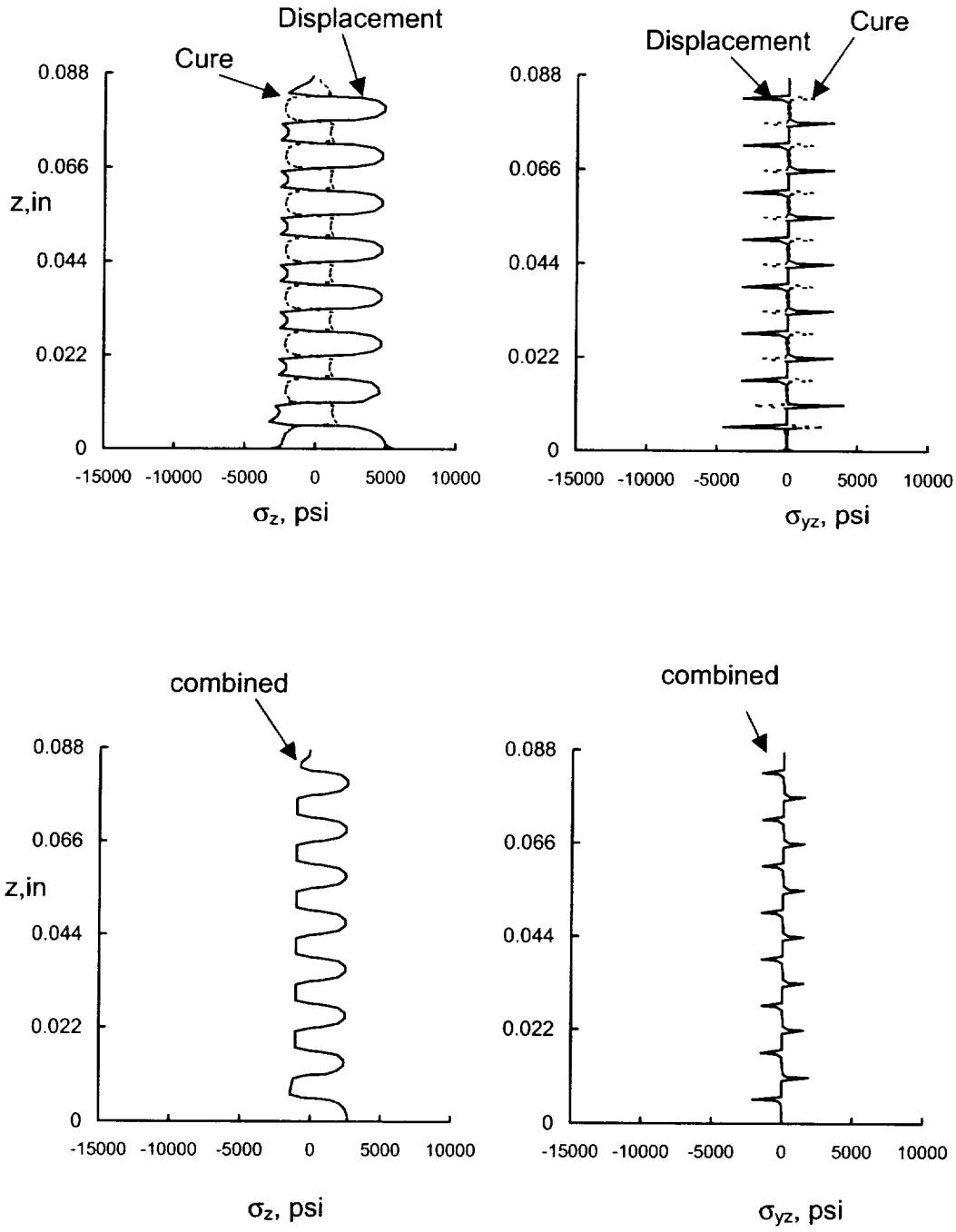

Figure 3.23. Interlaminar stresses through the thickness of the laminate two elements away from free edge at T=350°F.

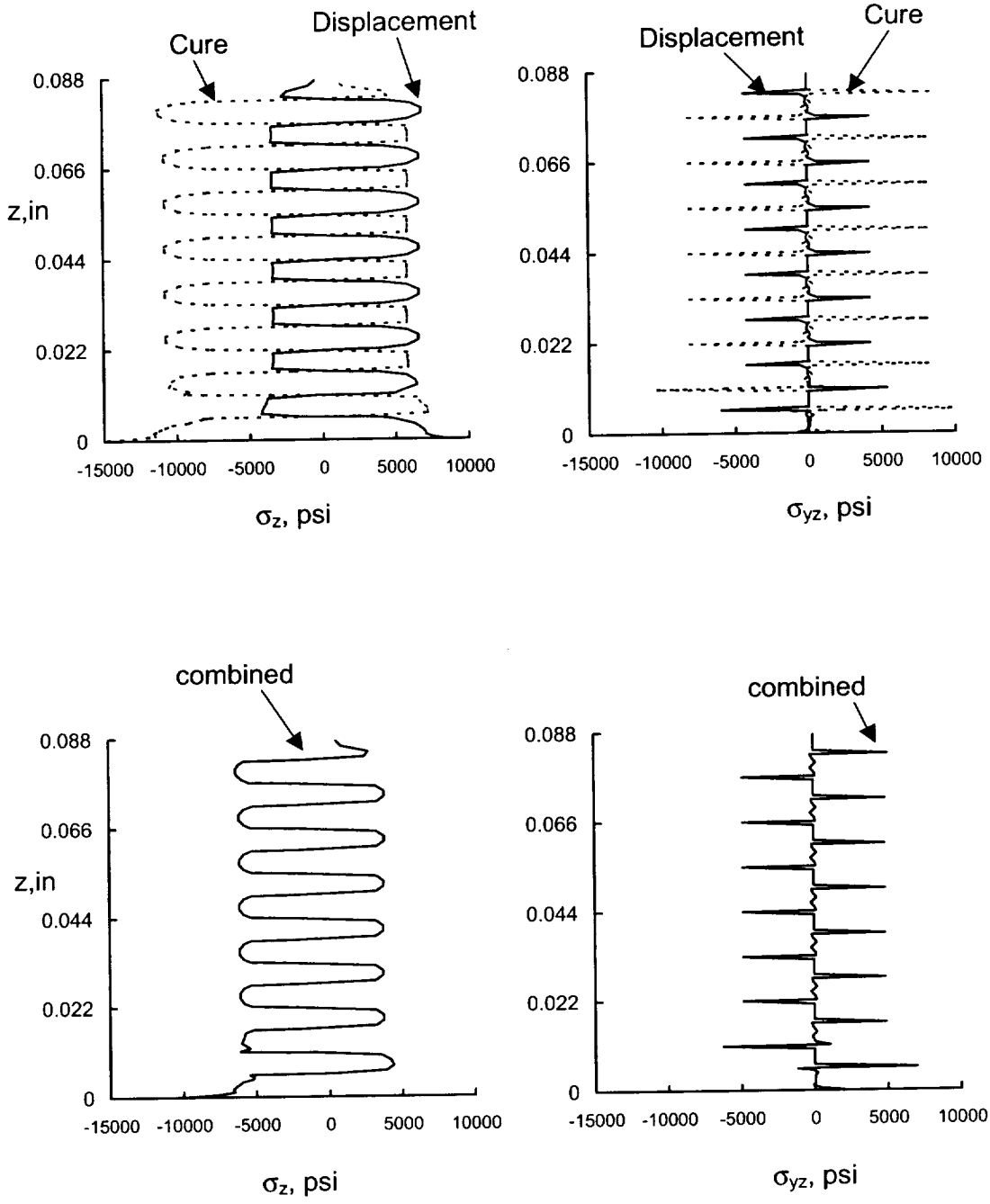

Figure 3.24. Interlaminar stresses through the thickness of the laminate two elements away from free edge at T=70°F.

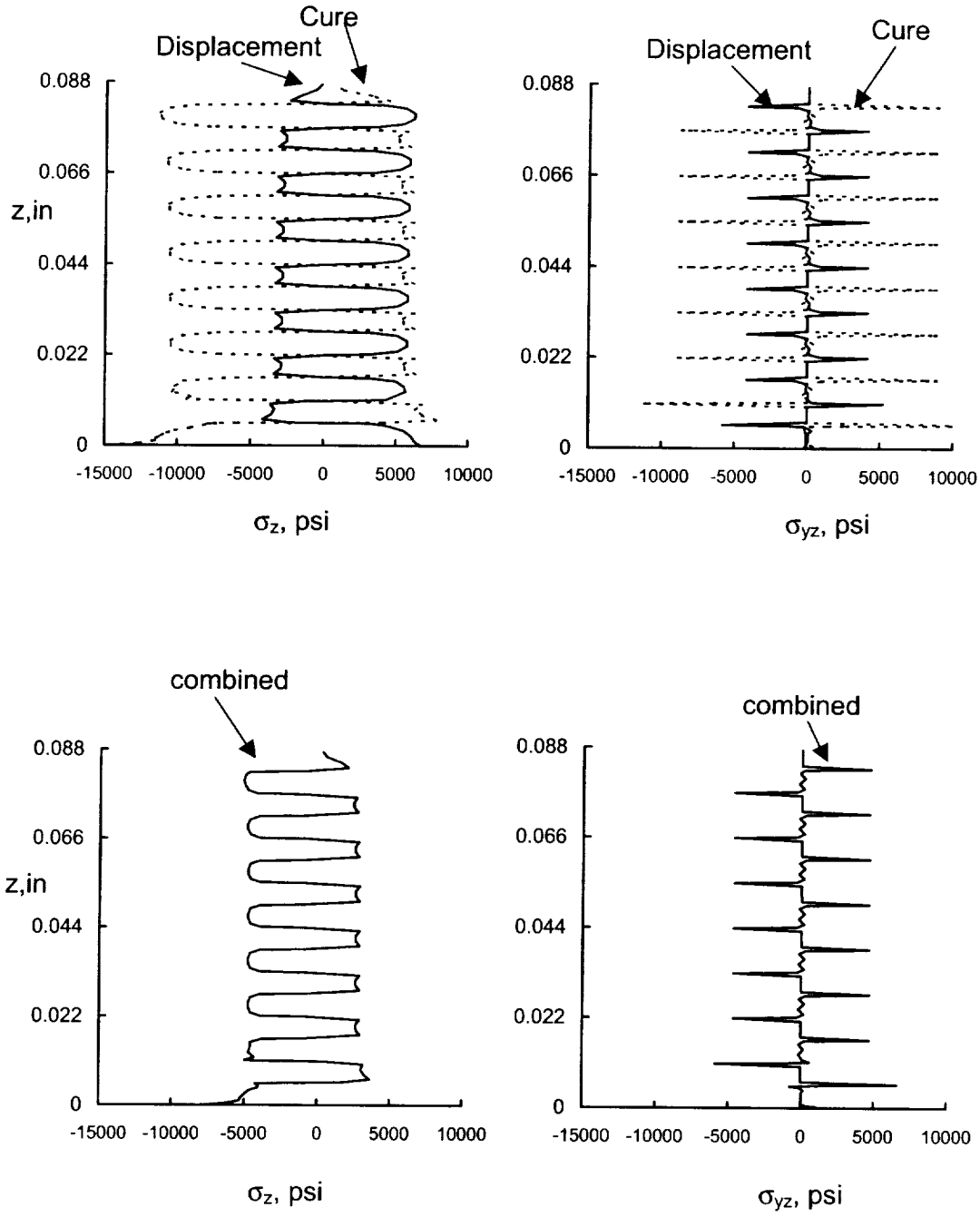

Figure 3.25. Interlaminar stresses through the thickness of the laminate two elements away from free edge at T=-200°F.

Chapter 4
Pin-Bearing Tests

An experimental investigation on the effect of temperature changes on the pin-bearing strength is pursued to establish the extent of bearing strength changes with a change in temperature for the IM7/PETI5 material system. Several lay-ups were investigated to observe the effect of lay-up on the extent of the strength change and to establish a possible optimal lay-up for maximum strength at varying temperatures. The test data for the $[90,0]_{8s}$ lay-up is utilized for validation of the computational model through qualitative comparison of experimental strength changes with temperature compared to changes in the state of stress at the bolt hole of the pin-bearing computational model with a change in temperature. Within this chapter the test procedure is described, followed by test configuration and mechanical operation, the test specimen details, and finally the test results.

4.1 Test Procedure

The pin-bearing tests were conducted within the guidelines of the American Society of Testing and Materials (ASTM) standard for determining the bearing response of a polymer matrix composite laminate.[4.1] The ASTM test method was also consistent with the recommendations of MIL-HDBK-17.[4.2] The double shear tensile loading procedure was chosen to provide pin bearing loads on a flat, rectangular composite laminate coupon with a centerline hole. The thickness of the composite at the hole boundary and the hole diameter are measured prior to testing. The composite laminate coupon is loaded at the hole in bearing as illustrated in Figure 1.4. The bearing load is applied through a close tolerance pin that is reacted in double shear by the fixture, creating a symmetric loading condition through the thickness of the composite laminate hole. The load is applied to the composite laminate specimen while both the load and hole deformation are monitored. The test is terminated when a maximum load has clearly been reached, and the load is removed immediately so as not to mask the initiation failure characteristics with additional damage. The bearing stress versus bearing strain is plotted and the failure mode is noted. The ultimate bearing strength is determined from the maximum load and the ultimate bearing strain is determined after correcting the strain data for the new effective origin as will be described later is Section 4.3.

4.2 Test Configuration and Operation

A schematic drawing of the test configuration is shown in Figure 4.1. A similar configuration was used by Crews in 1986 and later modified by Wright in 1997.[4.3,4.4] The test components shown in the figure include the test specimen, the pin for applying the bearing load to the test specimen, the extensometer and measurement wire for measuring the bolt hole elongation, and the clevis and grip which are the fixtures connecting the specimen to the test machine. The pin-bearing load is reacted in double shear by the clevis which is attached to the load frame while the end of the specimen constrained by the bolted grip is held

fixed. Photographs of the test configuration in the 22kip test machine, surrounded by the environmental test chamber, are shown in Figure 4.2.

The pin used for applying the bearing load is made of Vascomax C-300 steel.[4.4] The pin material was chosen for its high strength characteristics and ability to transfer high bearing loads without the possibility of pin failure during testing. The manufacturer's available pin properties of interest included,

$d = 0.249$ in
$E_p = 27.5 \times 10^6$ psi
$\alpha_p = 5.6 \times 10^{-6}$ in/in/F
$F_{CY} = 317.$ ksi
$F_{TY} = 290.$ ksi at T=70°F and $F_{TY} = 245.$ ksi at T = 600°F

The pin that goes through the specimen bolt hole is also placed through clearance fit bolt holes on both sides of a steel clevis in a double shear arrangement. An attachment rod connects the clevis with the load frame. The lower end of the specimen is held constrained with a steel bolted grip which is also connected to the test machine with an attachment rod as can be seen in the photograph in Figure 4.2. A 30 ft-lb torque was used for all six grip bolts.

The extensometer and measurement wire are used to measure the bolt hole elongation during testing. The measurement wire is made of 0.060 inch diameter stainless steel wire. A high temperature epoxy adhesive is used to fastener one end of the wire in the slot machined to fit the wire in the unloaded, bottom portion of the specimen bolt hole, and the other end of the wire is attached to the extensometer. The extensometer measures the relative displacement between its two arms. One arm is attached to the end of the clevis as shown in Figure 4.1 where the other arm attaches to the measurement wire. Assuming negligible pin bending, the displacement of the loaded top of the bolt hole is measured relative to the unloaded end where the measurement wire is fastened, giving the bolt hole elongation.

The environmental test chamber with the door open can be seen in the Figure 4.2 photograph, wherein the specimen is either convectively heated or cooled to the desired test temperature prior to applying the mechanical bearing load. For the –200°F and 350°F temperature tests, three thermocouples are monitored, one on each side of the specimen nearly adjacent to the bolt hole and one located on the clevis. After approximately one hour, when all thermocouple temperatures remain steady within two degrees of the desired operating temperature, the mechanical loading is applied to the specimen. The test machine is operated by displacing the clevis at a rate of 0.004 in/min while the mechanical load and bolt hole elongation are measured and recorded each second. The test is terminated at the onset of failure as observed by an obvious drop in the load.

4.3 Test Specimens

The composite laminate test specimens for the pin-bearing tests were designed with 32 plies to transfer large loads and hence be representative of a

joint in a high speed aircraft wing or launch vehicle intertank. The objective was also to design the specimens with sufficient edge, e, and width, w, distances to fail in the bearing mode for all test temperatures and eliminate premature failure by shearout or tension, seen in Figure 1.6. The test specimen geometry is shown in Figure 4.3. The length, L= 8 inches, was chosen to provide adequate gripping area to prevent any slipping on the fixed end of the specimen. The bolt holes were drilled in the specimens by first drilling under the specified diameter, D, and then reaming to size. A small hole of diameter 0.063 inch was also drilled adjacent to the bolt hole as shown, where the material between the small hole and bolt hole was then filed away to allow insertion of the measurement wire through the bolt hole. A specimen width, W = 2 inches, was used for all specimens except the specimens fabricated from the $[90]_{32}$ lay-up, where W= 4 inches, in an attempt to avoid a tension failure in these specimens with low tensile strength. A photograph of a 2. inch wide pin bearing test specimen is provided in Figure 4.4.

Pin-bearing specimens were made using five different laminate lay-ups as defined in Table 4.1. For each lay-up, three 12 in by 12 inch panels were fabricated where five replicate specimens were made from each panel. A total of 105 pin-bearing test specimens were fabricated for the pin bearing experiments.

4.4 Test Results

The pin-bearing experiments were conducted to determine the pin-bearing strength for all lay-ups tested at the three operating temperatures of 350°F, 70°F, and -200°F. The pin-bearing stress – bearing strain curve for one of the $[90,0]_{8s}$ laminates tested at 70°F is shown in Figure 4.5. This curve was typical for all specimens tested successfully. The pin-bearing stress is calculated as

$$\sigma_{br} = \frac{P}{Dt} \tag{4.1}$$

where P is the measured load transmitted , D is the bolt hole diameter, and t is the bolt hole thickness. The pin-bearing strain is calculated as

$$\varepsilon_{br} = \frac{\delta}{D} \tag{4.2}$$

where δ is the bolt hole elongation measured by the extensometer. The ultimate bearing strength is then determined as

$$F_{bru} = \frac{P_{max}}{Dt} \tag{4.3}$$

where P_{max} is the maximum load attained during testing. The ultimate bearing strain is determined as

$$\varepsilon_{bru} = \varepsilon_{brrmax} - \varepsilon_0 \tag{4.4}$$

where ε_{brrmax} is the bearing strain at the maximum load, and ε_0 is the bearing strain at the effective origin. In accord with the ASTM standard, an effective origin is computed from the initial linear portion of the stress-strain curve as illustrated in Figure 4.5. The initial nonlinearity is typical of a bearing test and attributable to initial joint translations and straightening.[4.1] The effective origin is computed from

the chord stiffness line intersection with the bearing strain axis. Similar to ε_{bru}, the bearing strain, ε_{bry}, is determined from the bearing yield strength, F_{bry}.

For the $[90,0]_{8s}$ specimens tested, in addition to the ultimate bearing strength, the ultimate bearing strain, bearing chord modulus, and bearing yield strength and bearing yield strain were also computed for comparison with the analysis models developed in Chapter 5. The chord modulus, E_{br}, is calculated from the slope of the linear portion of the stress-strain curve, where the curve between σ_{br} = 25 ksi and σ_{br} = 40 ksi is used in this report. For several specimens, the extensometer did not function properly during testing, but the ultimate bearing stress was still determinable. The test data for all specimens of Layup 1, the $[90,0]_{8s}$ laminate, is presented in Table 4.2. Also calculated are the average values for F_{bru}, ε_{bru} , and E_{br}. The ultimate bearing strength, F_{bru}, data for Layup 2, 3, 4, 5, 0, and 90 is presented in Tables 4.3- 4.8, respectively. Also presented in Tables 4.3-4.8 are the failure modes for each specimen.

Excluding the $[0]_{32}$ and $[90]_{32}$ lay-ups, all specimens tested failed in the bearing mode as illustrated in Figure 1.6, which was the desired failure mode for these tests. Some of the $[0]_{32}$ specimens failed in the shearout mode, and the number at -200°F that failed in shearout was greater than at 70°F, but no specimens tested at 350°F failed in shearout. This indicates that decreasing temperature increases the likelihood of the shearout mode, whereas as temperature increases, bearing strength decreases and the bearing failure mode becomes more likely. Although the $[90]_{32}$ specimens were made twice as wide as all other specimen, that was still not sufficient and most $[90]_{32}$ specimens failed in the tension mode, which would be expected for the $[90]_{32}$ specimens with low tensile strength.

The average ultimate bearing strength data for all specimens is plotted in Figure 4.6. Error bars show the range of values associated with the plotted average value. From this curve, it is obvious that for specimens that failed in the bearing mode, the bearing strength increases with decreasing temperature for all the lay-ups tested. Although the average bearing strength of Layup 3 was the greatest at all temperatures, due to the range in values at each temperature, it is not clear that this $[+45,-45,0,90]_{4S}$ quasi-isotropic lay-up is necessarily the optimum lay-up. Layup 1, with a $[90,0]_{8s}$ lay-up and Layup 4 with a $[+45,0,-45,90]_{4S}$ lay-up also faired well with the range of bearing strengths measured overlapping Layup 3. For the $[90]_{32}$ lay-up which failed in the tension mode, the strength remained almost constant as does the tensile strength of the material with varying temperature.

Further evaluation of some failed specimens included having the specimens carefully cut along the bearing load line for observation under a microscope. To observe internal damage, the specimens were cut along the dashed lines illustrated in Figure 4.7. Specimens where the external damage was minimally visible from Layup 1, 3, 4, and 5 were chosen to observe internal failure initiation characteristics. For Layup 1, the $[90,0]_{8s}$ laminate, specimens c-1, b-5 and a-4, as identified in Table 4.2, were evaluated. All three specimens have very similar internal failure characteristics. A series of three micrographs of

specimen c-1, tested at –200°F, with a nearly 50 times magnification, is presented in Figure 4.8. Extreme damage is evident in the outermost plies, with a transverse shear crack emanating from that region. These failure characteristics were also observed within specimens b-5 and a-4. The micrographs indicate the possibility of failure initiating in the $[90,0]_{8s}$ specimens due to the interlaminar shear stress at all test temperatures. These observations will be compared with pin-bearing analysis results in Chapter 5, to determine if there is any correlation with significant stresses predicted with the analysis model.

Several observations can be made in comparing the average pin-bearing ultimate strengths from Tables 4.2-4.6 to the corresponding laminate strengths presented in Table 2.1. First, pin-bearing strength is observed to be significantly lower than the corresponding laminate compressive strength in most cases. Only for Layup 3 and 4 at –200°F pin-bearing strength was greater and for Layup 4 at 70°F pin-bearing strength and laminate strength were equivalent. Also, the extent of pin-bearing strength degradation in the temperature range from 70°F to 350°F is observed to be lower than the laminate strength degradation for Layup 1 and 5, but the opposite is true for all other lay-ups in Table 2.1, where the pin-bearing strength degradation was greater than the laminate strength degradation. With a temperature decrease in the temperature range from 70°F to –200°F, the pin-bearing strength increase was greater than the laminate strength increase for all lay-ups. Although both laminate strength and pin-bearing strength similarly decrease with an increase in temperature, the extent of the laminate strength change differs from pin-bearing strength change. In general, the extent of both laminate strength change and pin-bearing strength change with a change in temperature is dependent on the lay-up of the IM7/PETI5 material and the temperature range.

4.5 References

4.1 Annual Book of ASTM Standards, Sec.15, Vol. 15.03, D5961M-96,1996, p. 310-323.

4.2 MIL-HDBK-17, Military Handbook, Polymer Matrix Composites, Vol. 1. Guidelines, U.S. Dept. of Defense, 1994.

4.3 Crews, J.H. and Naik, R.V.A.: Failure Analysis of a Graphite/Epoxy Laminate Subjected to Bolt-Bearing Loads, *Composite Materials: Fatigue and Fracture, ASTM STP 907*, American Society of Materials , Philadelphia, 1986, pp. 115-133.

4.4 Wright, R.J.; Johnson, W.S.; and Ahmad, H.: Bolt Bearing Behavior of Highly Loaded Composite Joints at Elevated Temperatures with and without Clampup. Department of Material Science and Engineering, Georgia Institute of Technology, Atlanta, Georgia,1997.

4.5 Teledyne Vasco, P.O. Box 151, LaTrobe, PA, 1982.

Table 4.1 Test Matrix – Pin-bearing Specimens.

LAY-UP	ID	W (in)	Test Temperature (^{o}F)	No. of Specimens
$(90,0)_{8s}$	1	2	-200	5
			70	5
			350	5
$(+45,-45)_{8s}$	2	2	-200	5
			70	5
			350	5
$(+45,-45,0,90)_{4S}$	3	2	-200	5
			70	5
			350	5
$(+45,0,-45,90)_{4S}$	4	2	-200	5
			70	5
			350	5
$(+45,0_2,-45,0_2,+45,0_2,-45,0_2,+45,90_2,-45)_s$	5	2	-200	5
			70	5
			350	5
$(0)_{32}$	0	2	-200	5
			70	5
			350	5
$(90)_{32}$	90	4	-200	5
			70	5
			350	5

Table 4.2 Pin-Bearing Test Data for Layup 1 – $[90,0]_{8s}$.

T = -200°F								
1	t (in)	D (in)	P_{max} (lb)	F_{bru} (ksi)	ε_{bru} (in/in)	E_{br} (Msi)	F_{bry} (ksi)	ε_{bry} (in/in)
c-1	.168	.249	4930	117.8	---	---		
c-2	.171	.250	5005	117.1	.0475	2.88	62.	.0215
c-3	171	.249	5417	127.2	.0510	2.97	62.	.0209
c-4	.172	.249	5094	118.9	.0560	2.51	64.	.0255
c-5	.171	.249	5412	127.1	.0610	2.50	65.	.0260
Average Value				121.6	.0539	2.72	63.	.0235
T = 70°F								
1	t (in)	D (in)	P_{max} (lb)	F_{bru} (ksi)	ε_{bru} (in/in)	E_{br} (Msi)	F_{bry} (ksi)	ε_{bry} (in/in)
a-1	.165	.252	3241	77.9	.0471	1.91	50.	.0265
a-2	.175	.249	3881	88.9	.0517	2.14	48.	.0229
a-3	.173	.249	3978	91.9	.0504	2.14	48.	.0229
b-4	.169	.249	3697	87.7	.0400	2.68	47.	.0178
b-5	.165	.249	3800	92.1	.0470	2.63	47.	.0184
Average Value				87.9	.0472	2.31	48.	.0217
T = 350°F								
1	t (in)	D (in)	P_{max} (lb)	F_{bru} (ksi)	ε_{bru} (in/in)	E_{br} (Msi)	F_{bry} (ksi)	ε_{bry} (in/in)
b-1	.169	.249	2673	63.5	.0466	1.40	41.	.0295
b-2	.166	.249	2467	59.7	---	---	---	---
b-3	.169	.249	2721	64.7	---	---	---	---
a-4	.172	.249	2623	61.2	.0459	1.32	45.	.0342
a-5	.168	.249	2646	63.3	.0477	1.48	41.	.0272
Average Value				62.5	.0467	1.40	42.	.0303

Failure Mode: All Layup 1- $[90,0]_{8s}$ specimens failed in the Bearing Mode.

Table 4.3 Pin-Bearing Test Data for Layup 2 – $[45,-45]_{8s}$.

T = -200°F					
2	t (in)	D (in)	P_{max} (lb)	F_{bru} (ksi)	Failure Mode
c-1	.167	.249	5017	121	Bearing
c-2	.178	.249	---	---	---
c-3	.180	.249	5466	122	Bearing
c-4	.179	.249	5413	121	Bearing
c-5	.174	.249	5076	117	Bearing
Average Value				120	
T = 70°F					
2	t (in)	D (in)	P_{max} (lb)	F_{bru} (ksi)	Failure Mode
a-1	.167	.249	3616	87	Bearing
a-2	.176	.249	4093	93	Bearing
a-3	.177	.249	4175	95	Bearing
a-4	.176	.249	3895	89	Bearing
a-5	.174	.249	3462	80	Bearing
Average Value				89	
T = 350°F					
2	t (in)	D (in)	P_{max} (lb)	F_{bru} (ksi)	Failure Mode
b-1	.170	.249	2499	59	Bearing
b-2	.187	.249	2750	59	Bearing
b-3	.187	.249	2487	53	Bearing
b-4	.187	.249	2830	61	Bearing
b-5	.179	.249	2221	50	Bearing
Average Value				56	

Table 4.4 Pin-Bearing Test Data for Layup 3 – $[+45,-45,0,90]_{4S}$.

T = -200°F					
3	t (in)	D (in)	P_{max} (lb)	F_{bru} (ksi)	Failure Mode
c-1	.177	.249	5450	124	Bearing
c-2	.179	.250	5680	127	Bearing
c-3	.177	.250	5408	122	Bearing
c-4	.178	.250	5647	128	Bearing
c-5	.179	.249	5534	124	Bearing
Average Value				125	
T = 70°F					
3	t (in)	D (in)	P_{max} (lb)	F_{bru} (ksi)	Failure Mode
a-1	.166	.249	4136	100	Bearing
a-2	.177	.249	4440	101	Bearing
a-3	.178	.249	4146	94	Bearing
a-4	.177	.249	4557	101	Bearing
a-5	.181	.249	3573	79	Bearing
Average Value				95	
T = 350°F					
3	t (in)	D (in)	P_{max} (lb)	F_{bru} (ksi)	Failure Mode
b-1	.169	.249	2777	57	Bearing
b-2	.170	.249	2829	67	Bearing
b-3	.173	.250	2671	62	Bearing
b-4	.173	.249	2758	64	Bearing
b-5	.179	.249	2811	63	Bearing
Average Value				63	

Table 4.5 Pin-Bearing Test Data for Layup 4 – $[+45,0,-45,90]_{4S}$.

T = -200°F					
4	t (in)	D (in)	P_{max} (lb)	F_{bru} (ksi)	Failure Mode
c-1	.174	.250	5394	124	Bearing
c-2	.184	.249	5854	128	Bearing
c-3	.185	.250	5708	123	Bearing
c-4	.184	.249	5696	124	Bearing
c-5	.184	.250	5759	125	Bearing
Average Value				125	
T = 70°F					
4	t (in)	D (in)	P_{max} (lb)	F_{bru} (ksi)	Failure Mode
a-1	.164	.249	3685	90	Bearing
a-2	.180	.249	4203	94	Bearing
a-3	.182	.249	4300	95	Bearing
a-4	.170	.250	4205	99	Bearing
a-5	.158	.250	3531	89	Bearing
Average Value				93	
T = 350°F					
4	t (in)	D (in)	P_{max} (lb)	F_{bru} (ksi)	Failure Mode
b-1	.171	.250	2168	51	Bearing
b-2	.172	.250	2613	61	Bearing
b-3	.174	.247	2714	63	Bearing
b-4	.181	.249	2324	52	Bearing
b-5	.177	.249	1775	40	Bearing
Average Value				53	

Table 4.6 Pin-Bearing Test Data for Layup 5 – $[+45,0_2,-45,0_2,+45,0_2,-45,0_2,+45,90_2,-45]_s$.

T = -200°F					
5	t (in)	D (in)	P_{max} (lb)	F_{bru} (ksi)	Failure Mode
c-1	.168	.250	4511	107	Bearing
c-2	.180	.249	5141	115	Bearing
c-3	.181	.250	4916	109	Bearing
c-4	.181	.251	4976	110	Bearing
c-5	.172	.249	5056	118	Bearing
Average Value				112	
T = 70°F					
5	t (in)	D (in)	P_{max} (lb)	F_{bru} (ksi)	Failure Mode
a-1	.167	.249	3477	84	Bearing
a-2	.178	.249	3914	88	Bearing
a-3	.184	.250	3986	87	Bearing
a-4	.176	.249	3980	91	Bearing
a-5	.162	.250	3426	85	Bearing
Average Value				87	
T = 350°F					
5	t (in)	D (in)	P_{max} (lb)	F_{bru} (ksi)	Failure Mode
b-1	.175	.249	2307	53	Bearing
b-2	.185	.249	2340	51	Bearing
b-3	.186	.250	2593	56	Bearing
b-4	.180	.250	2370	53	Bearing
b-5	.169	.250	2338	55	Bearing
Average Value				54	

Table 4.7 Pin-Bearing Test Data for Layup 0 – $[0]_{32}$.

T = -200°F					
0	t (in)	D (in)	P_{max} (lb)	F_{bru} (ksi)	Failure Mode
c-1	.156	.250	3780	97	Shearout
c-2	.176	.250	4252	97	Shearout
c-3	.182	.249	4177	92	Shearout
c-4	.181	.250	4348	96	Shearout
c-5	.174	.250	3514	80	Bearing
Average Value				93	
T = 70°F					
0	t (in)	D (in)	P_{max} (lb)	F_{bru} (ksi)	Failure Mode
a-1	.177	.250	2964	67	Bearing
a-2	.185	.250	3238	70	Shearout
a-3	.182	.250	3320	73	Bearing
a-4	.179	.250	3197	71	Shearout
a-5	.162	.249	2762	68	Shearout
Average Value				70	
T = 350°F					
0	t (in)	D (in)	P_{max} (lb)	F_{bru} (ksi)	Failure Mode
b-1	.160	.249	1535	39	Bearing
b-2	.177	.250	1539	35	Bearing
b-3	.184	.251	1635	35	Bearing
b-4	.182	.250	1717	37	Bearing
b-5	.176	.250	1604	36	Bearing
Average Value				36	

Table 4.8 Pin-Bearing Test Data for Layup 90 – $[90]_{32}$

T = -200°F					
90	t (in)	D (in)	P_{max} (lb)	F_{bru} (ksi)	Failure Mode
c-1	.175	.249	969	22	Tension
c-2	.175	.249	1009	23	Tension
c-3	.175	.249	962	22	Tension
c-4	.186	.249	1118	24	Tension
c-5	.188	.249	1344	29	Tension
Average Value				24	
T = 70°F					
90	t (in)	D (in)	P_{max} (lb)	F_{bru} (ksi)	Failure Mode
a-1	.183	.249	1198	26	Tension
a-2	.184	.249	1190	26	Tension
a-3	.181	.249	1233	27	Bearing
a-4	.184	.249	1153	25	Tension
a-5	.185	.249	1080	23	Bearing
Average Value				25	
T = 350°F					
90	t (in)	D (in)	P_{max} (lb)	F_{bru} (ksi)	Failure Mode
b-1	.184	.249	1171	26	Bearing
c-2	.183	.250	1217	27	Tension
b-3	.181	.249	1207	27	Tension
b-4	.185	.249	1151	25	Tension
b-5	.186	.250	1205	26	Tension
Average Value				26	

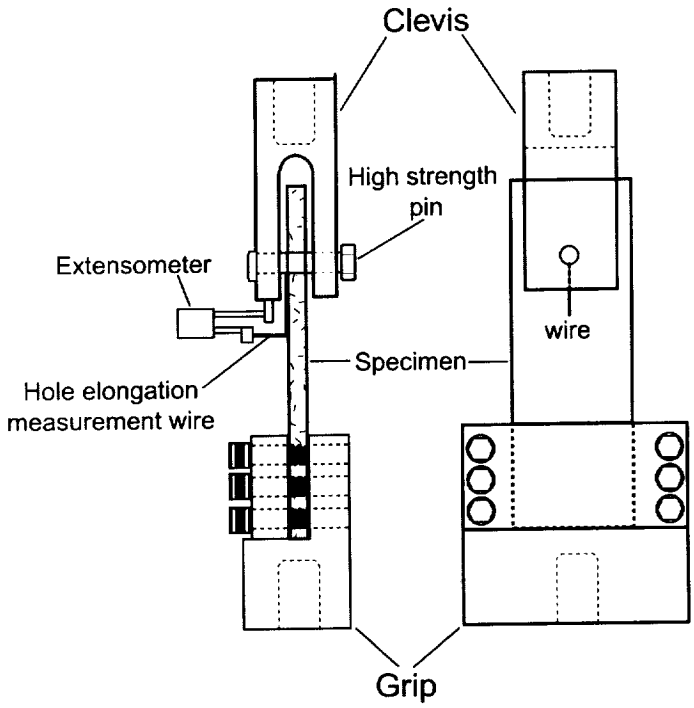

Figure 4.1. Schematic drawing of pin-bearing test configuration.

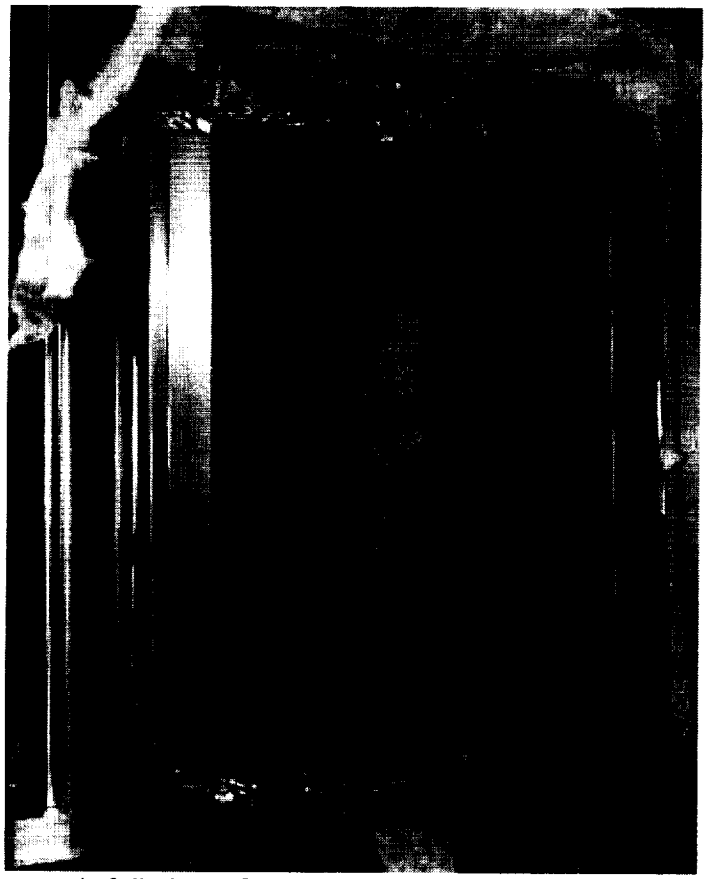

a) full view of test chamber with door open

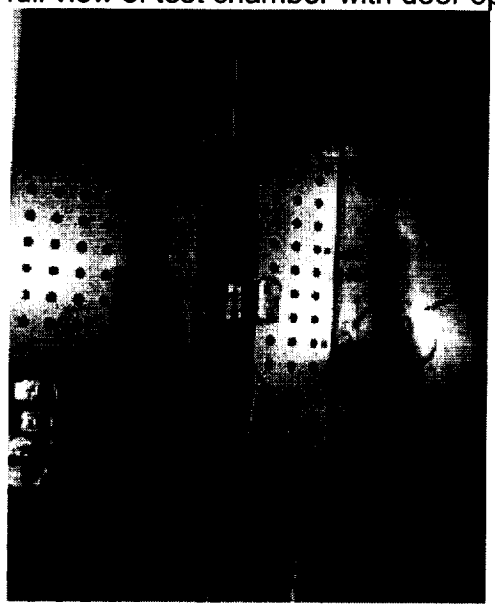

b) close-up

Figure 4.2. Photographs of test set-up in test machine.

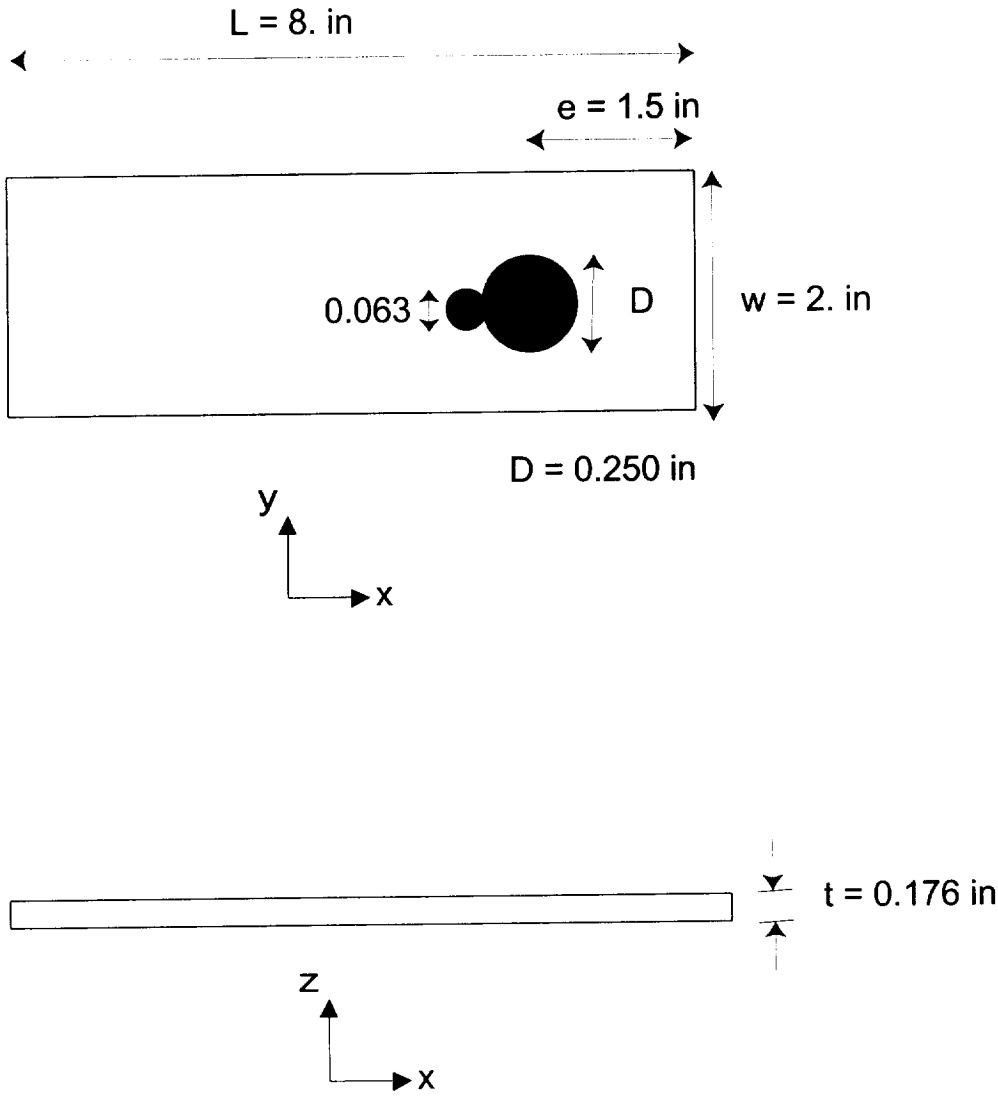

Figure 4.3. Pin-bearing test specimen geometry.

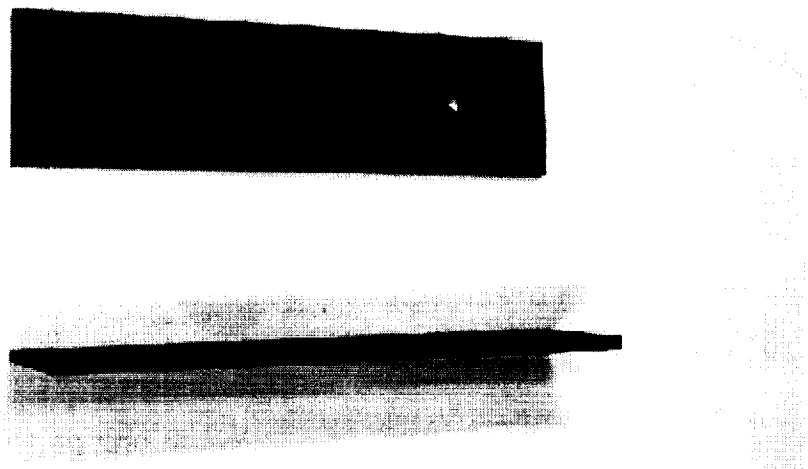

Figure 4.4. Photograph of pin-bearing test specimen.

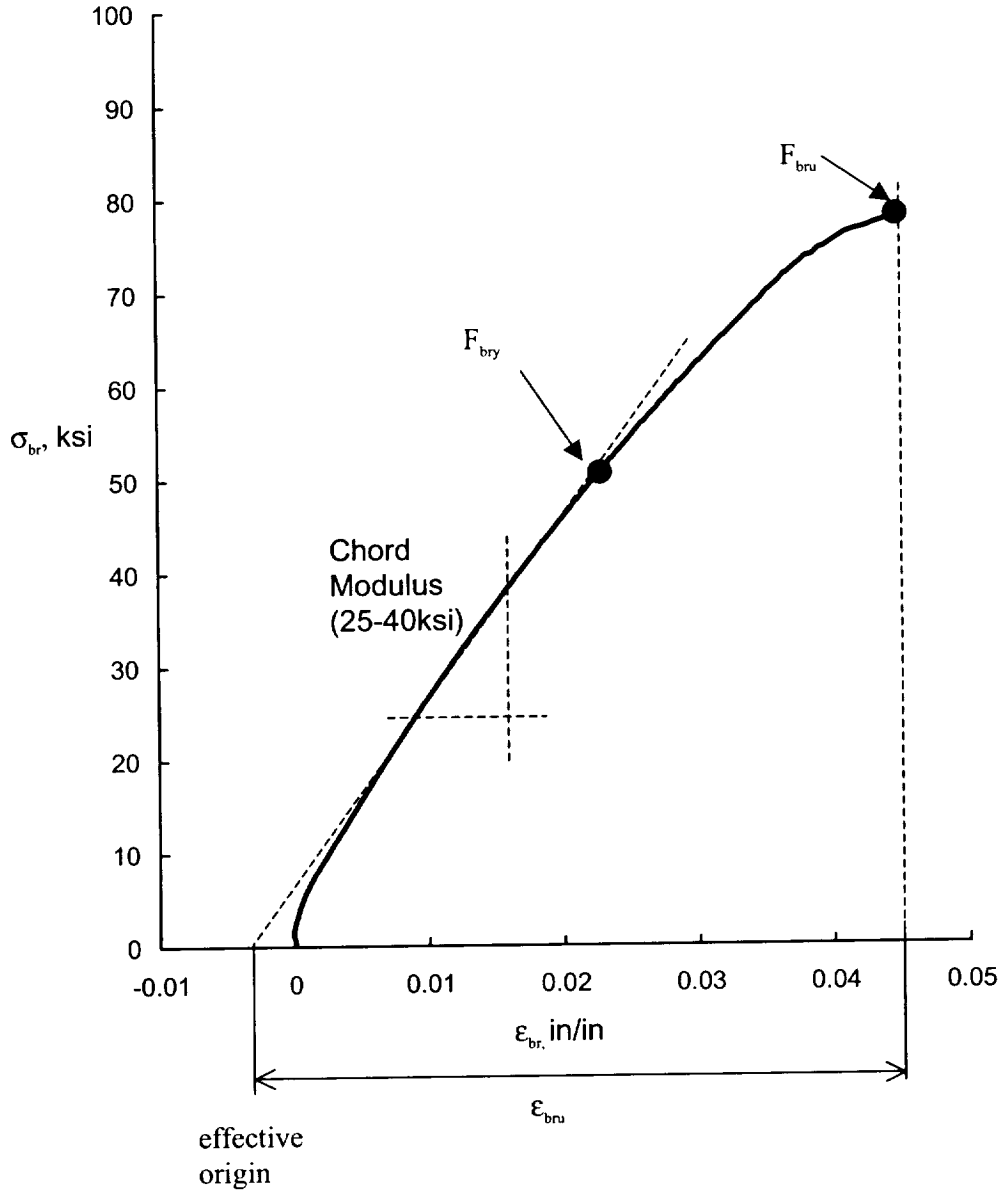

Figure 4.5. Bearing stress-strain curve for $[90,0]_{8s}$ specimen tested at 70°F.

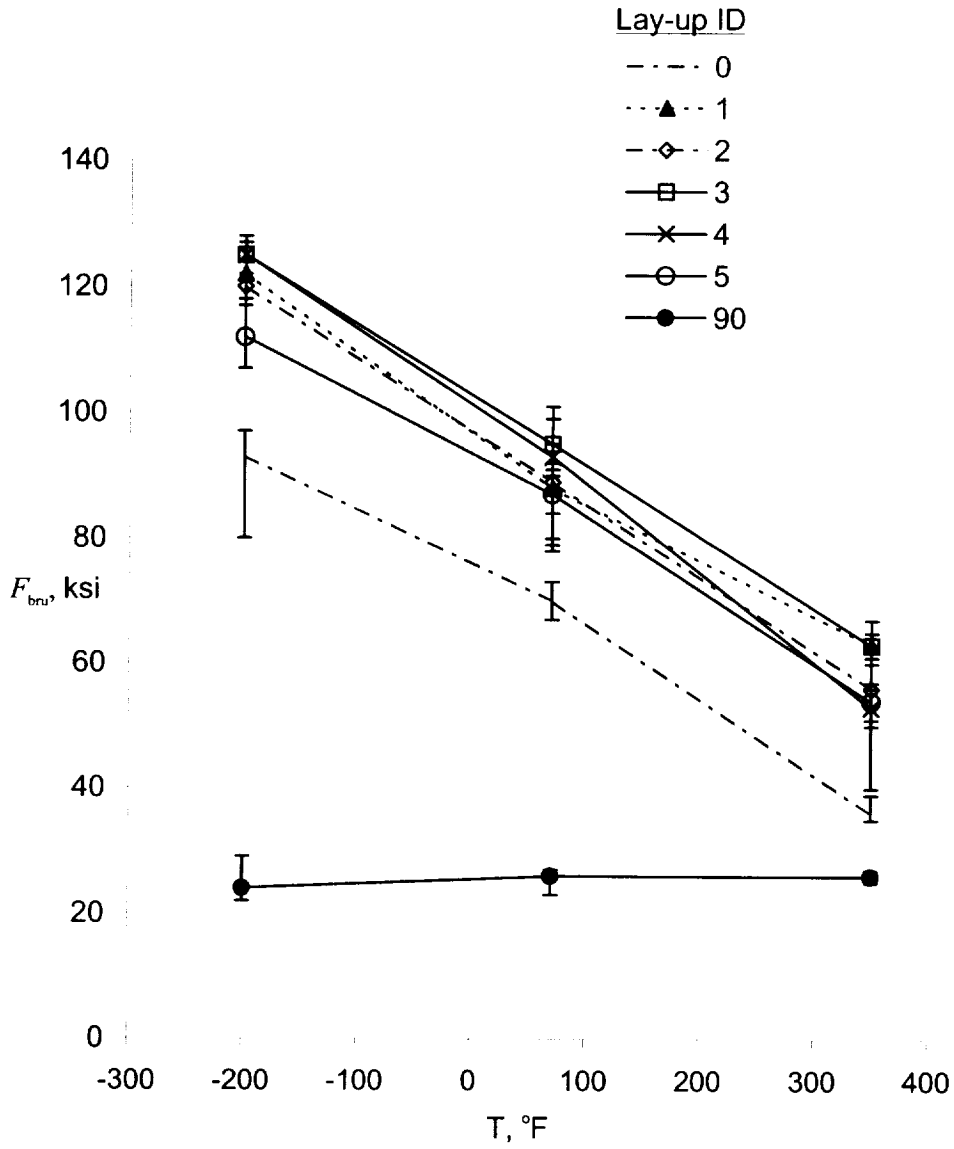

Figure 4.6. Ultimate bearing strength as determined from pin bearing testing.

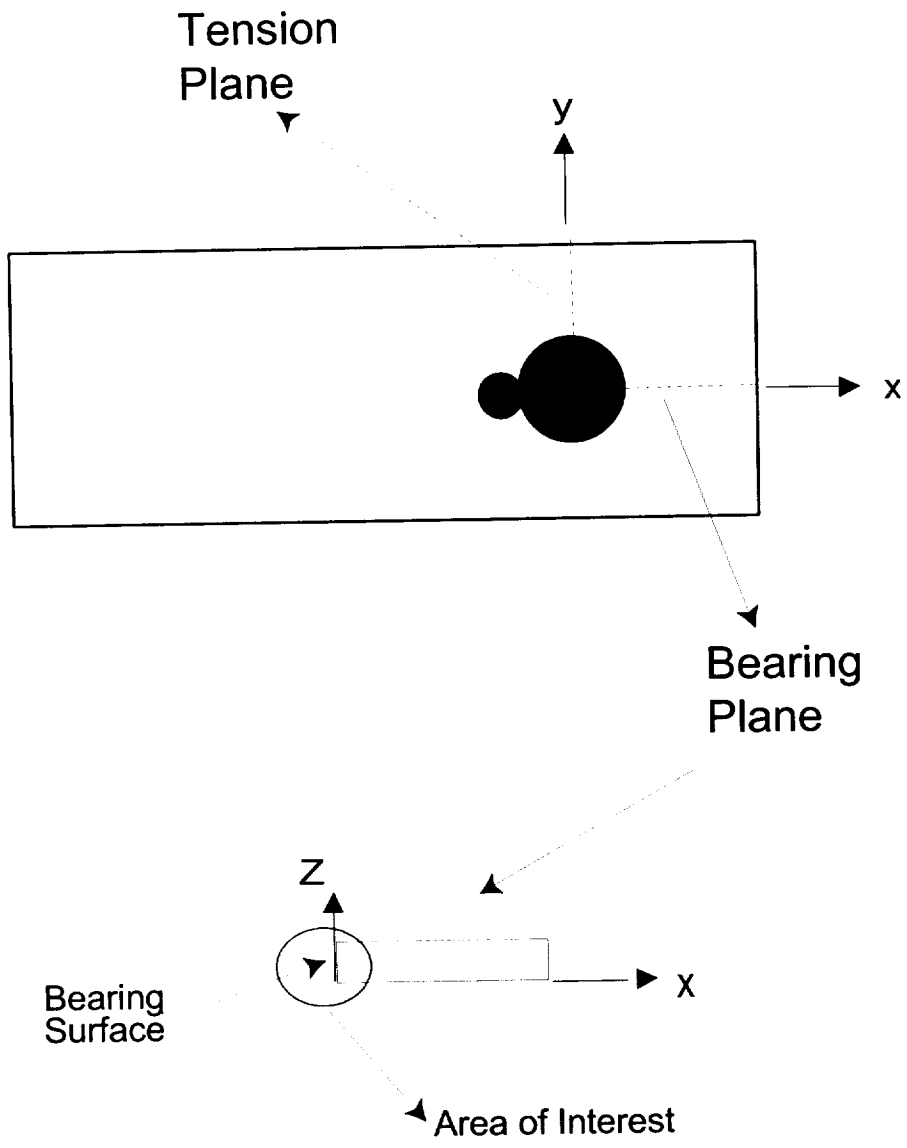

Figure 4.7. Illustration of failed specimen cut for observation of internal damage.

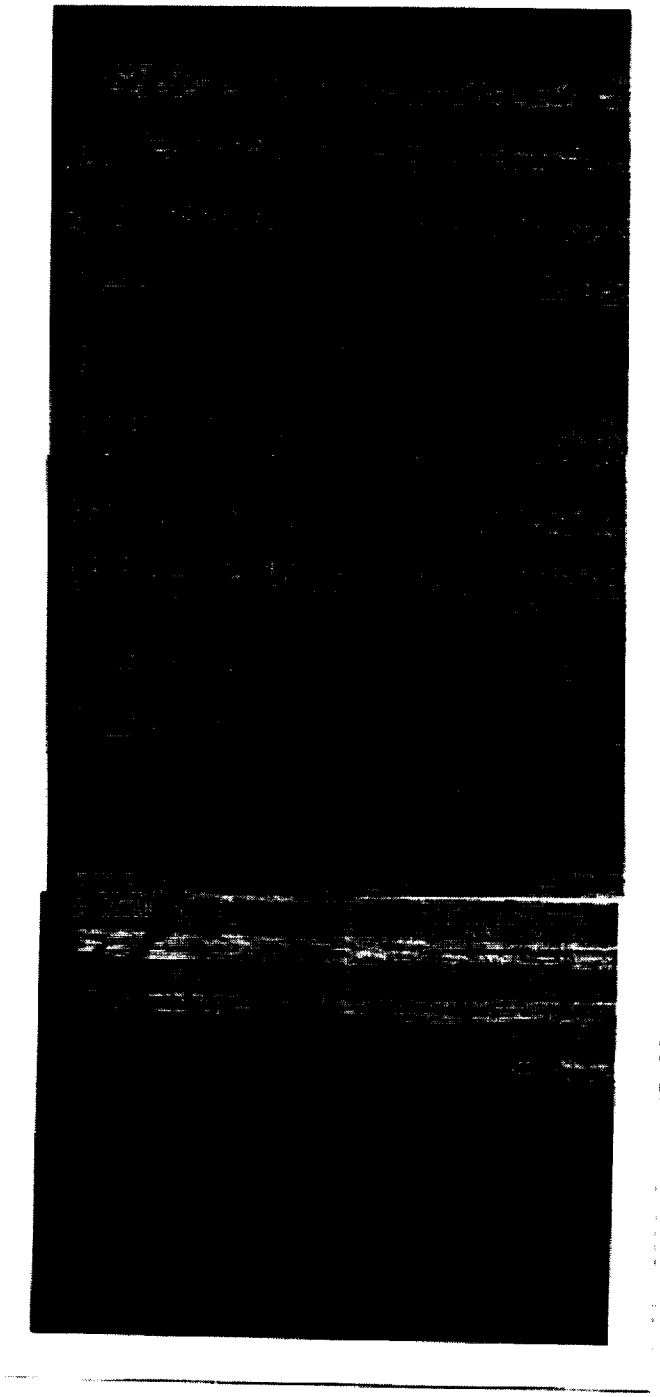

Figure 4.8. Series of three micrographs showing damage through the thickness at the bolt hole of specimen 1-c of the $[90,0]_{8s}$ specimens tested at –200°F.

Chapter 5
Computational Study

Computational models are developed to study the effect of temperature changes on the state of stress in a composite laminate subject to pin-bearing loads. The significance and role of each basic change, ΔS ,ΔM, ΔB, as defined by the hypothesis of this dissertation (see Chapter 1.3), is investigated. The finite element model of the composite laminate containing the bolt hole is first presented. Two preliminary studies are then introduced, one aimed at understanding the effect of temperature change on the state of residual stress in the vicinity of the bolt hole, ΔS, and another one for understanding the effect and significance of temperature change on the fastener fit, ΔB. The pin-bearing problem is then studied by first applying the pin-bearing load using the material properties at the three different operating temperatures. A solution combining residual stresses with pin-bearing stress results is presented. Finally, comparisons are made between computationally and experimentally determined results.

5.1 Finite Element Model

Following the guidelines developed in Chapter 3, the finite element method is used to perform three-dimensional analyses of a composite laminate containing a bolt hole. The $[90,0]_{8s}$ laminate is analyzed where in-plane symmetry as well as out-of-plane symmetry allow the computational model to be reduced to one-fourth of the actual configuration. This section presents model attributes that are consistent for all analyses to be conducted within this chapter. These model attributes include the geometry, finite element mesh, and material properties.

Geometry. The model geometry is illustrated in Figure 5.1. Symmetry planes exist about z=0, the laminate thickness symmetry, and about y=0, the in-plane symmetry. Although the geometry is symmetric about x=0, the pin-bearing loading condition is not and hence the model cannot be further reduced. The in-plane size of the laminate modeled was 0.5 inch wide and 2. inches in length. Although the pin-bearing test specimens were 2. inches wide and 8. inches in length, to reduce the computational size, the laminate size modeled was reduced. Through evaluation of analysis results forthcoming, the in-plane size of the laminate modeled proved to be sufficiently large, so that laminate size did not significantly alter the state of stress in the vicinity of the bolt hole. The through the thickness laminate geometry includes both ply layers and resin layers, where a total of 32 solid layers are contained in the model, wherein 8 layers are 0 degree plies, 8 layers are 90 degree plies, and 16 layers are resin layers. This is the same thickness laminate geometry modeled in Chapter 3 and depicted in Figure 3.13. Once again the ply thickness is h = 0.005 inch and the resin layer thickness is 0.1h, where only half the resin layer is modeled adjacent to the z=0 symmetry plane and the top 90 degree ply has a thickness of 0.00525 inch. The total laminate thickness modeled was 0.088 inch, which is half the actual laminate thickness of 0.176 inch.

Finite Elements. The finite element model was generated using 8-node hexahedral solid elements. A convergence study, using the room temperature thermal cure loading condition stress results, was conducted to determine an optimum mesh. The objective was to refine a mesh until all stress components were converged (when compared to a more refined mesh) two elements away from the free edge bolt hole boundary, but also so that the mesh was not more refined than necessary. Although less refinement may have been achievable with further study, an acceptable mesh was defined which contained a total of 63,498 elements. Figure 5.2 shows the finite element mesh in the x-y plane. Figure 5.2(a) shows the complete finite element model and Figure 5.2(b) displays an enlarged view showing just a 0.25 inch by 0.25 inch section to the right of the bolt hole on the z=0 plane. This section is where the largest stresses are expected in the pin-bearing model. Figure 5.2(b) also shows the origin, a rectangular coordinate system and a cylindrical coordinate system at the center of the bolt hole.

The two layers of elements closest to the bolt hole boundary were only 1.67×10^{-5} inch wide in the radial direction. The analysis results obtained in the two elements closest to the bolt hole boundary, within which the free edge singularity is contained, will not be presented. Alternatively, analysis results are presented at a distance of 3.3×10^{-5} inch in away from the bolt hole boundary where r = 0.125033 inch; hence *all stresses presented are assumed to be valid computational stresses.*

At the bolt hole boundary, a total of 108 layers of elements were located through the thickness of the laminate in the z-direction. The first resin solid layer adjacent to the z=0 symmetry plane and the next two plies (a zero degree ply and 90 degree ply) were modeled with five layers of uniformly spaced elements each. The remaining solid layers were discretized each with three layers of uniformly spaced elements, except the three outermost layers closest to z=0.088 inch. The three outermost layers were discretized each with five layers of graded elements so that the elements were smaller closest to the interfaces between layers. Between r = .1251 inch and r=.145 inch, the through the thickness mesh was transitioned to only one element per solid layer through the thickness of the laminate.

Material Properties. The material properties used in the analyses were assumed to be constant at the applied operating temperature. Through comparison with nonlinear temperature-dependent property analyses conducted in Chapter 3, the constant property assumption was determined to be sufficient for accurately predicting stresses at the operating temperatures being studied. For the operating temperatures of 350°F, 70°F, and –200°F, the material properties, as given in Table 2.1, were used. Since compression was the primary loading condition, compressive stresses were assumed to dominate. Hence for simplicity, and although tensile stresses were predicted with the analysis model, only the compressive moduli, E_{11c} and E_{22c}, are used in the analysis models.

5.2 Residual Stress Concentrations at Bolt Holes

The state of residual stress due to curing a composite laminate is an initial state of stress, and it is present in the laminate containing a bolt hole prior to applying the pin-bearing load. The study presented focuses on predicting the changes in the state of thermal residual stress, ΔS, in the vicinity of the bolt hole due to the change in temperature. The change in stress, ΔS, for the current problem is a function of both the change in temperature, ΔT, and the change in material properties of the constituent materials, ΔM. To predict the change in the state of residual stress accurately from room temperature to an elevated or reduced temperature, knowledge of the residual stress concentrations due to curing present in the laminate at room temperature is required.

In this study, the composite laminates were first cured, where subsequently, at room temperature, the bolt hole was drilled and reamed to size in the composite laminate having an initial state of residual cure stresses. However, the finite element analysis for evaluation of residual stresses at a room temperature of 70°F is performed on a model containing the bolt hole at the stress free temperature of 460°F, where a temperature change to room temperature is applied as the thermal load. Moreover, the state of residual stress in the vicinity of the bolt hole is assumed here to be altered insignificantly by modeling the bolt hole in the laminate at the stress free temperature, and then curing to room temperature.

In the three previous published studies on thermal residual stresses in composite laminates containing a bolt hole the same modeling assumption was used where the bolt hole was assumed present throughout the cure cycle. In the first study[5.1], three-dimensional finite element analyses of 6-ply symmetric laminates were performed on a model with a very crude mesh containing only 32 elements with only three elements through the thickness. Only the interlaminar normal stress result was presented at the bolt hole boundary. Accordingly, the interlaminar stress result presented, being at the free edge bolt hole boundary, must be invalid as discussed earlier in this dissertation. In the second study[5.2], a very simplified one-dimensional analysis through the thickness of the bolt hole was conducted to predict only the interlaminar normal stress due to combined thermal and bearing loading, neglecting all other stress components. The final study[5.3] was a two-dimensional study that showed in- plane stress concentrations at the bolt hole due to thermal loading. Hence, the study presented here on the thermal residual stresses in the vicinity of a bolt hole in a composite laminate is believed to be of much greater resolution then has previously been attained. In the present study, valid interlaminar stress concentrations at a bolt hole due to thermal loading and the manner in which the residual stresses change with a change in temperature, are investigated for the first time.

5.2.1 Residual Stress Analysis Model

The analysis of residual stresses was initially performed on only the section on the computational model given in Figure 5.2(b). The analyses were performed subsequently on the entire finite element model given in Figure 5.2(a), where no variations on residual stress components in the partial section were

observed between analysis models. This result shows that the residual stress concentrations for the current problem are confined to the region modeled in section b), and this section is sufficient for predicting residual stresses in the vicinity of the bolt hole for laminates of that size and larger.

Boundary Conditions. For the residual stress analysis of the complete model, the boundary condition constraints included: 1) symmetry about z=0, where displacements in the z-direction were constrained, 2) symmetry about y=0, where displacements in the y-direction were constrained, and 3) displacements in the x-direction along the x = -1. inch boundary were constrained.

Thermal Loading. The three operating temperature cases of 350°F, 70°F, and –200°F were applied as thermal loads to the analysis model with corresponding material properties, all having a reference stress free temperature of T_{SFT} = 460°F. A linear static analysis was performed for each thermal load case.

5.2.2 Analysis Results

Linear static thermal-structural analyses are performed to predict the thermal residual stresses in the vicinity of the bolt hole due to curing. At the bolt hole boundary, the in-plane residual stresses at T=70°F, predicted around the circumference of the bolt hole, are presented in Figure 5.3. For each stress component, the distribution presented is at the z-coordinate location through the thickness of the laminate where the maximum of that stress component occurred. Note that for σ_y, only the material matrix direction stresses were considered for the determination of the maximum in this study. This resulted in the maximum σ_y occurring in a resin layer. For the in-plane stresses, the most significant stress concentration due to the bolt hole occurred with σ_x, where a maximum of -32.ksi was observed at the bolt hole boundary. The σ_x stress at the bolt hole boundary was twice the σ_x due to curing in the laminate without a bolt hole, where a value of -15. ksi was determined and presented in Table 3.2.

The interlaminar stress distributions due to curing, determined at T=70°F, are presented in Figure 5.4 around the bolt hole boundary. Once again, for each stress component, the distribution is presented at the z-coordinate location through the thickness of the laminate where the maximum of that stress component occurred. As can be observed, very large interlaminar stresses occur at the bolt hole boundary, where each component has its peak at a different circumferential location. Table 5.1 presents the peak interlaminar stresses at the bolt hole boundary along with the peak interlaminar stresses at the straight free edge that were predicted in Chapter 3. As can be observed from Table 5.1, residual stresses due to a bolt hole boundary as compared to a straight free edge are dramatically larger. The σ_z stress concentration is over twice as large at the bolt hole boundary compared to the straight free edge. Where σ_{zx} is zero for a straight free edge, a σ_{zx} of 16. ksi is predicted at the bolt hole boundary, and where a maximum positive σ_{yz} of 11.5 ksi is predicted at a straight free edge, a larger negative σ_{yz} of -17.9 ksi is predicted at the bolt hole boundary. At the other operating temperatures studied, the circumferential stress distributions were similar with maximum values occurring at the same location. The only difference observed was in the magnitude of the stress components.

All peak stress components predicted in the laminate containing a bolt hole, at each operating temperature, are presented in Table 5.2. The variation of the maximum in-plane stress, σ_x, in the radial direction at $\theta = 90^\circ$, from the bolt hole boundary, is presented in Figure 5.5, as predicted at the three operating temperatures being studied. Away from the bolt hole boundary, the stress concentration quickly reduces to the value predicted in a laminate without a bolt hole, where the values without a bolt hole are given in Table 3.2. Similarly, the variation of the maximum interlaminar stresses in the radial direction are presented in Figure 5.6, 5.7 and 5.8 for the σ_z, σ_{xz}, and σ_{yz} components, respectively. All interlaminar stresses quickly reduce to zero within a small distance from the bolt hole boundary. The behavior for the cure residual stresses at a bolt hole boundary is similar to the behavior of cure stresses in a laminate at a straight edge, where the interlaminar stresses also approach zero within one laminate thickness away from the free edge.

5.3 Fastener Fit

When the pin bearing configuration, as illustrated in Figure 1.4, is exposed to a change in operating temperature, both the bolt hole diameter, depth and shape and the pin diameter may change due to either thermal expansion or contraction. The aforementioned pin-bearing configuration changes affecting the fastener fit have the potential to change the actual pin bearing surface area of the composite laminate. A change in the pin-bearing surface area can alternatively be caused by a change in the manufacturing clearance between the fastener and pin. The effect of clearance has been previously studied in the literature, and changing the pin-bearing surface contact area has been shown to affect the pin-bearing load capacity.[5.4] Additionally, pin bearing strength has been shown to be dependent on the bolt hole diameter size.[5.5] Hence, the study presented here is focused on determining the change in both the bolt hole diameter size, ΔD, and the bolt hole clearance, λ, due to a change in temperature.

The change in the diameter of the isotropic pin can easily be determined as a plane strain problem of a cylinder subject to a uniform change in temperature. The unrestrained change in pin diameter due to a change in temperature is computed as

$$\Delta d = \alpha_p \, \Delta T \, d \tag{5.1}$$

where α_p is the coefficient of thermal expansion of the pin, ΔT is the change in temperature, and d is the original diameter of the pin. The pin properties used in the current study are presented in Chapter 4.

The change in the geometry of the bolt hole of the composite laminate due to a change in temperature was predicted in the finite element analyses conducted for determining residual stresses in section 5.2. Analysis results revealed that for the $[90,0]_{8s}$ IM7/PETI5 lay-up and the current operating temperatures considered, the changes in bolt hole geometry were extremely small. For the cure cycle from the cure temperature of $T_{SFT} = 460^\circ F$ down to a room temperature of $T = 70^\circ F$, a maximum change in the bolt hole diameter of only -2.82×10^{-4} inch was predicted. The variation is only a 0.1% change in

diameter and is much smaller than the bolt hole tolerance of 0.001 inch used for machining the pin-bearing specimens. Additionally, a maximum change in laminate thickness of only – 8.19 x 10^{-4} inch was predicted, which is only a 0.9% change and is much less then the variation in manufacturing thickness of the laminates, which were as large as 0.02 inch. The clearance, λ, resulting from a change in temperature from a room temperature of 70°F to another operating temperature, is defined as

$$\lambda = \Delta D - \Delta d \tag{5.2}$$

where ΔD is the maximum bolt hole diameter change computed from the differences between the finite element analysis results, and Δd is pin diameter change computed from Equation 5.1.

The pin-bearing configuration changes affecting fastener fit, determined for the elevated and reduced operating temperatures being studied, are given in Table 5.3. Presented in Table 5.3 are the temperature change, ΔT, pin diameter change, Δd, laminate diameter change, ΔD, resulting clearance, λ, and laminate thickness change, Δt. All diameter changes are extremely small relative to the dimensions of the pin-bearing problem. The net resulting clearances are also small, where for the elevated temperature of 350°F, a small decrease in clearance of -1.84 x 10^{-4} is determined, and at the –200°F a small increase in clearance of 4.06 x 10^{-4} is predicted. In relation to the effect of change in clearance on changes in pin bearing load capacity, a previous study[5.4] used a clearance of 0.01 and determined a decrease in load capacity of 12%. Therefore, the much smaller clearances predicted here due to temperature changes are assumed to have an insignificant effect on pin-bearing strength. Overall, changes in fastener fit due to the temperature changes of the current problem being studied are determined to be negligible and consequently will not be considered in the forthcoming pin bearing analysis models.

5.4 Pin-Bearing Analysis

A pin-bearing analysis model is developed where much of the detail is based on the findings of the previous studies presented in this dissertation. The effect of temperature changes on the state of stress at the bolt hole will be investigated for the pin-bearing load condition. The significant factors influencing the change in bearing strength with a change in temperature will be investigated.

5.4.1 Load and Boundary Conditions

Several methods of applying the pin-bearing load to the finite element model were considered to determine the optimum loading condition that could be modeled using NASTRAN. Many methods used in the literature were considered. The conditions to be discussed include: applied cosine load at the bolt hole boundary, fixed displacements at the bolt hole boundary, plate elements in the bolt hole, radial constraint at the bolt hole boundary, circumferential contact area, and nonlinear contact conditions including friction.

The method of applying a cosine distributed load on the loaded half of the bolt hole boundary has been used in the literature on two-dimensional models of composite laminate.[5.6,5.7] However, the method proved to be inaccurate for

composite problems with highly orthotropic properties.[5.8] The method was tested on the current problem and resulted in unrealistic stress concentrations at the interfaces between plies. Some authors have completely fixed the displacements on the loaded half of the bolt hole while applying a uniform force or displacement to the far end of the analysis model.[5.7,5.9] The method simulates a rigid pin with infinite friction, as in the case of a bonded pin. One study showed the method to result in unrealistic displacements for the bolt hole.[5.7] The method was also tested on the current problem. At $\theta = 90^{\circ}$, the intersection between the fixed displacement constraint and free bolt hole boundary, unrealistically high tensile stresses were observed. To account for pin elasticity, other authors have modeled the pin with bars and plate elements.[5.10,511] However, for problems with zero clearance and high stiffness pins, the pin elasticity effect was negligible as predicted from both two- and three-dimensional nonlinear contact analyses.[5.4,5.12] Since a high stiffness pin and zero clearance are the conditions of the current problem, the effect of pin elasticity should not be a significant factor and will consequently not be considered in the current pin-bearing analyses.

The effect of friction between the pin and composite laminate has been studied using both two- and three-dimensional nonlinear contact analyses.[5.4, 5.12] As observed in the studies using a coefficient of friction of 0.2, the effect of friction has been to decrease the normal contact traction at $\theta = 0$ by about 25% while inducing a tangential contact traction. As θ increases from 0° to 40° around the circumference of the bolt hole, the stress results approach the same stresses as were predicted in the case of no friction. Three studies[5.12,5.13,5.14] were found in the literature that performed three-dimensional nonlinear contact analyses of the pin bearing problem including friction. All the analyses used very crude meshes with a maximum of four ply layers modeled, and they all did not show any verification of the accuracy of the solution in the vicinity of the bolt hole boundary. The three-dimensional contact problem is highly nonlinear, requires significant computational resources, and may easily become unstable and produce erroneous results.[5.15] Since the current model contains an extremely large number of elements, modeling nonlinear three-dimensional contact is not practical. Also, since temperature effects on the pin-bearing problem are being studied for the first time in a three-dimensional high resolution model, a more reliable and efficient boundary condition was desired.

The boundary condition of constraining only the radial displacements on the loaded half of the bolt hole was used to simulate a rigid frictionless pin.[5.16] The load was then applied to the straight edge of the composite as a uniformly distributed load. This procedure was adopted for the current analysis as the most appropriate method of modeling the pin-bearing load. An initial analysis was performed where the radial constraint was applied from $\theta=0^{\circ}$ to $\theta=90^{\circ}$ on the bolt hole boundary. This condition resulted in erroneous tensile radial stresses at $\theta=90^{\circ}$, which would not be the case of a laminate free to separate from the pin at this location. It was desired for the solution to only contain negative radial stresses in contact with the pin, which would be a realistic scenario of pin contact. The radial constraint was subsequently reduced by applying it to only the bolt hole boundary between $\theta=0^{\circ}$ and $\theta=80^{\circ}$, simulating the case for a pin

having a slightly smaller diameter than the bolt hole, i.e., a pin with a clearance fit. This resulted in compressive radial stresses for pin contact between θ=0° and θ=80°.

Since the effect of friction was observed to be most significant only between θ=0° and θ=40° in a previous nonlinear contact analyses, the modeling of infinite friction was investigated here by constraining all displacements at the bolt hole boundary for the case of infinite friction between, θ = 0° to 45° and in another case between θ = 0° to 10°, while continuing to constrain only the radial displacement to θ = 80°. Both cases resulted in unrealistic tensile stresses at the intersection between the fixed constraint and radial only constraint, which was θ = 45° in the first case and θ = 10° in the second case. Hence, only radial constraints between θ = 0° and 80° produced acceptable boundary stresses and these boundary conditions are used.

In summary, the pin-bearing boundary and loading conditions used in the current analysis model are illustrated in Figure 5.9 and include

1) radial displacement constraints applied to the bolt hole boundary between θ = 0° and θ = 80°
2) y-displacement constraints on y=0 plane
3) z-displacement constraints on z=0 plane
4) uniform surface traction S_g at x = -1. inch.

The first boundary condition simulates the conditions of a rigid pin by constraining radial displacement at the bolt hole boundary and assumes a frictionless interface between the pin and composite laminate by leaving tangential and z-displacements unconstrained. The y- and z- model symmetry are prescribed with the second and third boundary conditions, and finally the load is applied in the negative x-direction by S_g.

For the pin-bearing analyses, a pressure load equivalent to the pin-bearing yield stress, F_{bry}, is applied for the evaluation of the state of stress in the linear range. Therefore, S_g is determined as

$$S_g = \frac{F_{bry} D}{W} \tag{5.3}$$

where D = 0.25 inch is the bolt hole diameter, and W = 1. inch is the finite element model laminate width. For each operating temperature analyzed, the corresponding average F_{bry} as determined from experiment (Table 4.2) was used for determining the S_g used in the analysis as presented in Table 5.4.

5.4.2 Pin-Bearing Analysis Results

Pin-bearing analyses were conducted to determine the state of stress at the three operating temperatures of 350°F, 70°F, and –200°F due to the pin-bearing load condition. For the room temperature operating condition, T= 70°F, in-plane stresses around the circumference of the bolt hole are displayed in Figure 5.10. The in-plane stress component plotted is at the z-coordinate location were the maximum occurred for that stress component. The interlaminar stress components are displayed in Figure 5.11, once again at the z-coordinate location were the maximum occurred for that stress component.

The distributions shown in Figures 5.10 and Figure 5.11 are very similar in shape to the distributions plotted in Ref. 5.16, where a three-dimensional pin-bearing analysis of a $[90_4,0_4]_s$ graphite/epoxy laminate was conducted using similar boundary conditions. The boundary condition differed from the current analysis in that the radial constraint was applied at the bolt hole between $\theta = 0^\circ$ and $\theta = 90^\circ$. Both analyses had similar σ_x distributions with a compressive maximum at $\theta = 0^\circ$ and a tensile maximum at $\theta = 90^\circ$. Where Ref. 5.16 shows a tensile σ_z peak at approximately $\theta=90^\circ$, a peak positive σ_{xz} at $\theta=45^\circ$, and a peak negative σ_{yz} at approximately $\theta = 22^\circ$, the current analysis model produced a peak σ_z at approximated $\theta = 85^\circ$ a peak σ_{xz} at 50°, and, a peak σ_{yz} at 27.5°. Overall, the similarity in appearance of the distributions gives validity to the current analysis model.

The peak values for all stress components predicted from the analysis models at all three operating temperatures are given in Table 5.5 and the predicted bearing yield strain is presented in Table 5.6. Also presented in Table 5.6 are the experimentally determined bearing yield strain, which will be discussed later in section 5.5. For all three operating temperatures, analysis results are plotted together for σ_x, σ_z, and σ_{yz} in Figures 5.12-5.14, respectively. For each stress component, the distribution is presented at the z-coordinate location where the maximum value of that stress component occurred. The stress components plotted were chosen to show the similarity in the distributions between the three operating temperatures analyzed. The distributions were also similar for σ_y, σ_{xy}, and σ_{xz}, between the three operating temperatures, which were not plotted. It is important to note that the cause for variations in the state of stress are the variations in the lamina properties used for the analysis models at the different temperatures, in addition to the change in the magnitude of the load, S_g, used in the analyses. Most importantly, variations in lamina properties with a change in temperature affect the state of stress at the bolt hole boundary and consequently should affect changes in the pin-bearing strength with a change in temperature.

Additionally, to check the effect of modeling the full size specimen, an analysis was performed on an enlarged finite element model as can be seen in Figure 5.15. The full size model contained 80,310 elements, where the discretization in the 0.25 in by 0.25 in region adjacent to the bolt hole was not altered from the previous model given in Figure 5.2. A pin-bearing analysis was performed at the 70°F operating temperature, and the applied load was accordingly adjusted to S_g = 6000. ksi. Except for the in-plane shear stress and interlaminar normal stress, the results showed less than 1% change in maximum stress magnitudes and no change in location. However, a 9% change in σ_{xy} was observed were the maximum stress changed from –29. ksi to –32. ksi at $\theta = 22.5^\circ$ and z=0.0818 in. Also, the maximum σ_z magnitude changed by 12% from 18. ksi to 16. ksi, but the location or distribution was not altered. Although the changes in stress are significant in magnitude and indicate that the larger model results would be more appropriate for application of failure theories, the findings of the dissertation are not altered, and so the smaller model being used is concluded to be adequate for the current study.

5.4.3 Combined Analysis Results

The state of stress due to the combined effect of pin-bearing load conditions and thermal residual cure stresses is obtained by superposition of solutions. The initial state of stress obtained from the analysis due to thermal cure loads at the operating temperature of interest is combined with the stress results obtained from the pin-bearing load conditions applied to the finite element model.

At the room temperature operating condition of 70°F, the initial cure stresses are plotted along with the combined stress results around the circumference of the bolt hole for each stress component in Figures 5.16-5.21. Each stress component has been plotted at the z-coordinate location where the maximum of that stress component occurred. Unlike the in-plane stresses, all interlaminar stress components had the maximum occur at the same location as in the case of pin-bearing load only. The presence of the residual cure stresses only affected the magnitudes of the interlaminar stress component, and not the location of the maximum. Where the presence of cure stresses resulted in a lower maximum for the σ_x stress component as can be observed in Figure 5.16, this was not the case for the other stress components. For all other stress components, the magnitude of the peak stresses were intensified with the presence of the thermal residual cure stresses. For all interlaminar stresses plotted in Figures 5.19-5.21, the θ location where the peak thermal cure stress occurred was near the same location where the peak pin-bearing stress occurred, resulting in intensified interlaminar stresses due to residual cure stresses. This effect is contrary to what was observed in Chapter 3 for the laminate, where the presence of residual stresses reduced the interlaminar stress magnitudes that were predicted under compressive loading.

For the other operating temperatures of 350°F and –200°F, analysis results were similar, where changing the operating temperature did not affect either the location of the maximum or the appearance of the distribution. Therefore, their distributions were not plotted. Only the magnitude of the combined stresses varied with varying temperature. The maximum stresses predicted for each stress component and for each operating temperature are presented in Table 5.7.

5.5 Comparisons with Experimental Results

The computational results obtained in this chapter are evaluated through comparisons with experimental results.

The magnitudes of the peak residual stress components are presented in Table 5.2. Through comparison with lamina strengths given in Table 2.1, their values reveal significant interlaminar stresses at all temperatures due to curing. The maximum σ_z exceeds the F_{zz} strength predicted at all temperatures while σ_{yz} and σ_{xz} exceed the F_{1z} strength at the operating temperatures of 70°F and –200°F. However, the strengths given in Table 2.1 only represent the average strength of the cross-section used in the property test and neglect stress concentrations in the test specimen. Note that the predicted maximum σ_z is

tensile, and hence a tensile modulus, E_{33T}, would have been more appropriate in the elements where σ_z were positive. Since E_{22T} is lower then the E_{22c} modulus used in the analysis, and $E_{33}=E_{22}$ is assumed in the model, lower stresses would be expected if a tensile modulus were utilized. However, a qualitative perspective can be gained from the analysis results presented.

The magnitudes of the maximum stress components are presented in Table 5.5. Through comparison with lamina strengths given in Table 2.1, their values reveal significant stresses for all stress-components due to the pin-bearing load condition. For pin-bearing loading only, the in-plane shear stress and all interlaminar stresses exceed the strength values. Consequently, the case of pin-bearing loading only over-predicts stresses at the bolt hole in the composite laminate.

The bearing yield strain predicted from the pin-bearing analysis is compared to the measured values from the experiment in Table 5.6. Large discrepancies are observed. Unfortunately, the previous studies that used the same method for measuring bearing strain did not attempt to verify their results with an analysis as was attempted here.[5.17,5.18] There is a possibility here that the measured values are erroneous and that the extensometer used did not measure the bolt hole elongation accurately. Although the measured values are questionable, the bearing strain measurement is still useful and necessary for indication of the yield and ultimate strength values obtained from the experiment. Also, an observation can be made that both the measured and predicted bearing strains were lower at room temperature than at the elevated or reduced operating temperatures.

The maximum stress failure criterion is used here to gain perspective on the severity of the stresses predicted from the analysis. The maximum stress criterion states that each stress component must be less than the respective strength, otherwise, failure is said to have occurred.[5.19] A failure ratio is computed as

$$\text{F.R.} = \frac{\sigma_{ij}}{F_{ij}} \tag{5.4}$$

where σ_{ij} is the maximum stress for the ij component and F_{ij} is the strength of the corresponding stress component. Then, a failure ratio of F.R. > 1 indicates failure. The failure ratios computed from the maximum stresses are given in Table 5.8. All in-plane shear stresses and interlaminar stresses are well above the failure ratio, indicating failure had occurred before the applied loads were reached. Consequently, either the strengths have been under-predicted from the experiments or the model has over-predicted stresses.

With respect to the strength data, the interlaminar strengths given in Table 2.1 do not account for stress concentrations during the experiment and may actually under-predict the strength in the absence of stress concentrations. Also, since resin layers are present even in unidirectional laminates, residual stresses can also be present and affect the lamina strength data, where a correction could be made to the lamina strength data to account for residual stresses.

With respect to the stresses predicted by the model, several reasons can be offered for over-prediction. First, as mentioned earlier in evaluation of

residual stresses, the tensile modulus E_{22T} is lower than the compressive modulus E_{22c} at all operating temperatures (see Table 2.1). Consequently, appropriate use of the tensile E_{22T}, in elements where a tensile stress was predicted should lead to lower tensile stresses. The high failure ratio for σ_{xy} at the 350°F operating temperature could be lessened by appropriately modeling the nonlinear material behavior, as obviously would be necessary in this case. Finally, the effect of friction at the bolt hole boundary, as was neglected here could result in lower boundary stresses.

In conceding to over-prediction, however, additional observations can be made on the predicted state of stress. With the failure ratios being near the same value if not greater with increasing operating temperature, and with the lower average bearing yield strengths values being used as loading with the increasing operating temperatures, the analyses reveal that increasing temperature reduces the pin-bearing yield strength. This observation corresponds to the experimental results of decreasing strength with increasing temperature.

The distribution of the maximum interlaminar stresses through the thickness of the laminate, at the bolt hole boundary and θ location where the maximum occurred, are presented in Figures 5.22-5.24. Plotted are only the distributions for the case of T=70°F, since similar distributions were observed at the other operating temperatures. As seen in Figure 5.22, the maximum interlaminar normal stress occurs in the lower 90° ply at the interface with the lower resin layer. The peak layer stress is then observed to diminish as the outer plies are approached. In contrast, the interlaminar shear stress maximum, σ_{xz}, occurs in the outermost resin layer interface with the 0° ply, and the maximum σ_{yz} occurs in the second resin layer from the top interface with the outermost 0° ply, where both interlaminar stress layer peaks lessen as the center of the laminate is approached. In comparison with the failed specimen micrograph (see Figure 4.8), the maximum interlaminar shear stress locations could be used to explain the severe damage observed in the specimens in the outermost two resin layers. Consequently, failure of the composite may initiate from excessive interlaminar shear stresses.

To aid in understanding the contribution of thermal residual stresses on the maximum stress result, the magnitude of the cure stresses at the location where the maximum combined stress occurred are presented in Table 5.9. As can be observed from the table, significant changes in residual stress occur between T=350°F and T=70°F with a ΔT=280°F. The changes in residual stress are significant in comparison to the change in bearing strength, where a ΔF_{bry} of only -6ksi was determined from experiment. Also, since the residual stresses are lower at T=350°F than at T=70°F, the effect of thermal residual stress is concluded to lessen the degradation in pin-bearing strength than would be expected in the absence of cure stresses. With the changes in residual stresses being more negligible between 70°F and -200°F, the change in pin-bearing strength to the reduced temperature appears to be affected by only the change in the lamina material properties. Here, a greater change in F_{bry} of +15 ksi was measured for ΔT= -270°F. Perhaps the change in strength is greater since there

are no changes in thermal residual stresses lessening the change in strength as there was between 70°F and 350°F.

The presence of residual stresses has been shown previously to intensify the magnitude of the maximum in-plane shear and interlaminar stresses obtained under pin-bearing loads for all temperatures. Consequently, residual cure stresses appear to contribute to the reason why the bearing strengths in general are lower than the compressive strength of the composite laminate. This is true for all lay-ups tested, where all laminate strengths presented in Table 2.4 are greater than the corresponding average ultimate bearing strengths presented in Tables 4.2, 4.4, 4.5, and 4.6.

Most importantly, from the results of this analysis, in addition to a change in lamina material properties, changes in the residual cure stresses with a change in temperature have the potential to affect the change in pin-bearing strength with temperature change. Hence, both $\Delta M(\Delta T)$ and $\Delta S(\Delta T)$ are factors that cannot be ignored in an investigation on the change in bearing strength with a change in temperature, $\Delta F_{br}(\Delta T)$.

5.6 References

5.1 Rybicki, E.F. and Schmueser, D.W.: Three-dimensional Finite Element Stress Analysis of Laminated Plates Containing a Circular Hole. Technical Report AFML-TR-76-92, August 1976.

5.2 Smith, P.A. and Pascoe, K.J.: The Effect of Stacking Sequence on the Bearing Strengths of Quasi-isotropic Composite Laminates. *Composite Structures*, Vol. 6, Issue 1-3, 1986, pp. 1-20.

5.3 Chang, H.T.: Nonlinear Curing Analysis For Advanced Composite Materials. 35th International SAMPE Symposium, April 2-5, 1990, pp. 604-615.

5.4 Hyer, M.W., Klang, E.C., and Cooper, D.E.: The Effect of Pin Elasticity, Clearance, and Friction on the Stresses in a Pin-Loaded Orthoptropic Plate. *Journal of Composite Materials*, Vol. 21, March 1987, pp. 190-206.

5.5 Garbo, S.P, and Ogonowski, J.M.: Effect of Variances and Manufacturing Tolerances on the Design Strength and Life of Mechanically Fastened Composite Joints. AFWAL-TR-81-3041, April 1981.

5.6 Collings, T.A., On the Bearing Strengths of CFRP Laminates, *Composites*, July 1982, pp. 241-252.

5.7 Tsujimoto, Y. and Wilson, D.: Elasto-plastic Failure Analysis of Composite Bolted Joints. *Journal of Composite Materials*, Vol. 20, May 1986, pp. 236-252.

5.8 De Jong, T.: Stresses Around Pin-Loaded Holes in Elastically Orthotropic or Isotropic Plates. *Journal of Composite Materials*, Vol. 11, July 1977, PP. 313-331.

5.9 Marshall, I.H., Arnold, W.S., and Wood, J.: Observations on Bolted Connections in Composite Structures. *Composite Structures*, Vol. 13, 1989, pp. 133-151.

5.10 Mathews, F.L., Wong, C.M., and Chryssafitis, S.: Stress Distribution Around a Single Bolt in Fibre-Reinforced Plastic. *Composites*, 13, July 1982.. pp. 316-322.

5.11 Sperling, U.O., Three-Dimensional Stress Distribution Around Pin Loaded Holes in Composite Laminates, AIAA 85-0826, 1985, pp. 743-750.

5.12 Chen, W.H., Lee, S.W., and Yeh, J.T.: Three-dimensional Contact Analysis of a Composite Laminate with a Bolted Joint. *Composite Structures*, Vol. 30, 1995, pp. 287-297.

5.13 Serabian, S. M., The Effect of Nonlinear Intralaminar Shear Behavior on the Modeling Accuracy of [(0/90)3,0]s and [+45/-45]3s Pin-Loaded Laminates, *Journal of Composites Technology and Research*, Vol.13, Winter 1991, pp. 236-248.

5.14 Persson, E., Madenci, E., and Eriksson, I.: Delamination Initiation of Laminates with Pin-Loaded Holes. *Journal of Theoretical and Applied Fracture Mechanics*,714, July 1998.

5.15 MARC User Information, MARC Analysis Research Corporation, Palo Alto, CA, Volume A, 1994.

5.16 Shokreih, M.M. and Lessard, L.B.: Effects of Material Nonlinearity on the Three-Dimensional Stress State of Pin-Loaded Composite Laminates. *Journal of Composite Materials*, Vol. 30, No. 7, 1996, pp.839-861.

5.17 Crews, J.H. and Naik, R.V.A.: Failure Analysis of a Graphite/Epoxy Laminate Subjected to Bolt-Bearing Loads, *Composite Materials: Fatigue and Fracture, ASTM STP 907*, American Society of Materials , Philadelphia, 1986, pp. 115-133.

5.18 Wright, R.J.; Johnson, W.S.; and Ahmad, H.: Bolt Bearing Behavior of Highly Loaded Composite Joints at Elevated Temperatures with and

without Clampup. Department of Material Science and Engineering, Georgia Institute of Technology, Atlanta, Georgia,1997.

5.19 Jones, Robert M.: *Mechanics of Composite Materials*, 2nd Edition, Taylor & Francis, Inc., Philadelphia, PA, 1998.

Table 5.1 Peak Interlaminar Residual Stresses Predicted at T=70°F.

Stress Component	Straight Free Edge	Bolt Hole Boundary
σ_z (ksi)	7.	16.7
σ_{xz} (ksi)	0.	16.0
σ_{yz} (ksi)	11.5	-17.9

Table 5.2 Peak Residual Stresses in Laminate Containing the Bolt Hole.

	Temperature		
Stress Component (ksi)	350°F	70°F	-200°F
σ_x	-6.9	31.9	31.7
σ_y	5.7	21.9	23.7
σ_{xy}	-0.86	-4.5	-6.2
σ_z	3.5	16.7	16.1
σ_{xz}	3.2	16.	16.7
σ_{yz}	-3.6	-17.9	-18.7

Table 5.3 Changes in Fastener Fit Due to Temperature Changes.

Temperature (°F)	ΔT (°F)	Δd (inches)	ΔD (inches)	λ (inches)	Δt (inches)
350	280	3.92×10^{-4}	1.94×10^{-4}	-1.98×10^{-4}	5.8×10^{-4}
-200	-270	-3.78×10^{-4}	0.14×10^{-4}	3.92×10^{-4}	0.

Table 5.4 The Pin-bearing Load, S_g, for each Operating Temperature

Temperature (°F)	F_{bry} (ksi)	S_g (ksi)
-200	63.	-15.75
70	48.	-12.00
350	42.	-10.50

Table 5.5 Maximum Stresses due to Pin-Bearing Loads.

	Temperature		
Stress (ksi)	350°F	70°F	-200°F
σ_x	214.	206.	265.
σ_y	-30.	-31.	-21.
σ_{xy}	-26.	-29.	-41.
σ_z	10.	18.	14.
σ_{xz}	24.	23.	31.
σ_{yz}	35.	35.	44.

Table 5.6 Bolt Hole Bearing Yield Strain.

Temperature (°F)	Experiment ε_{bry} (μin/in)	Analysis ε_{bry} (μin/in)
350	30300.	11400.
70	21700.	10920.
-200	23500.	13680.

Table 5.7 Maximum Stresses from Combined Solution – Pin-Bearing Loads and Thermal Residual Cure Stresses.

	Temperature		
Stress (ksi)	350°F	70°F	-200°F
σ_x	211.	189.	246.
σ_y	22.	45.	44.
σ_{xy}	-29.	-35.	-49.
σ_z	12.	27.	24.
σ_{xz}	26.	34.	41.
σ_{yz}	37.	47.	55.

Table 5.8 Maximum Stress Failure Ratios for Combined Solution.

	Temperature		
F.R.	350°F	70°F	-200°F
σ_x	.69	.62	.73
σ_y	.82	1.22	1.07
σ_{xy}	4.39	2.40	2.75
σ_z	3.70	6.00	4.62
σ_{xz}	2.17	1.97	1.92
σ_{yz}	3.08	2.72	2.58

Table 5.9 Cure Stresses at Combined Solution Maxima.

	Temperature		
Stress (ksi)	350°F	70°F	-200°F
σ_x	-1.	-17.	-18.
σ_y	3.	15.	15.
σ_{xy}	-1.	-5.	-5.
σ_z	2.	9.	9.
σ_{xz}	2.	10.	11.
σ_{yz}	2.	12.	11.

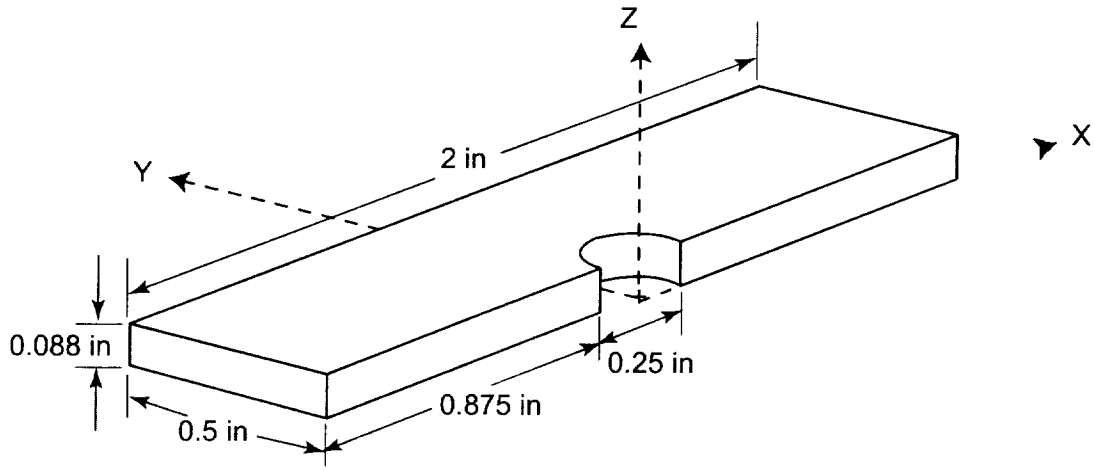

Figure 5.1. Pin-bearing composite laminate computational model geometry.

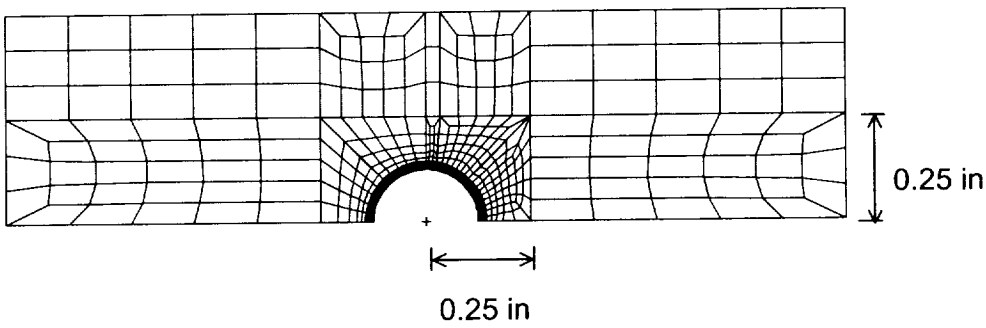

a) complete finite element model shown in x-y plane.

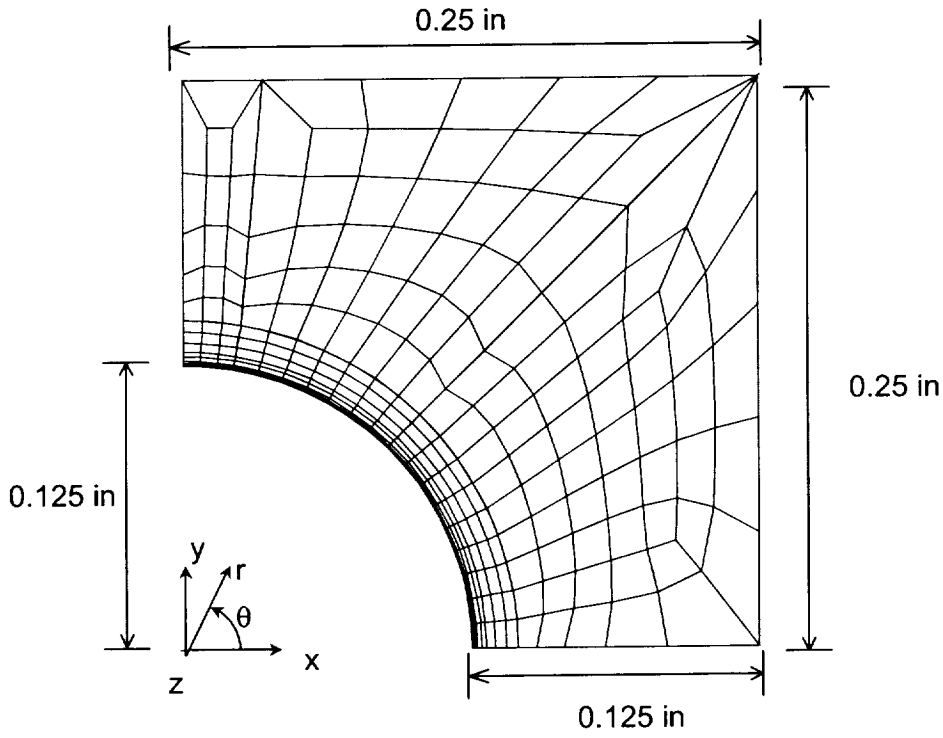

b) Section of finite element model showing discretization at z=0 in x-y plane.

Figure 5.2. Finite element model discretization in x-y plane.

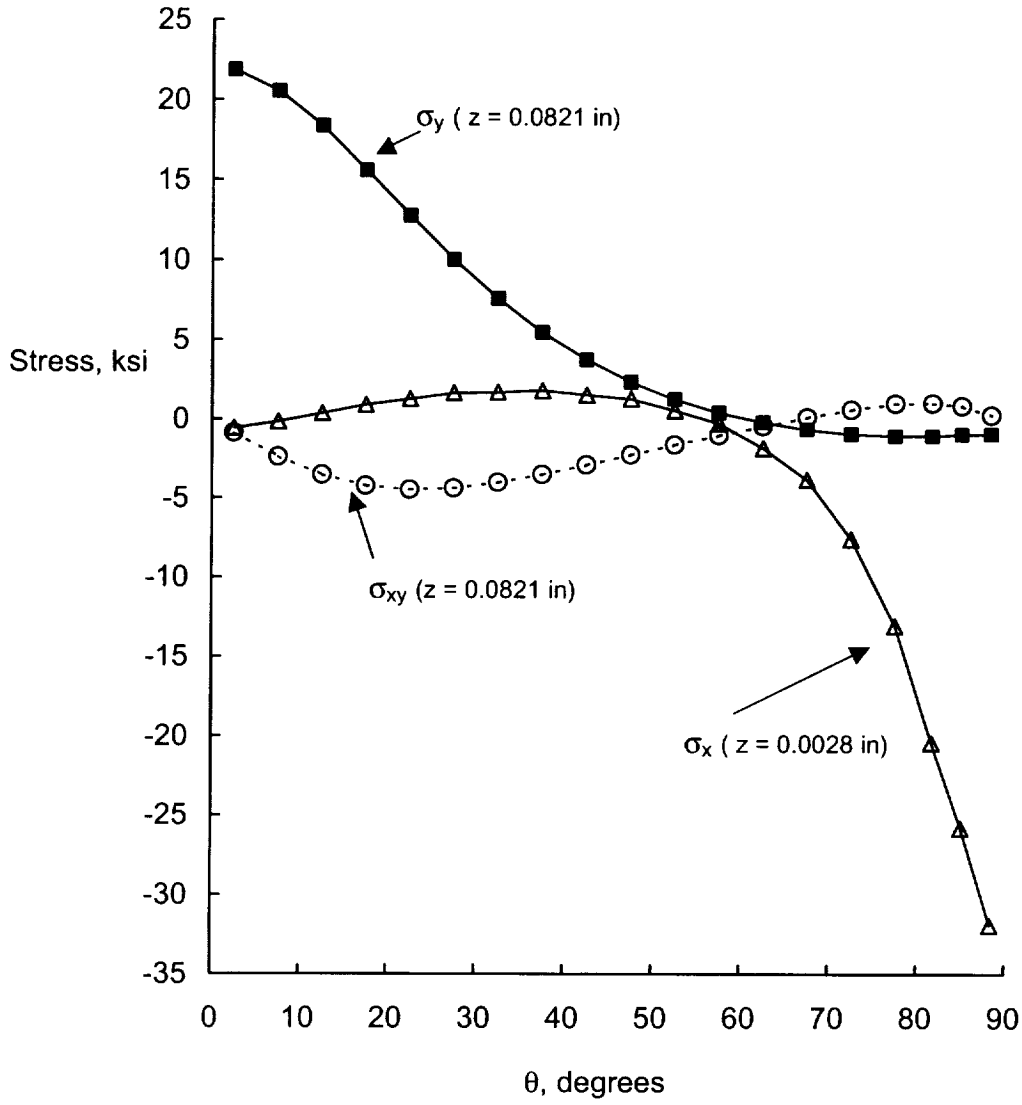

Figure 5.3. Variation of in-plane stresses around circumference of bolt hole due to curing, T = 70°F.

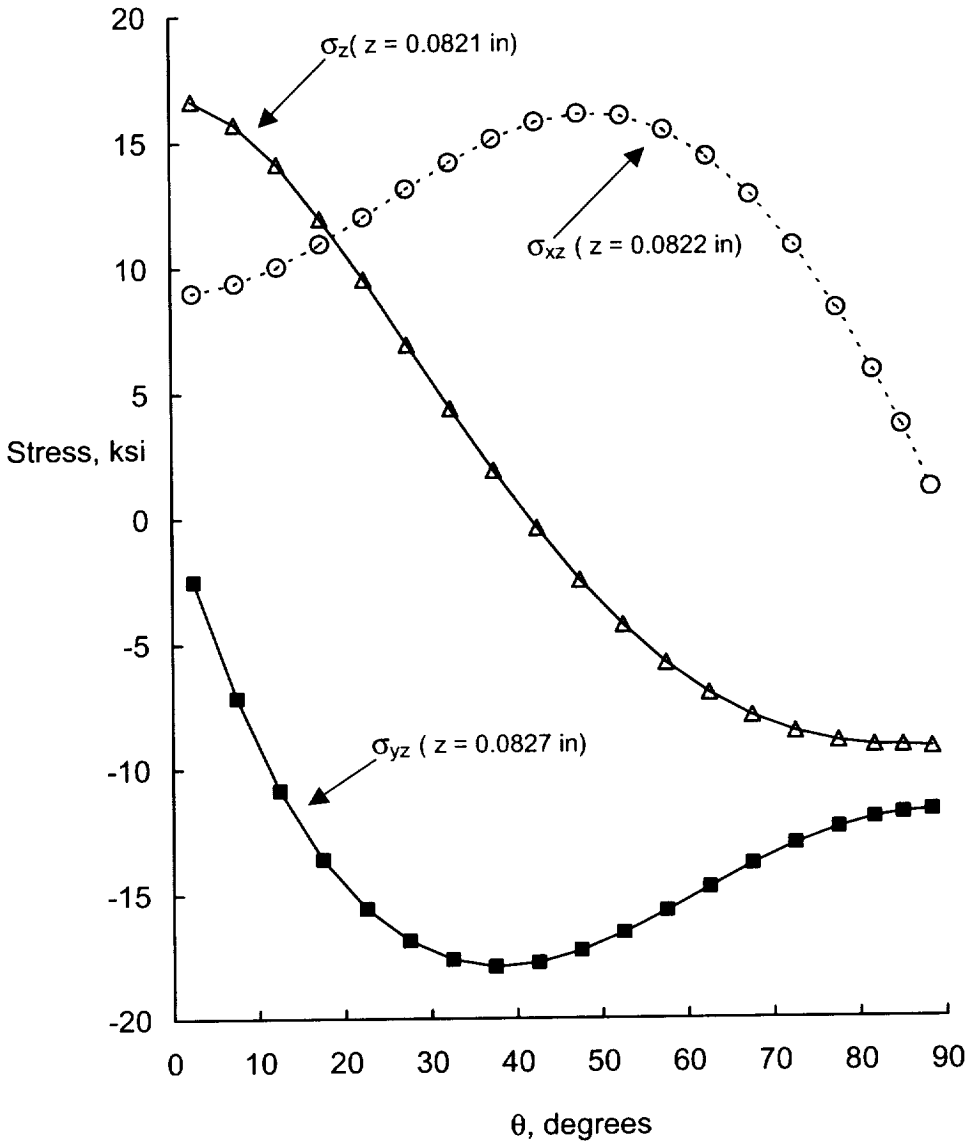

Figure 5.4. Variation of interlaminar stresses around circumference of bolt hole due to curing, T=70°F.

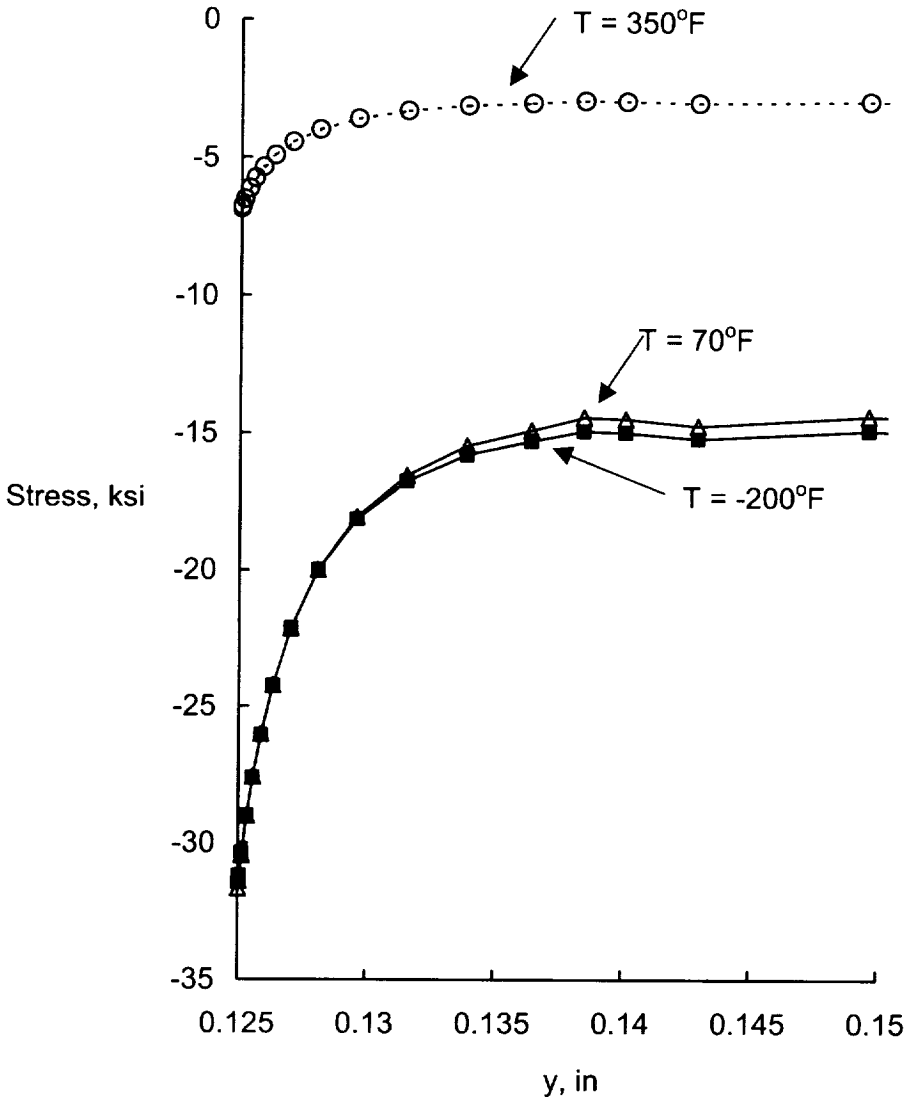

Figure 5.5. Radial distribution of σ_x at θ = 90 degrees due to curing, for T= -200°F, 70°F, 350°F.

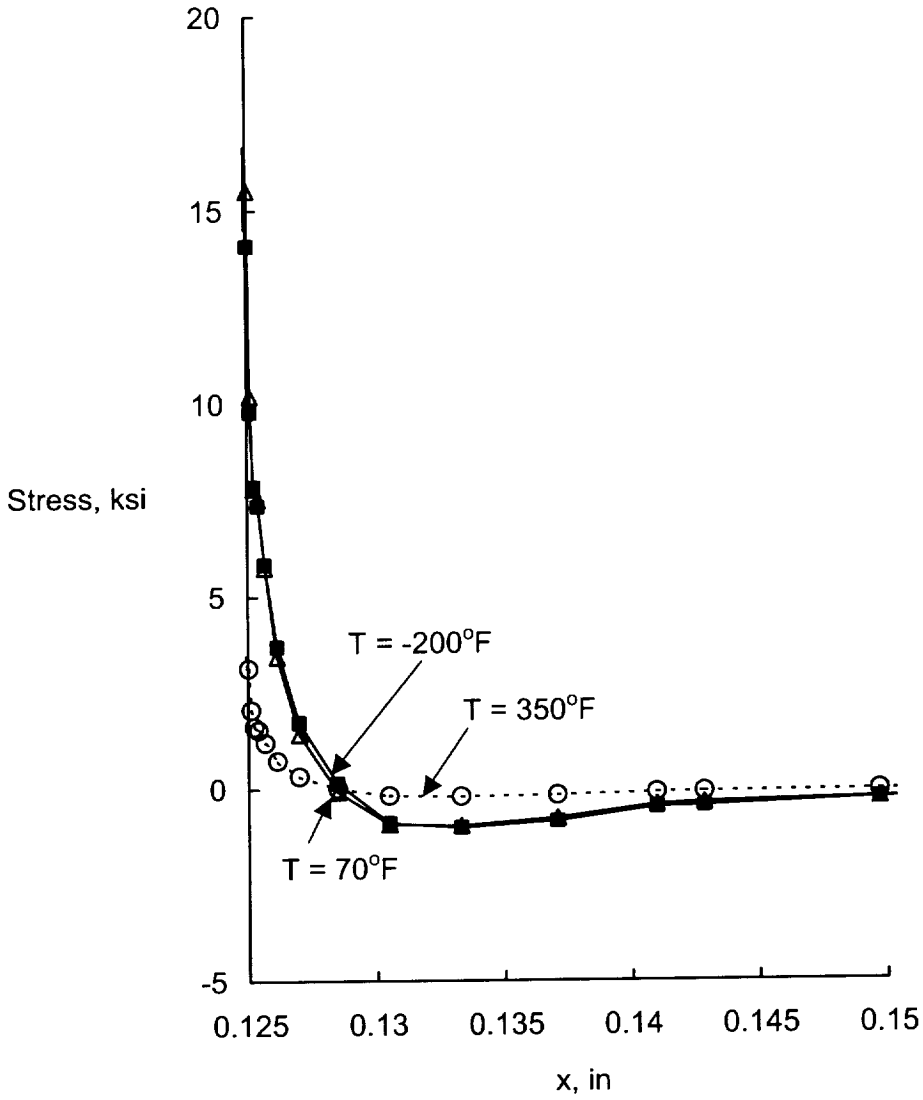

Figure 5.6. Radial distribution of σ_z at $\theta = 0$ degrees due to curing, at T = -200°F, 70°F, 350°F.

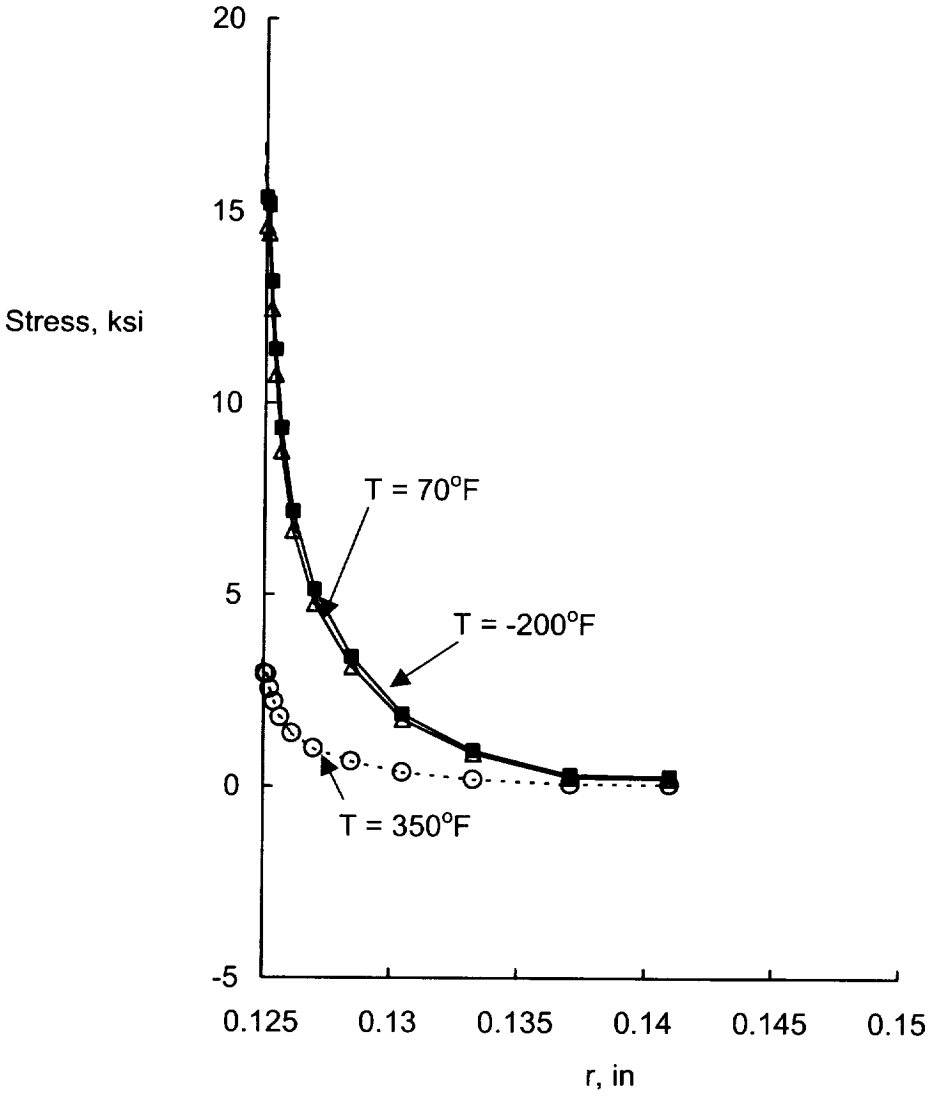

Figure 5.7. Radial distribution of σ_{xz} at θ = 52.5 degrees due to curing, at T = -200°F, 70°F, 350°F.

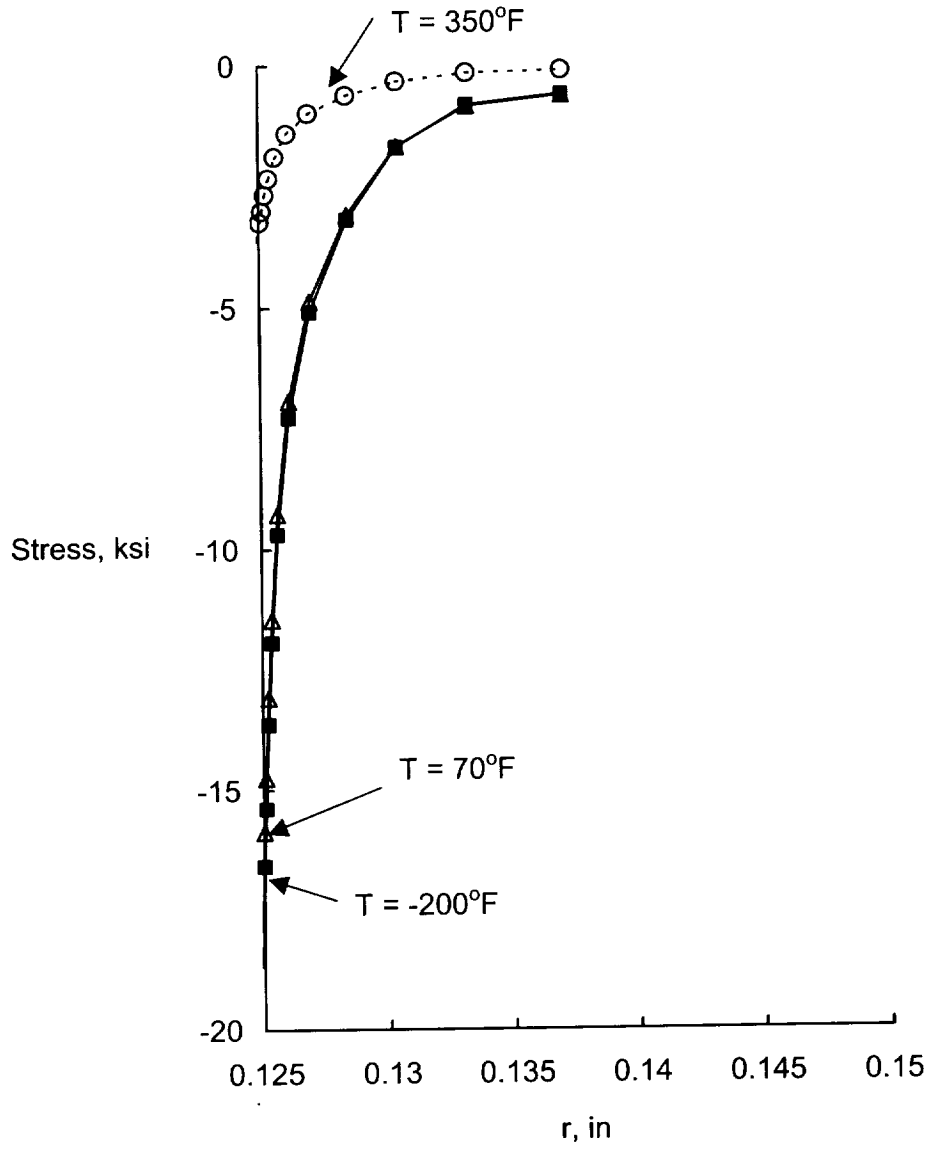

Figure 5.8. Radial distribution of σ_{yz} at θ = 37.5 degrees due to curing, at T = -200°F, 70°F, 350°F.

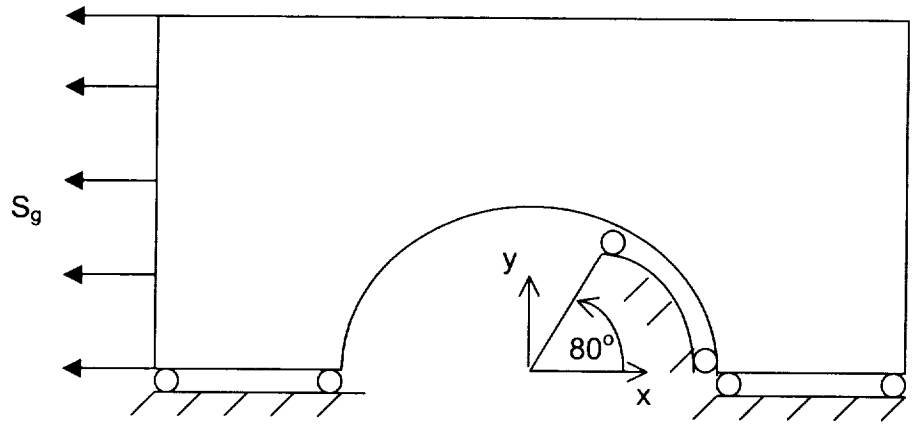

Figure 5.9. Illustration of pin-bearing boundary and loading conditions.

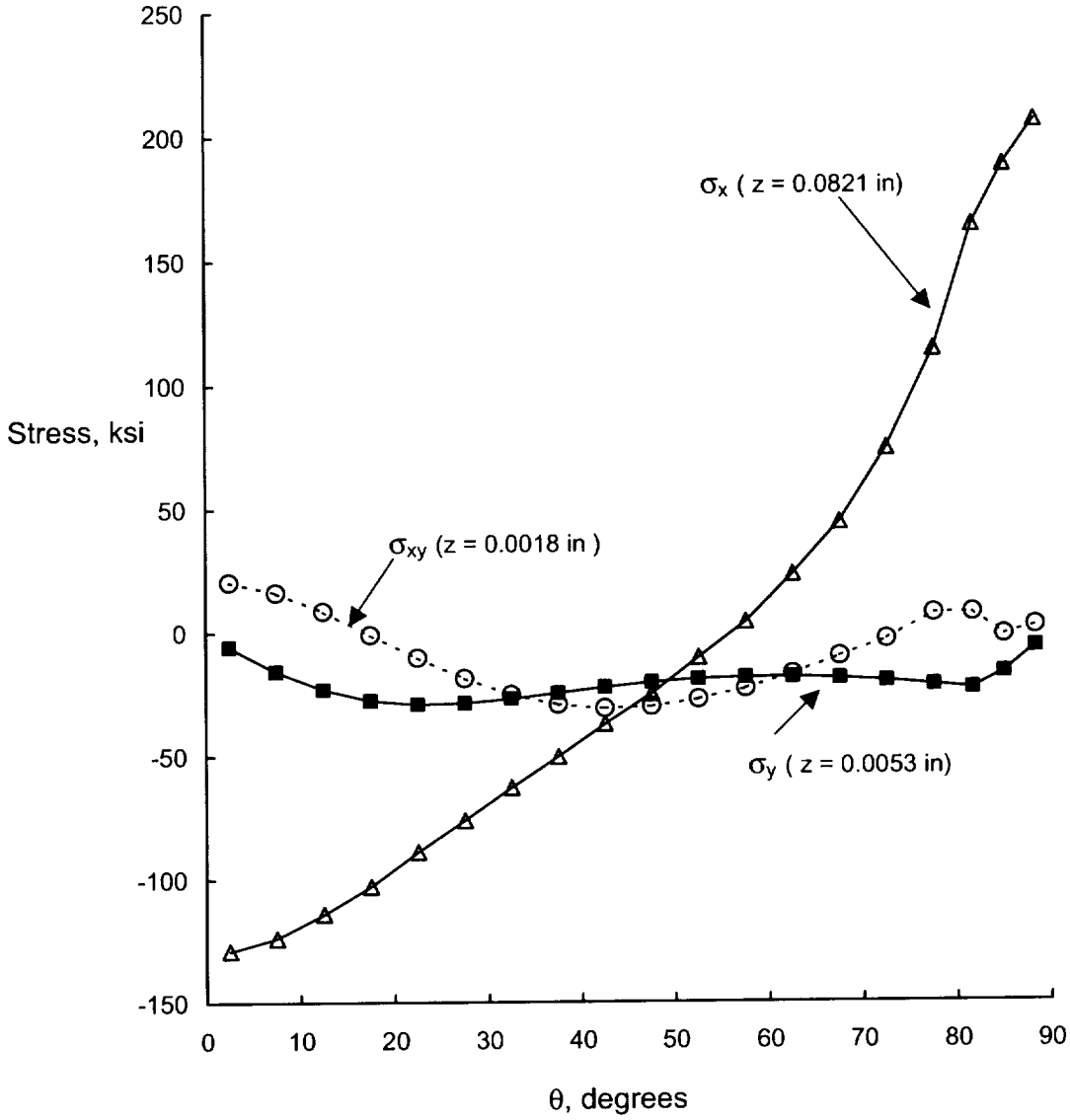

Figure 5.10. Variation of in-plane stresses around circumference of bolt hole due to pin-bearing load condition at T=70°F.

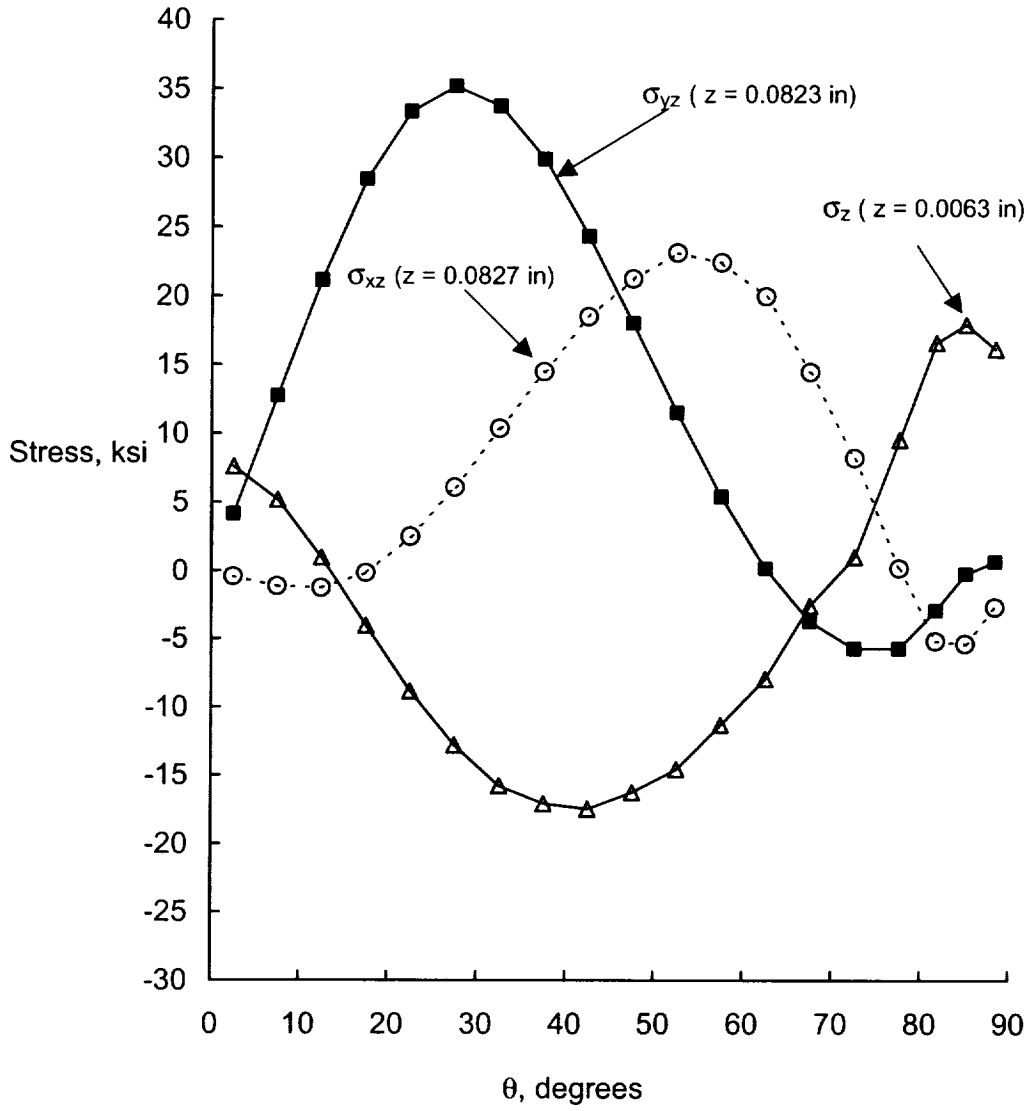

Figure 5.11. Variation of interlaminar stresses around circumference of bolt hole due to pin-bearing load condition at T=70°F.

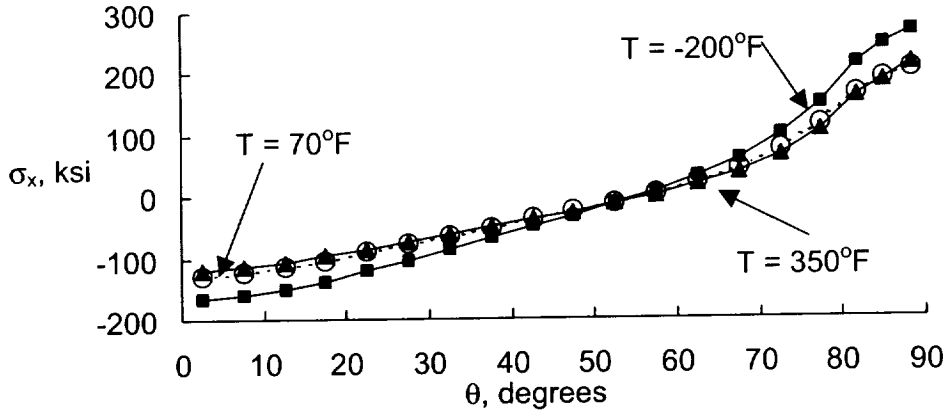

Figure 5.12. In-plane stress, σ_x, due to pin-bearing load at z = 0.0821 inch.

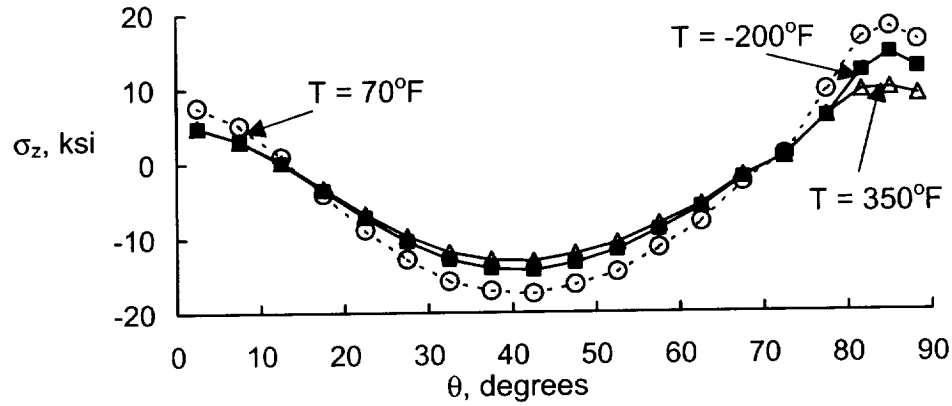

Figure 5.13. Interlaminar normal stress, σ_z, due to pin-bearing load at z = 0.0063 inch.

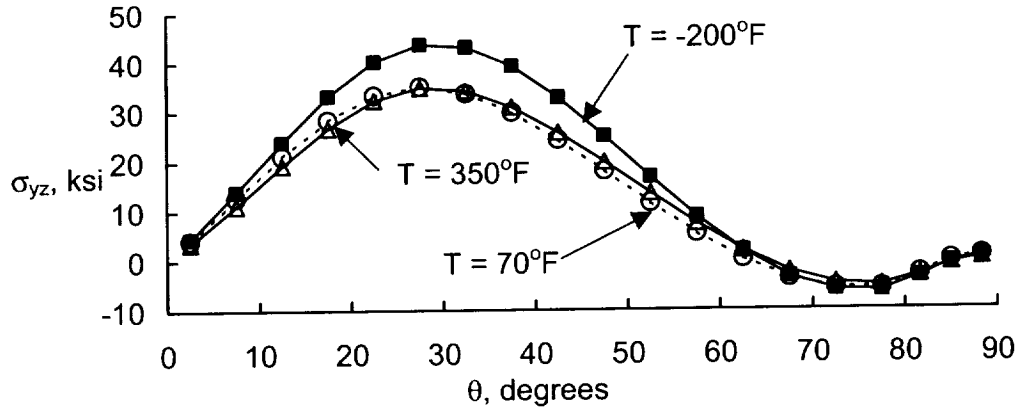

Figure 5.14. Interlaminar shear stress, σ_{yz}, due to pin-bearing load at z = 0.0823 inch.

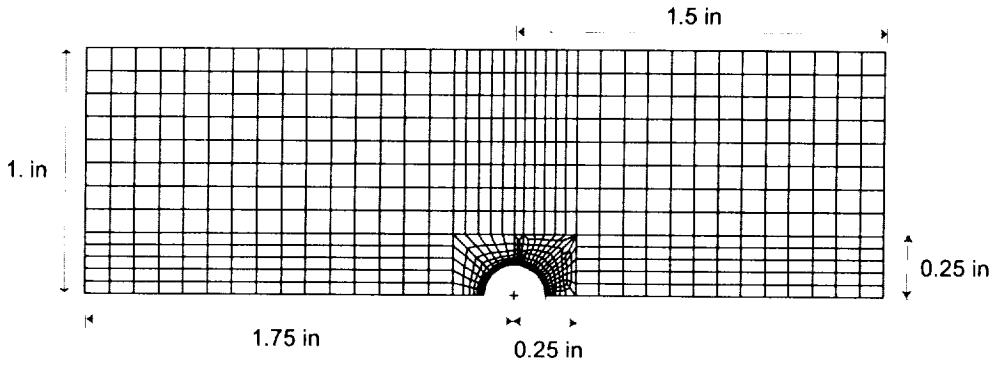

Figure 5.15. Finite element model for model size evaluation.

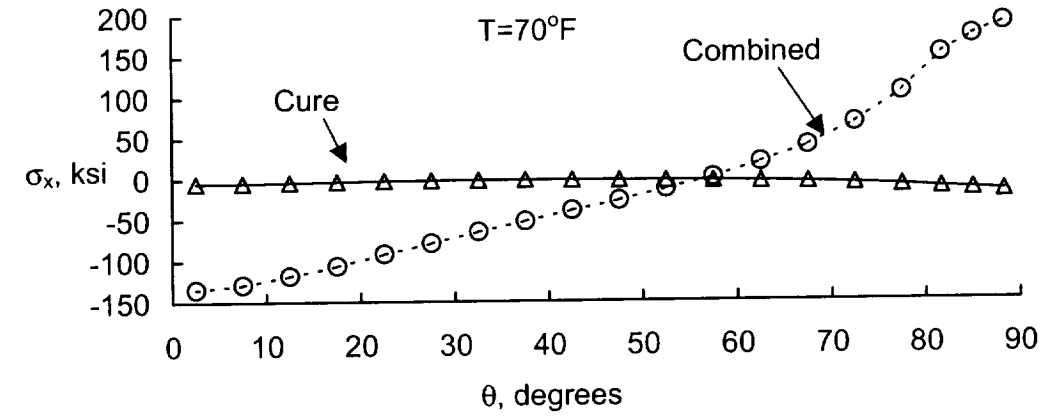

Figure 5.16. σ_x around circumference of bolt hole at z = 0.0821 inch.

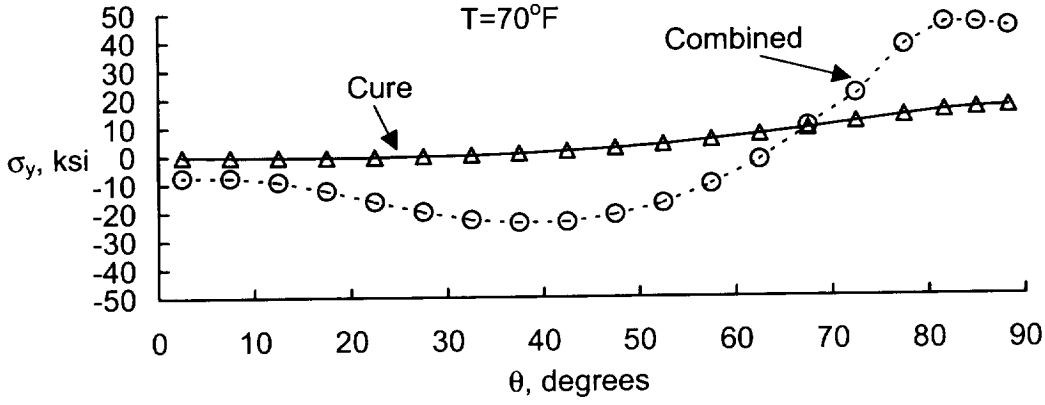

Figure 5.17. σ_y around circumference of bolt hole at z = 0.0083 inch.

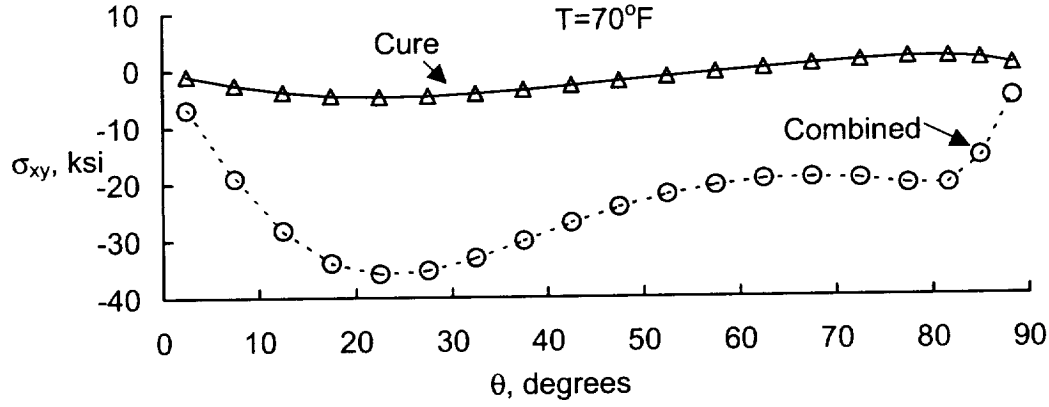

Figure 5.18. σ_{xy} around circumference of bolt hole at z = 0.0802 inch.

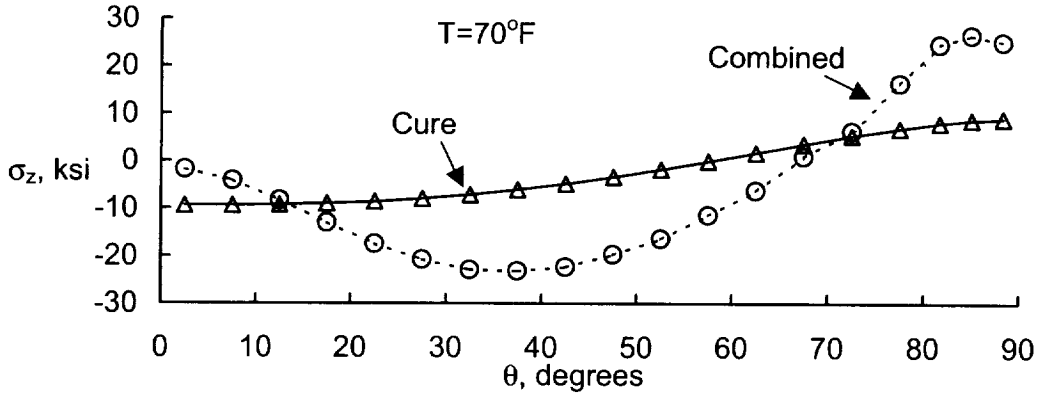

Figure 5.19. σ_z around circumference of bolt hole at z = 0.0063 inch.

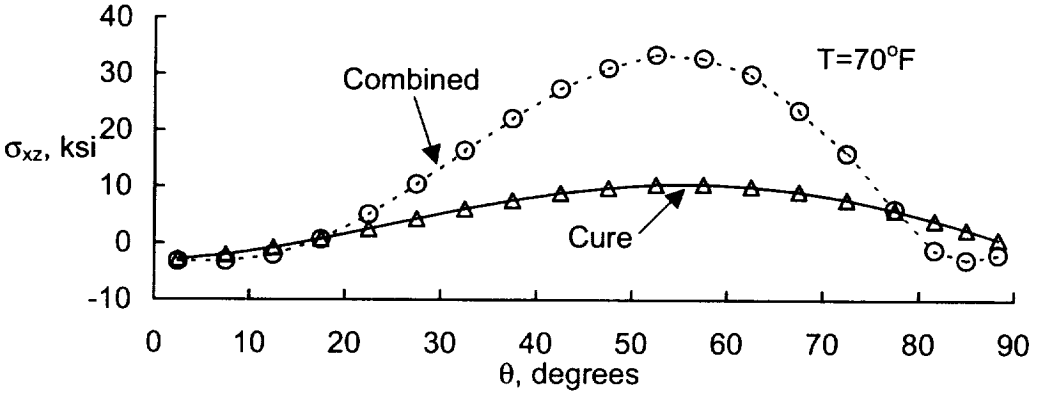

Figure 5.20. σ_{xz} around circumference of bolt hole at z = 0.0827 inch.

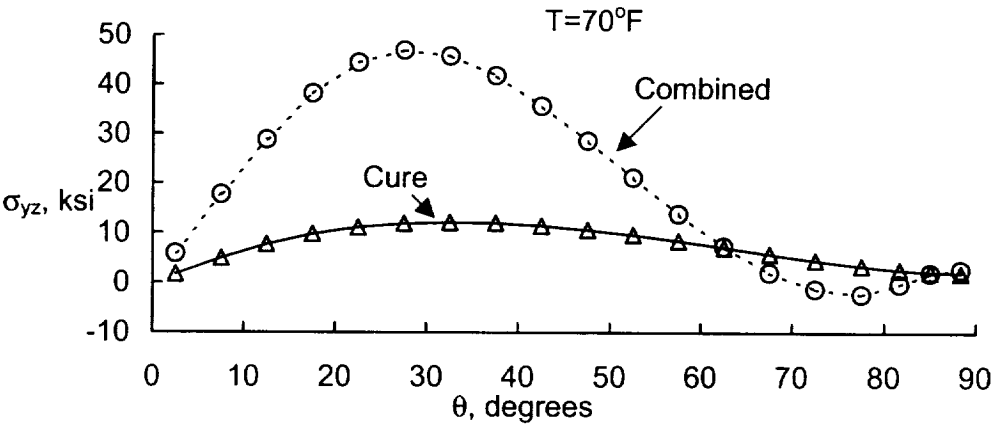

Figure 5.21. σ_{yz} around circumference of bolt hole at z = 0.0772 inch.

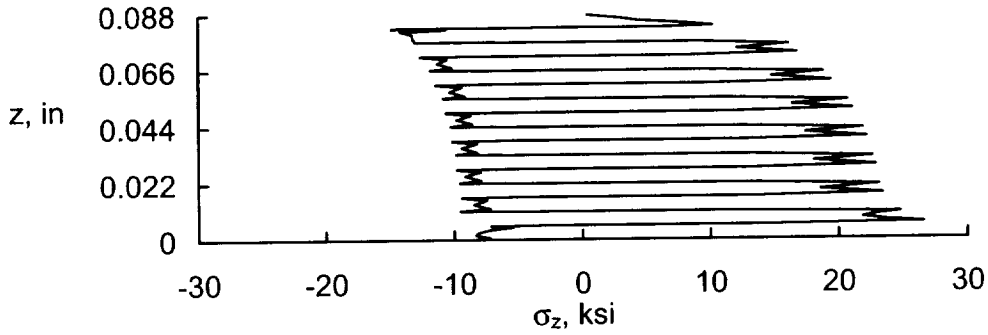

Figure 5.22. Combined solution σ_z distribution at bolt hole boundary and $\theta = 85^\circ$ for T=70°F.

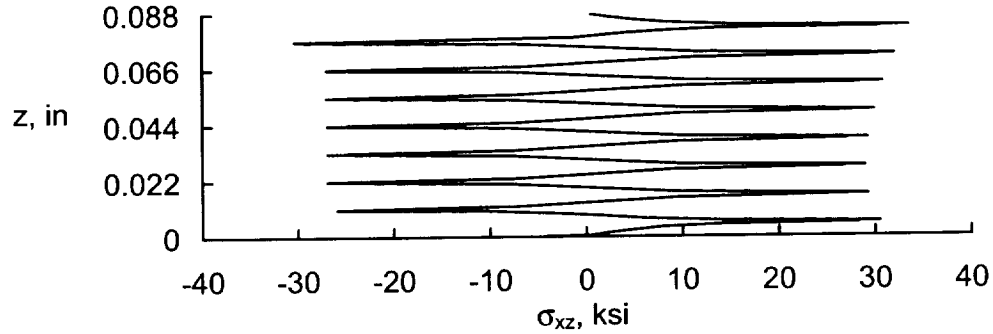

Figure 5.23. Combined solution σ_{xz} distribution at bolt hole boundary and $\theta = 52.5^\circ$ for T=70°F.

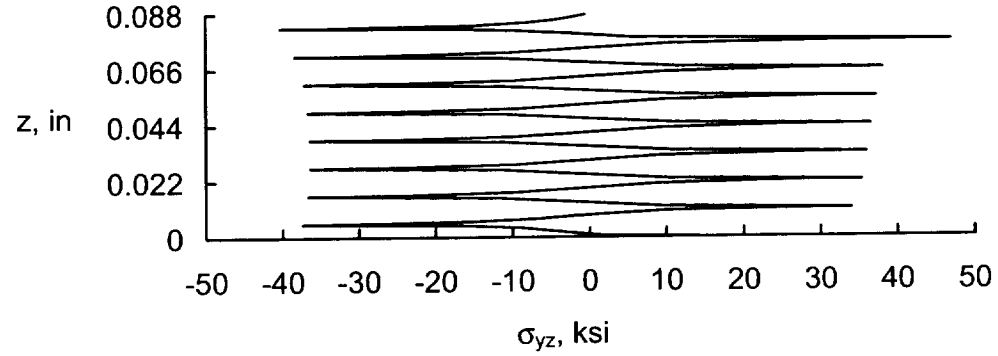

Figure 5.24. Combined solution σ_{yz} distribution at bolt hole boundary and $\theta = 27.5^\circ$ for T=70°F.

Chapter 6
Conclusions

An overview of the dissertation research accomplishments and findings is presented within this chapter. First, a summary reviewing the major results is presented. Then, specific conclusions from the research are presented. Finally, recommendations for future work are given.

6.1 Summary

Advanced technology vehicles require numerous composite structural panels to be mechanically joined and to operate at temperature extremes. Experimental studies have shown that elevated temperatures reduce the strength of polymer joints to an extent not explained by conventional understanding of joint behavior. A review of previous research did not identify a comprehensive study showing the factors contributing to the strength change. Consequently, the goal of this dissertation is to develop a fundamental understanding on the mechanisms that cause strength changes with a change in temperature. A fundamental understanding is necessary to design an efficient composite joint able to withstand a change in operating temperature without the risk of premature failure. A hypothesis was developed relating the change in pin-bearing strength to three basic changes in a specific joint subject to temperature change. The proposed factors contributing to a strength change with a change in temperature include: a change in the state of residual thermal stress, a change in the material properties of the constituent materials, and a change in the fastener fit. The specific objectives are then given with the goal of the research being to investigate the significant factors contributing to a strength change with a change in temperature. The objectives include: characterizing the material system to model structural response accurately, conducting pin-bearing experiments under thermo-mechanical loads, and developing computational models to study the effect of temperature changes on the state of stress.

The material system characterization to model the IM7/PETI5 material system utilized in this study is presented. The temperature-dependent lamina engineering constants were determined between temperatures of 495°F and –200°F. The glass transition temperature of the IM7/PETI5 was determined to be 460°F, and this temperature was assumed to be the stress free temperature below which curing stresses develop in the laminate. Lamina strength properties were determined at operating temperatures of –200°F, 70°F, and 350°F. Nonlinear stress-strain behavior was presented for the in-plane shear modulus and the matrix-direction compressive modulus. Laminate strength properties for several lay-ups of interest were also determined for comparisons with computational results and pin-bearing test data.

As a preliminary step in developing a computational model of the pin-bearing problem, analysis results for the composite laminate were studied. Classical lamination theory, as pertained to the current problem of interest, was introduced, and the derivation of the classical lamination theory expression for computing in-plane stresses due to both mechanical in-plane loads and a uniform

temperature change was presented. Key background information on interlaminar stresses and residual cure stresses revealed the need for a three-dimensional analysis of the composite laminate. Accordingly, a three-dimensional finite element model of a composite laminate was developed using NASTRAN and validated with an analysis found in the literature. The model was used to investigate laminate attributes that significantly affect the state of stress in the laminate and hence need to be incorporated in the pin-bearing analysis. The need for modeling the resin layers between lamina and residual stresses in the laminate was established. For the operating temperatures under investigation, using constant material properties determined at the operating temperature of interest in a linear analysis provided an accurate stress solution, as opposed to modeling temperature-dependent properties and conducting nonlinear analyses. Also, for the $[90,0]_{8s}$ lay-up, analysis results revealed the in-plane shear stresses and interlaminar shear stresses, τ_{13}, to be virtually zero, eliminating the need for nonlinear stress-strain characterization of the laminate model.

A combined solution was produced where the residual stresses due to curing were combined with the solution of the composite laminate subject to a compressive load. The interlaminar stresses present in the laminate due to curing were found to be reduced with the application of the mechanical compressive load. Therefore, the cause of failure in a composite laminate subject to compressive load is most likely not due to excessive interlaminar stresses. Results of the combined analysis also revealed that a change in laminate strength with a change in temperature is governed by the change in the fiber-direction compressive lamina strength, F_{11c}, with a change in temperature. The possibility that the residual stresses present in the laminate may lessen the change in strength was explored. Moreover, a three-dimensional analysis was concluded to be necessary to determine the role of interlaminar stresses in the pin-bearing problem.

Pin-bearing experiments were conducted to produce pin-bearing strength data for developing understanding on the pin bearing behavior of the IM7/PETI5 material system. The tests were conducted at the three operating temperatures of interest, 350°F, 70°F, and –200°F. As expected based on previous studies, for all lay-ups that failed in the bearing mode, strength degradation was observed with increasing temperature. Only the $[90]_{8s}$ lay-up, which failed in the tension mode, did not show any significant strength change with changing temperature. In comparing laminate and pin-bearing strength changes with temperature change, the extent of the strength change differs between the laminate and pin-bearing strength and also varies with lay-up change. Also, most pin-bearing strengths were significantly lower than laminate strengths. Since the computational study was limited to the $[90,0]_{8s}$ lay-up, this lay-up was scrutinized more thoroughly than the others. For all lay-ups, the ultimate bearing strengths and failure modes were presented. For the $[90,0]_{8s}$ lay-up, the bearing yield strength, bearing yield strain, and bearing ultimate strain were also computed and presented for all specimens tested. Micrographs taken on failed specimens cut along the bearing plane revealed severe damage in the outermost two plies. Also emanating from that region were transverse shear cracks. This observation

raised the possibility that ultimate failure could be due to the interlaminar shear stresses in the region of severe damage.

The computational study of the pin-bearing problem was finally presented. A three-dimensional finite element model of the composite laminate containing the bolt hole was developed. The model was highly discretized at the bolt hole boundary and contained a total of 63,498 elements. The residual stresses present in the laminate due to curing from the assumed stress free temperature of 460°F down to the operating temperature were studied. The free edge stresses at the bolt hole boundary were found to be dramatically different than in the case of a straight free edge. All interlaminar stress components intensified with extremely large stress concentrations at the hole boundary. As with the straight free edge, the interlaminar stresses quickly reduced to zero within one laminate thickness away from the free edge boundary. The residual stress distributions were similar for all three operating temperatures studied. Where the magnitudes of the maximum stresses of each component were lowest at 350°F, there was not much difference in residual stresses between the 70°F and –200°F operating temperatures. The effect of fastener fit changes with a change in temperature was also studied and found to be negligible for the current pin-bearing problem.

The finite element model was analyzed subject to pin-bearing loads. Assuming a rigid frictionless pin, the pin-bearing load was modeled assuming radial displacement constraints at the bolt hole boundary between $\theta = 0^{\circ}$ and 80°, and a uniform negative pressure load to the straight end of the model at $x = -1.$ inch. For each temperature analyzed, the load applied was equivalent to the average pin-bearing yield strength determined from the experiments of Chapter 4. Analysis results revealed extremely high stresses for all stress components at different locations around the bolt hole boundary. Distributions were similar for all three operating temperatures analyzed, where variations in only the magnitude of the maximum stresses were observed. Variations in material properties were obviously concluded to affect the magnitude of stresses significantly at the bolt hole boundary.

Finally, a combined solution was obtained that included the thermal residual cure stresses in the state of stress for the pin-bearing problem. The presence of cure stresses in the laminate intensified maximum pin-bearing stresses at the bolt hole boundary for all operating temperatures studied. Consequently, residual stresses could possibly contribute to the reason why pin-bearing strengths are lower than compressive strengths of the composite laminate. The observation was also made that the presence of residual stresses may lessen the extent of changes in pin-bearing strength with a change in temperature. Failure ratios much greater than one were predicted for many of the stress components, indicating the possibility that the finite element model did not include enough detail to accurately predict stresses. However, the distributions predicted peak interlaminar stresses in the outermost two resin layers of the composite laminate at the bolt hole. The micrograph of the failed specimens also revealed severe damage in the outmost two layers, indicating the possibility of failure initiating in that region.

6.2 Conclusions

The following conclusions were reached based on the experimental and computational studies investigating the effect of temperature changes on changes in pin-bearing strength of an IM7/PETI5 composite laminate:

1. Changes in both residual stresses and material properties with a change in temperature are factors influencing the changes in pin-bearing strength with temperature changes as proposed in the hypothesis.
2. The effect of changes in fastener fit with a change in temperature are negligible on pin-bearing strength changes and can be neglected from the hypothesis for the pin-bearing problem studied in this dissertation.
3. A three-dimensional analysis model including the resin layers between plies and thermal residual stresses due to curing is required to investigate accurately the state of stress in the pin-bearing problem.
4. The presence of residual stresses due to cure have the potential to reduce the overall pin-bearing strength of a composite laminate.
5. Residual stresses due to curing have the positive affect of lessening the extent to which bearing strength decreases with a temperature increase from 70°F to 350°F for the pin-bearing problem studied.
6. Residual stresses do not significantly change when temperature decreases from 70°F to –200°F and material property changes are the dominant factor influencing the increase in pin-bearing strength for the pin-bearing problem studied.
7. Analysis results reveal a decrease in the pin-bearing strength with increasing temperature, which qualitatively corresponds to the experimental pin-bearing strength reductions with increasing temperature.
8. The finite element model did not include sufficient detail to predict stresses accurately for the pin-bearing problem.
9. The reduced strength and stiffness properties of the polymer matrix material with increasing temperature drives pin-bearing strength degradation with increasing temperature and the residual thermal stresses due to curing only influence the extent of the strength degradation. The extent of the strength reduction with increasing temperature can only be lessened by the presence of the thermal residual stresses, which decrease with increasing temperature.
10. Until an accurate pin-bearing computational model is developed to predict strengths accurately, an IM7/PETI5 (or similar advanced material) joint design, with a defined lay-up, needs to be tested at the desired operating temperature to determine its pin-bearing strength at that temperature. The upper bound operating temperature will determine the joints minimal pin-bearing load capacity.

6.3 Recommendation

The following recommendations for future studies are based on the findings of this dissertation.

A more accurate finite element model is needed to predict stresses for the evaluation of pin-bearing behavior including thermal residual stresses. First, the effect of friction on the magnitude of the stresses at the bolt hole boundary needs to be investigated. A three-dimensional nonlinear contact analysis capability is recommended for modeling the effect of friction. Secondly, due to the large variation of key stresses between very high negative and positive values, both the tensile and compressive moduli should be incorporated in the analysis. A non-linear iterative scheme, where the determination on whether the stress was positive or negative for an element is made with increasing load, so the appropriate modulus can be determined and utilized for that element, is recommended. Finally, due to the large shear stresses predicted for the pin-bearing problem, modeling of the nonlinear stress-strain behavior is recommended. The non-linear moduli need to be modeled independently, where for the IM7/PETI5 material, the fiber direction properties are linear, and the matrix and shear properties have differing nonlinear profiles.

Due to the shortcomings of NASTRAN to include any of the aforementioned detail, an alternative analysis tool with the ability to model three-dimensional contact, tension and compression moduli simultaneously, and nonlinear moduli independently, needs to be identified, or if necessary, developed.

With large discrepancies observed between the measured and computed bolt hole elongation, evaluation and if necessary modification of the measurement technique used in this dissertation is recommended.

Appendix

Material Property Testing

The tests conducted to determine the moduli and strength properties are outlined in Table 1. The table shows the type of test followed by the test method, specimen size, the number of plies in the laminates tested, and finally the material properties obtained from the test. The ASTM test methods are published by the American Society of Testing and Materials (ASTM) in their Annual book of ASTM Standards. The lamina property testing was conducted under grant at the University of Wyoming (exluding F_{11c}), while the laminate property testing and the F_{11c} property tests were conducted at NASA Langley Research Center (LaRC).

The CLC method uses the Combined Load Compression(CLC) fixture developed at the University of Wyoming.[1] The CLC method was chosen here over the ASTM standards for compression testing of composites, since sample $[90,0]_{8s}$ specimens tested using the CLC method yielded higher ultimate compressive strengths. In addition, there was increased simplicity of conducting the test using the CLC fixture. While using the CLC fixture in testing at LaRC for the F_{11c} strength and the laminate compression strengths, it was discovered that additional clamp-up on the fixture was needed to prevent premature failure on the loaded ends of the specimen for the 350°F tests. An increase in torque to 60 in-lbs (from the recommended 25. in-lbs given in the user instructions) was found to be sufficient for failure to occur in the gage section. It was also found that using a torque too high, i.e. greater then 25 in-lb for the -200°F tests, resulted in premature failure occurring in the gage section adjacent to the fixture.

The property testing was conducted at the three operating temperatures of –200°F, 70°F, and 350°F and at an upper temperature of 495°F, which was preliminarily determined to be the glass transition temperature, T_g, of the material. Later, the glass transition temperature, T_g, of the current IM7/PETI-5 material was determined, by Wallace Vaughn[1], to be 460°F. The test data presented in Chapter 2 are typically the average values of four replicate specimen. When specimens were determined to have failed prematurely, the data was not used in calculating the average value presented. The coefficients of thermal expansion presented in Table 2.1 were determined at NASA Langley Research Center by Wally Vaughn and Craig Ohlhorst.[1]

Reference

1. Adams, D.F. and Welsh, J.S.: The Wyoming Combined Loading Compression Test Method. *Journal of Composites Technology and Research*, JCTRER, Vol. 19, No. 3, 1997, pp. 123-133.

[1] Aerospace Technologist, Enviromental Interactions Branch, NASA Langley Research Center, Hampton, VA.

Table 1 Material Property Test Information for Material Characterization.

Lamina Properties				
Type	Method	Specimen Size (inxin)	# of plies	Properties
Axial Compression	CLC**	0.5 x 5.5	20	E_{11C}, F_{11C}
Transverse Compression	CLC**	0.75 x 5.5	32	E_{11C}, F_{11C},ν_{23}
Axial Tension	ASTM D3039*	0.5 x 11.	8	E_{22T}, F_{22T},ν_{12}
Transverse Tension	ASTM D3039*	0.75 x 11.	20	E_{11T}, F_{11T}
Shear	ASTM D5379*	0.5 x 3.	20	E_{12}, F_{12}
ILSS+	ASTM D2344*	0.5 x 1.	32	F_{XZ}
ILNS++	Modified ASTM C 297*	1. x 1.	32	F_{zz}
Laminate Properties				
Compression	CLC**	0.5 x 5.5	32	E_{XXC}, F_{XXC}
Tension	ASTM D3039*	0.5 x 11.	32	E_{XXT}, F_{XXT}

* ASTM D# – American Society for Testing and Materials Designation Number
** CLC – Combined Load Compression
\+ ILSS – Interlaminar Shear Strength
++ ILNS – Interlaminar Normal Strength